Results in Engineering 23 (2024) 102712

Contents lists available at ScienceDirect

Results in Engineering

journal homepage: www.sciencedirect.com/journal/results-in-engineering

Review article

A comprehensive review on MIMO antennas for 5G smartphones: Mutual coupling techniques, comparative studies, SAR analysis, and future directions

Nazrin Haziq Jemaludin [a], Ahmed Jamal Abdullah Al-Gburi [a,*], Rania Hamdy Elabd [b], Tale Saeidi [c], Muhammad Firdaus Akbar [d], Imran Mohd Ibrahim [a], Zahriladha Zakaria [a]

[a] Center for Telecommunication Research & Innovation (CeTRI), Fakulti Teknologi Dan Kejuruteraan Elektronik Dan Komputer (FTKEK), Jalan Hang Tuah Jaya, 76100, Durian Tunggal, Melaka, Universiti Teknikal Malaysia Melaka (UTeM), Malacca, Malaysia
[b] Department Electronic and Communication, Higher Institute of Engineering and Technology in New Damietta, Damietta, Egypt
[c] WiSAR Lab, Atlantic Technological University (ATU), Letterkenny, Co. Donegal F92 FC93, Ireland
[d] School of Electrical and Electronic Engineering, Universiti Sains Malaysia, Engineering Campus, Nibong Tebal, Pulau Pinang 14300, Malaysia

ARTICLE INFO

Keywords:
Multiple-input multiple-output (MIMO)
5G
Smartphones
Mutual coupling
Specific absorption rate (SAR)
Isolation

ABSTRACT

Multiple-input multiple-output (MIMO) technology has become a key enabler for 5G smartphones, significantly enhancing data throughput and connectivity. By incorporating multiple antennas into the compact design of modern smartphones, MIMO technology improves spectral efficiency and network capacity. This comprehensive review examines the fundamental characteristics of MIMO antennas designed for 5G smartphones. The study explores various mutual coupling techniques used to mitigate interference between closely spaced antennas, thereby enhancing system performance. A comparative analysis of different MIMO antenna configurations is presented, highlighting their respective advantages and limitations in 5G applications. Additionally, the review includes specific absorption rate (SAR) analysis to ensure user safety by adhering to regulatory standards and addressing health concerns associated with prolonged exposure to electromagnetic fields. Finally, the paper outlines future directions for MIMO antenna research, emphasizing the need for innovative design strategies to accommodate the evolving landscape of wireless communication.

1. Introduction

In the past few years, mobile communication advancements have had an important impact on economic and social progress. The emergence of 5G technology is crucial for the future, offering revolutionary and evolutionary solutions such as ultra-high data rates, minimal latency, increased capacity, and enhanced quality of service. It symbolizes the next step in technological advancement [1–3].

Antenna designs in the modern era face several challenges, such as limited space, compatibility, support for multiple frequency bands, and compliance with specific absorption rate (SAR) regulations [4,5]. Several parameters determine the effectiveness of MIMO antennas. Far-field gain measures the radiation intensity in the far-field region. Analyzing diversity gain is crucial for evaluating the signal quality enhancements achieved through the use of multiple antennas [6–8]. The envelope correlation coefficient assesses the correlation between antenna elements. The total active reflection coefficient measures the losses and reflections within the antenna system. The mean effective gain determines the average directional gain [9].

The worldwide use of smartphones has experienced a significant increase in recent years. Currently, smartphones are utilised by approximately 4.88 billion individuals, which accounts for 60.25 % of the global population, as reported by Bankmycell [10]. Conversely, the global population comprising 49.40 % of the total was represented by 3.7 billion users in 2016. The Asia-Pacific region has experienced a surge in smartphone utilization due to the widespread availability of cost-effective service plans and affordable mobile phones. The smartphone adoption rate in this region was 64 % in 2019, and it is anticipated to reach 81 % by 2025 [11]. As a result of this upward trend, Malaysia's mobile market is anticipated to expand swiftly, with a potential annual growth rate of roughly 5 %.

With the rapid expansion of technology user bases, there is an urgent

* Corresponding author.
E-mail addresses: ahmedjamal@ieee.org, engahmed_jamall@yahoo.com (A.J.A. Al-Gburi).

https://doi.org/10.1016/j.rineng.2024.102712
Received 18 June 2024; Received in revised form 28 July 2024; Accepted 8 August 2024
Available online 10 August 2024

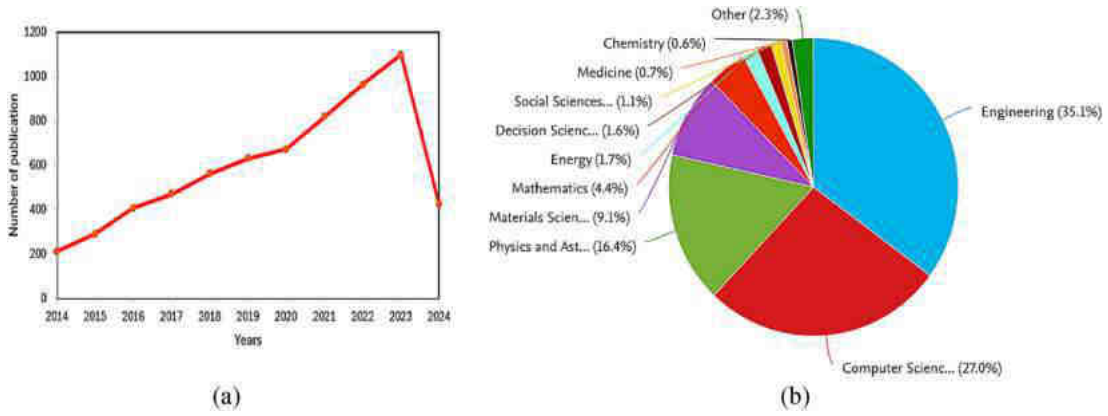

Fig. 1. Distribution of research publications on 5G MIMO antennas for smartphones, as extracted from Scopus, categorized by (a) the number of publications over the years and (b) the distribution of these documents by subject area.

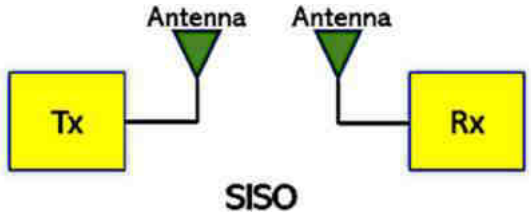

Fig. 2. SISO Antenna system [22].

need for smaller antenna systems that can support higher data rates and wider bandwidths [12]. Multiple-Input Multiple-Output (MIMO) antenna systems are increasingly recognized as a viable solution to this challenge. These systems enable simultaneous transmission and reception of data through independent channels within the same radio spectrum, effectively tackling multipath propagation issues by leveraging multiple transmit-and-receive antennas [13,14].

As the forefront of wireless communication, MIMO systems offer a compelling solution to the data rate limitations encountered by Single-Input Single-Output (SISO) systems [15]. By integrating multiple antennas, these systems enhance system reliability, increase channel capacity, and improve signal quality and gain. However, the adoption of MIMO antenna systems introduces complexities in design and increases physical footprint. Achieving adequate signal independence and isolation in MIMO operation requires careful spatial separation of antennas, which poses challenges for portable devices due to space constraints and the need for extended feedlines [16]. Although reducing the proximity of antenna elements may address space limitations, it can also lead to increased mutual coupling.

This review aims to address these challenges by exploring various isolation techniques discussed in the literature. These techniques aim to enhance efficiency, bandwidth, envelope correlation coefficient (ECC), and gain in different antenna configurations. Implementing antenna diversity techniques within MIMO systems has proven highly effective in improving performance by reducing co-channel interference and mitigating multipath fading [17,18]. Depending on specific needs, diversity gain is attained through various means, including spatial, polarization, and pattern diversities.

The sustained interest in this topic is evident from its continued prominence on the Scopus website. Fig. 1 illustrates the number of publications on this subject over the past decade, highlighting trends and growth patterns in research output. The graph not only shows the overall number of publications but also breaks down the data by subject area, offering a comprehensive view of the various disciplines contributing to this field. This detailed categorization by subject area underscores the interdisciplinary nature of the research, indicating how different academic and scientific communities are engaging with and advancing the topic.

The aim of this review paper is to offer a comprehensive overview of the current state of MIMO antenna design. We focus on essential topics such as mutual coupling methods, performance comparisons, SAR analysis, and prospects. The objective of this review is to compile current research, address critical obstacles, and propose innovative approaches to enhance the compatibility and performance of antennas. Our objective is to establish a valuable resource for researchers and engineers, facilitating the development of innovative and efficient MIMO antennas that meet the rigorous standards of next-generation 5G networks. Ultimately, this review aims to advance 5G technology by ensuring reliable, high-performance connectivity for future mobile communications.

2. Categorization according to input and output ports

2.1. Fundamental of SISO

Many researchers utilize the SISO antenna in 5G applications because it can serve as both a single-element and multi-element antenna. The SISO antenna is easy to design and implement, making it well-suited for integration into 5G communication devices. However, achieving substantial gain with a single-element antenna typically necessitates a larger size [19]. Signal degradation results in a reduction in the quality of service in frequency bands that exceed 6 GHz, which results in increased propagation losses. Thus, it is crucial to substitute a single-element antenna with a multi-element antenna to ensure consistent and optimal performance [20]. Despite the primary goal of a multi-element antenna being to increase antenna gain, this enhancement is achieved at the expense of increased physical dimensions and design complexity [21]. As illustrated in Fig. 2, SISO configurations consist of a single antenna on both the transmitter and receiver sides.

Compared to other system categories, Single Input Single Output (SISO) systems are characterised by their simplicity, as they lack diversity or additional processing. Although its simplicity makes it potentially applicable in fields such as Wi-Fi, television, and broadcasting, its bandwidth constraints continue to be a major challenge, as outlined by Shannon's Laws [23]:

$$C = B\,log_2(1 + SNR)[bit/s] \quad (1)$$

Where C is channel capacity; B channel bandwidth; SNR signal to noise ratio.

2.2. Fundamental of MIMO

Multipath fading, interference, and radiation losses are all potential

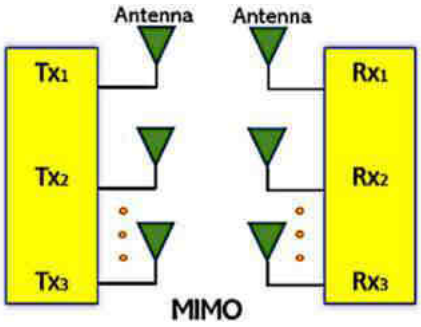

Fig. 3. MIMO Antenna system [22].

factors that can affect wireless communication. These issues become more apparent at higher frequencies [24,25]. Using MIMO antennas is crucial for overcoming these challenges. MIMO extends transmission range without requiring additional signal power. Consequently, 5G networks implement MIMO configurations to enhance overall efficiency, maximize throughput, and achieve low latency [26–28]. In MIMO systems, the coordinated transmission of multiple signals is facilitated by multiple antennas, significantly increasing channel capacity. MIMO systems utilize multiband antennas to minimize the number of antennas, these provide coverage for a variety of wireless applications [29]. Additionally, antennas for MIMO can be differentiated by their bandwidth regions, which are classified as either wideband or multiband. As illustrated in Fig. 3, the MIMO mode utilizes multiple transmit antennas to transmit signals through any antenna and travel through various paths to reach the receiving end.

Furthermore, MIMO antennas with improved isolation are a better choice for compact devices designed to achieve higher transmission rates [30]. Various enhancement techniques are applied across different antenna structures to enhance overall efficiency, broaden bandwidth, improve envelope correlation coefficient (ECC), minimize mutual coupling between antennas, and achieve higher gain. The electromagnetic interaction among antenna elements within MIMO systems is referred to as mutual coupling (MC) [31,32]. In MIMO systems, the receiving device of one antenna absorbs energy emitted by another antenna. Therefore, minimizing mutual coupling between antenna elements is essential. The following is a mathematical expression of this relationship [33]:

$$MC_{mn} = exp\left(-\frac{2x_{mn}}{\lambda}(\alpha + n\pi)\right), m \neq n \tag{2}$$

$$MC_{mn} = 1 - \frac{1}{N}\sum_{m}\sum_{m \neq n} MC_{mn} \tag{3}$$

Here, MC_{mn} represents MC, and x_{mn} denotes the space between the mth and nth elements of an antenna. The parameter α controls the level of coupling, and N denotes the total number of MIMO elements. Mutual coupling is typically assessed using scattering parameters and decibel measurements (dB).

The ECC is another critical parameter in MIMO systems, as it quantifies the correlation between the incoming signals at the MIMO terminals. The following formula can be employed to determine the ECC [33]:

$$|P_{mn}(e)|^2 = 1 - \frac{\eta_{max}}{\eta_m \eta_n} \tag{4}$$

In this formula, the correlation coefficient between the mth and nth ports is denoted by $P_{mn}(e)$. The combined efficiency of the radiating elements is represented by $\eta_m\eta_n$, where η_{max} indicates the maximum efficiency. It is recommended that the ECC value remains at or below 0.5 [33].

3. Fifth generation (5G) and mmWave revolution context

5G represents the next generation of wireless telecommunication technology, offering faster speeds, lower latency, and greater bandwidth compared to earlier generations such as 4G and 3G [34–36].

Key features of 5G include.

1. 10 Gbps for uplink and 20 Gbps for downlink peak data rates [34].
2. Latency reduced to as little as 1 ms in Ultra-Reliable Low Latency Communication (URLLC) environments [34].
3. Capacity to connect more devices simultaneously by expanding the radio spectrum resources from the sub-3 GHz range used in 4G to 100 GHz and beyond [35].
4. Smaller transmitters that can be placed unobtrusively on buildings, trees and other objects [35].

3.1. The evolution of cellular technology towards the deployment of 5G

The first generation (1G) networks, introduced in the late 1970s, were mainly created to facilitate voice calls and operated on analogue technology. They employed frequency modulation (FM) for signal transmission. These networks were vulnerable to espionage and interference. As the first digital cellular networks, the second generation (2G) networks emerged in the early 1990s, utilizing technologies such as TDMA and CDMA to improve the quality and capacity of voice calls. Furthermore, short messaging service (SMS) was implemented by 2G networks for text messaging. The introduction of third-generation (3G) networks in the early 2000s significantly improved the speed and data capacity of networks. These networks utilised technologies such as HSPA and WCDMA to facilitate multimedia messaging, video conferencing, and mobile internet access. Fourth-generation (4G) networks were subsequently developed in the late 2000s. They substantially improved network speed and data capacity by utilizing LTE technology,

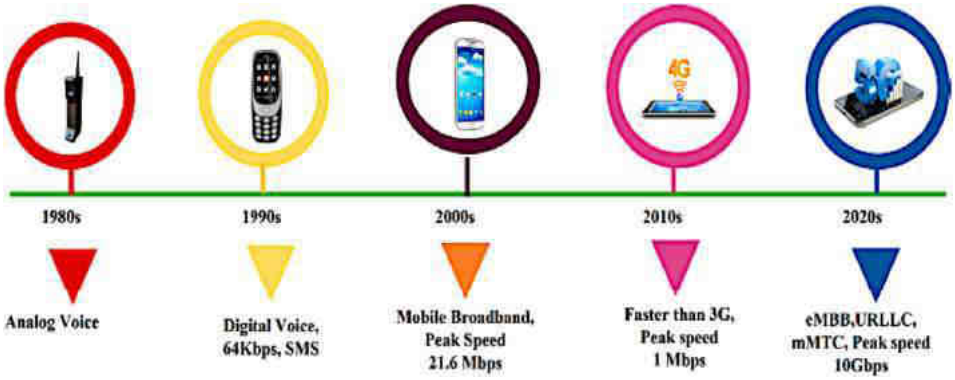

Fig. 4. Evolution of cellular communication generation [38].

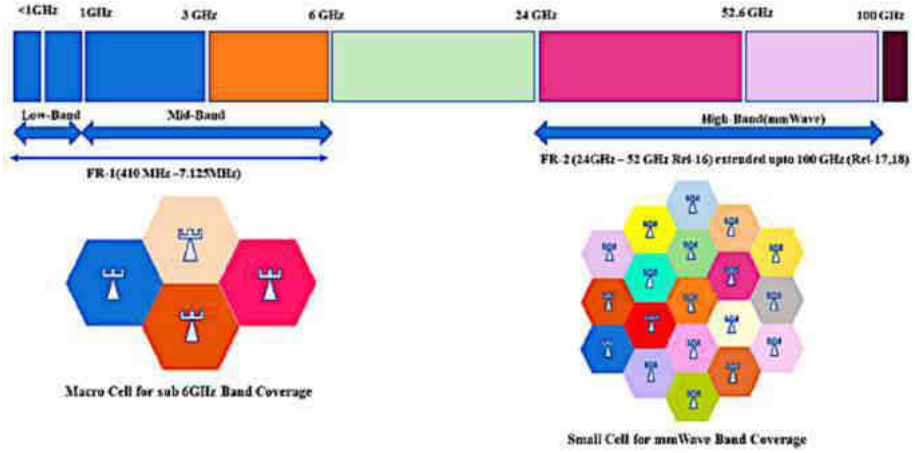

Fig. 5. 5G NR frequency spectrum in frequency range 1 (FR1 and frequency range 2 (FR2) with cell size requirements [38].

resulting in broader coverage, lower latency, and quicker upload and download rates. Consequently, advanced applications like cloud computing, online gaming, and video streaming became increasingly prevalent. In the 2010s, fifth-generation (5G) networks were introduced to further enhance network speeds, reduce latency, and increase data capacity beyond what 4G networks could provide. These networks utilised cutting-edge radio technologies such as massive MIMO and mmWave. This represents the latest advancement in technology. Moreover, 5G networks enable the development of innovative applications such as autonomous vehicles, smart cities, and virtual and augmented reality [37].

The evolution of cellular technology from 1G to 5G is shown in Fig. 4. Since the introduction of 1G networks in the 1980s, significant progress has been made. Network speed, capacity, and functionality have been enhanced with each successive iteration, facilitating the development of mobile devices and applications that are becoming increasingly sophisticated.

3.2. Millimeter-wave (mmWave)

5G cellular communication is significantly influenced by millimeter-wave (mmWave) technology, which applies to mmWave channels operating within the NR FR1 and FR2 as shown in Fig. 5. These higher-frequency channels enable greater capacity, reduced latency, and faster data transfer. Frequency Range 1 (FR1) encompasses sub-6 GHz frequency bands, specifically ranging from 410 MHz to 7.125 MHz, and includes many bands previously used in earlier mobile communication standards, such as 4G LTE. The FR1 bands support a significant portion of traditional cellular traffic and utilize both Frequency Division Duplex (FDD) and Time Division Duplex (TDD) methods, allowing for various configurations of uplink and downlink channels. Frequency Range 2 (FR2), which includes higher frequency bands from 24.25 GHz to 52.6 GHz, commonly referred to as mmWave frequencies, provides very high data rates over short distances, making them suitable for applications requiring high bandwidth, such as enhanced mobile broadband services. However, mmWave transmissions, due to their smaller wavelengths, are more susceptible to fading induced by objects such as trees and buildings. To resolve this obstacle, 5G networks that implement mmWave technology must establish access points or base stations closer to one another.

The optimization of 5G network performance depends on the distinctions between macro cells for sub-6 GHz coverage and small cells for mmWave coverage. Macro cells are well-suited for outdoor coverage because they can cover vast areas with sub-6 GHz frequencies, which have superior penetration through obstacles. In contrast, small cells offer coverage over shorter distances using mmWave frequencies, which are more susceptible to physical obstructions but offer higher capacity and speed. Small cells are cost-effective and can be readily integrated into existing urban infrastructure, even though macro cells are more expensive to deploy and have lower capacity in densely populated regions. The integration of macro and small cells results in a heterogeneous network that optimizes user experience, capacity, and coverage. Macro cells provide broad coverage, while small cells fill gaps in high-demand areas.

Despite its challenges, the utilization of mmWave technology provides numerous advantages to 5G networks. However, other wireless transmissions and environmental conditions such as rain and mist can interfere with these higher-frequency frequencies. To mitigate these issues, 5G networks employ sophisticated beamforming and signal processing techniques. Quality is enhanced and interference is diminished by concentrating signals in specific directions. The benefits are as follows: increased capacity, reduced latency, and faster data transmission rates—all of which are crucial for bandwidth-intensive applications, including augmented reality (AR), virtual reality (VR), and high-definition video streaming.

Recent research has demonstrated numerous techniques to reduce mutual coupling in mmWave antenna arrays. For example, the efficacy of advanced materials and configurations has been highlighted by substantial improvements in isolation achieved through innovative approaches in MIMO dielectric resonator antennas [39,40]. Additionally, studies implementing near-field techniques have effectively improved isolation within mmWave arrays, achieving coupling reductions from −17 dB to below −23.2 dB within the specified frequency ranges [41,42]. Furthermore, the integration of electromagnetic bandgap (EBG) structures and metamaterials has shown promising results in minimizing interference and enhancing performance. These advancements collectively contribute to more efficient and reliable mmWave communication systems.

3.3. 5G miniaturized antennas in smartphone

5G technology has transformed how consumers interact with mobile devices' internet access. 5G, the fifth-generation wireless technology, provides extensive enhancements over its predecessors, such as expanded capacity, reduced latency, and quicker speeds. These developments have created various innovative applications and services for mobile devices, unleashing new opportunities.

Key attributes of 5G on smartphones.

1. Speed: 5G smartphones can achieve download speeds of up to 20 Gbps, which is significantly faster than the 1 Gbps speeds of 4G

Fig. 6. 5G frequency band.

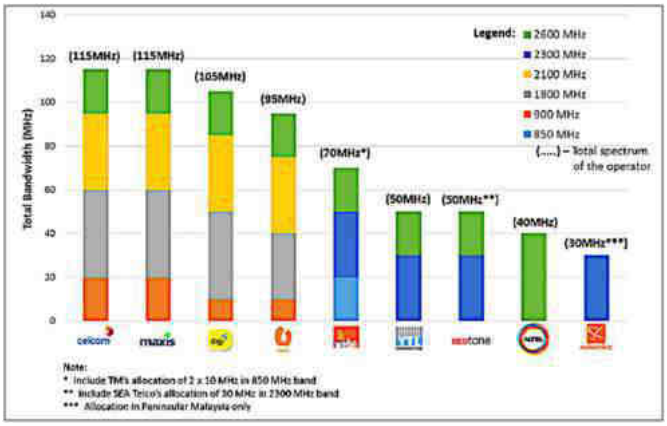

Fig. 7. Frequency spectrum allocation by operators in Malaysia [56].

networks. This means that users can pick up movies in minutes and songs in seconds [43,44].

2. Latency: The latency of 5G technology is reduced to as little as 1 ms, an important advance over the 40 ms of advanced 4G networks. The following reduced latency allows more efficient response times and more seamless interactions with applications and services [44,45].
3. Capacity: 5G networks are ideal for applications that demand extensive IoT connectivity by virtue of their ability to handle a significant number of devices and connections [44].

5G-enabled smartphones offer several benefits. Firstly, they enhance the mobile experience by providing a more responsive and immersive environment. Users can enjoy online gaming, streaming HD movies, and other data-intensive activities without any lag or buffering. Secondly, 5G networks enable new use cases, including augmented and virtual reality, autonomous vehicles, and remote healthcare services. Lastly, improved IoT connectivity supports the widespread adoption of connected devices by providing the necessary infrastructure [43–46].

The demand for smaller and more efficient devices capable of operating at higher frequencies is the primary driver behind the essential role of compact antennas in implementing 5G technology. This investigation focuses on exploring a variety of compact antenna designs, applications, and performance attributes optimized for 5G deployment.

In the field of 5G antenna technology, various key designs and technologies are driving advancements towards smaller size and enhanced performance. In Ref. [47], Fractal antennas have been specifically designed for 5G Ka-band applications, using a simple geometry to achieve broad-spectrum performance suitable for high-frequency demands. Next [48], explains millimeter-wave antennas designed for the 5G-II band exhibit notable features, including a wide 70.4 % impedance bandwidth and strong return loss capabilities of −35 dBi across frequencies ranging from 16.2 GHz to 33.8 GHz, with a central frequency at 25 GHz, adaptable for applications across Ka and Ku bands. Author in Ref. [49] presents a dual-band rectangular patch antenna that also emerged, utilizing slotted patch configurations to reduce size while maintaining efficiency in the 28 GHz and 38 GHz bands for 5G millimeter-wave applications. Furthermore, efforts to miniaturize Massive MIMO base station antennas prioritize optimizing gain-to-volume and isolation-to-volume ratios, highlighting current innovations and future prospects in base station applications for 5G networks as discussed in Ref. [50].

Various sectors benefit from miniaturized 5G antennas, supporting compact designs and high-speed data transmission in mobile devices like smartphones and wearables. In IoT devices, these antennas ensure efficient communication among interconnected devices. Moreover, in 5G infrastructure, they optimize extensive MIMO systems in base stations, boosting capacity and coverage through integration in smaller spaces. This capability enhances the reliability and resilience of contemporary telecommunications networks.

Modern wireless communication systems require miniaturized 5G antennas. There has been significant progress in developing smaller and more efficient antennas that perform better, demonstrated by the use of fractal shapes, millimeter-wave capabilities, and dual-band configurations. Ongoing research aims to improve these technologies by addressing challenges related to size, performance, and integration into various devices and systems, driven by the increasing demand for 5G connectivity.

In modern wireless communication systems, mobile antennas are indispensable, particularly with the evolution of 5G technology. This investigation explores the intricacies of mobile antenna design, the challenges they face, and recent advancements. The article covers practical applications, bandwidth capabilities, and various decoupling methods.

There are several critical aspects to consider when designing mobile antennas. Innovative designs and configurations are essential to ensure antennas can operate within the confined space of mobile devices while delivering optimal performance, with compactness being the highest priority. Additionally, mobile antennas must support multiple frequency bands to accommodate various communication standards, including LTE and 5G, necessitating designs capable of efficiently managing wide bandwidths. Decoupling techniques play a crucial role in minimizing mutual coupling between closely spaced antennas. Methods such as metamaterials, parasitic elements, neutralization lines, and others are employed to enhance antenna performance in mobile communication systems. These factors highlight the delicate balance between effective signal management, bandwidth requirements, and size constraints in modern mobile antenna development [51]. The future evolution of mobile connectivity is expected to be significantly influenced by smartphones that incorporate 5G technology, which have the potential to revolutionize the way people use mobile devices.

3.4. Frequency spectrum allocations for 5G MIMO antennas

A variety of low, mid, and high-frequency channels are utilised by global wireless operators, as illustrated in Fig. 5, to deliver a comprehensive experience with 5G that meets evolving consumer demands. By integrating these bands, 5G networks can effectively leverage diverse service benefits, significantly impacting both speed and coverage [52,53].

Although less vulnerable to physical obstacles and offering wider coverage, low-frequency bands compromise transmission capacity and speed. High-capacity and low-latency networks are facilitated by the mid-band spectrum, which typically ranges above 3.5 GHz and has a bandwidth range of 50–100 MHz. Meanwhile, 5G applications perform optimally in the high-band mm-wave range, spanning 24–70 GHz [54]. Fig. 6 provides a detailed overview of the frequency channels allocated to various services by different operators in Malaysia. This allocation is essential to maximize the utilization of the radio frequency (RF) spectrum and minimize interference between different services [55–58] (see Fig. 7).

3.5. Analysis of specific absorption rate (SAR)

The SAR quantifies the RF radiation absorbed by human body tis-

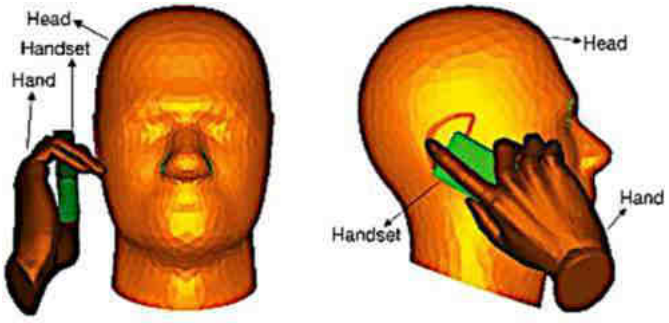

Fig. 8. SAM Head, Hand and Handset model [75].

sues, expressed as the average energy absorption rate per kilogram of tissue (W/kg). This measurement is essential for guaranteeing that mobile phones stick to safety regulations [59–61]. Exposure limits are set below the threshold where biological damage could occur, considering the body's ability to dissipate heat from tissues absorbing energy from the phone. The Federal Communications Commission (FCC) of the United States has established a Specific Absorption Rate (SAR) limit of 1.6 W per kilogram (1.6 W/kg) for exposure to mobile phone RF radiation [61]. The International Commission on Non-Ionizing Radiation Protection (ICNIRP) mandates that the SAR in the head should not exceed 2 W/kg averaged over any 10 g of tissue [62]. This standard is based on the finding that a SAR of 4 W/kg results in a slight increase in body temperature. The measurement of electromagnetic (EM) energy absorbed by the human body during smartphone usage is quantified by the SAR, as detailed in reference [63,64]. The SAR is frequently assessed for internal exposure and quantifies the amount of electromagnetic energy absorbed per unit mass. SAR is defined by CENELEC, the European Committee for Electrotechnical Standardisation, as [65]: " The time rate of change of the incremental energy (dW) absorbed by (dissipated in) an incremental mass (dm) within a volume element (dV) of a specified density (ρ)" or " The time rate of change of the incremental energy (dW) absorbed by (dissipated in) an incremental mass (dm) within a volume element (dV)" [66]:

$$SAR = \frac{d}{dt}\left(\frac{dW}{dm}\right) = \frac{d}{dt}\left(\frac{dW}{\rho dV}\right) \tag{5}$$

SAR may be obtained by Ref. [67]:

$$SAR = \frac{\sigma |E|^2}{\rho} \tag{6}$$

$$SAR = C_i \frac{dT}{dt} \tag{7}$$

$$SAR = \frac{J^2}{\rho\sigma} \tag{8}$$

The electrical field strength within body tissue, denoted as (E), is defined as voltage per meter (V/m):

$$E = \sqrt{E_x{}^2 + E_y{}^2 + E_z{}^2} \tag{9}$$

The x, y, and z components of the electric field's root mean square (rms) values are denoted as E_x, E_y, and E_z, respectively.

σ = The electrical conductivity characteristics of human tissues (S/m);

ρ = Density of human body tissue (kg/m^3);

C_i = Specific heat capacity of human tissue in J/kg °C;

dT/dt = Rate of change of body tissue temperature in °C/s;

J = Current density induced in body tissue in A/m^2.

3.5.1. *Safety standards and regulatory organizations of SAR*

Based on the latest information, various national and international organizations have established safety guidelines. A few notable organizations include.

1. **National Radiological Protection Board (NRPB)**: The NRPB, advising the Health and Safety Commission, was among the first to propose specific absorption rate (SAR) limits for both ionizing and non-ionizing radiation [68].
2. **The European Committee for Electrotechnical Standardisation (CENELEC):** has released comprehensive guidelines for assessing human exposure to electromagnetic fields [54].
3. **American National Standards Institute (ANSI)**: ANSI, a non-profit organization, oversees the C95.1 committee (now managed by IEEE). The ANSI-IEEE document [69], initially issued in 1991 and revised in 1999, serves as the American standard for exposure limits. The latest edition was published in 2019 [70].
4. **International Radiation Protection Association (IRPA)**: IRPA's International Non-Ionizing Radiation Committee (INIRC) investigates risks associated with non-ionizing radiations. In 1991, IRPA founded the International Commission on Non-Ionizing Radiation Protection (ICNIRP), which issued guidelines on limiting exposure to time-varying electric, magnetic, and electromagnetic fields (up to 300 GHz) [71]. An updated version was published in 2020.
5. **European Communities' Commission**: Currently, the European Economic Community (EEC) Commission is in the process of formulating radiation protection regulations. These regulations encompass directives for the safety of workers and machinery, covering both ionizing and non-ionizing radiation levels [72].

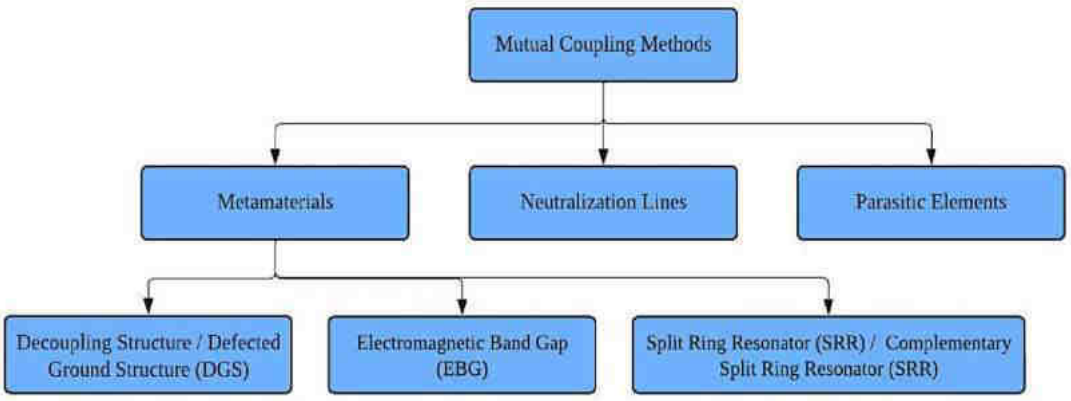

Fig. 9. Mutual coupling methods.

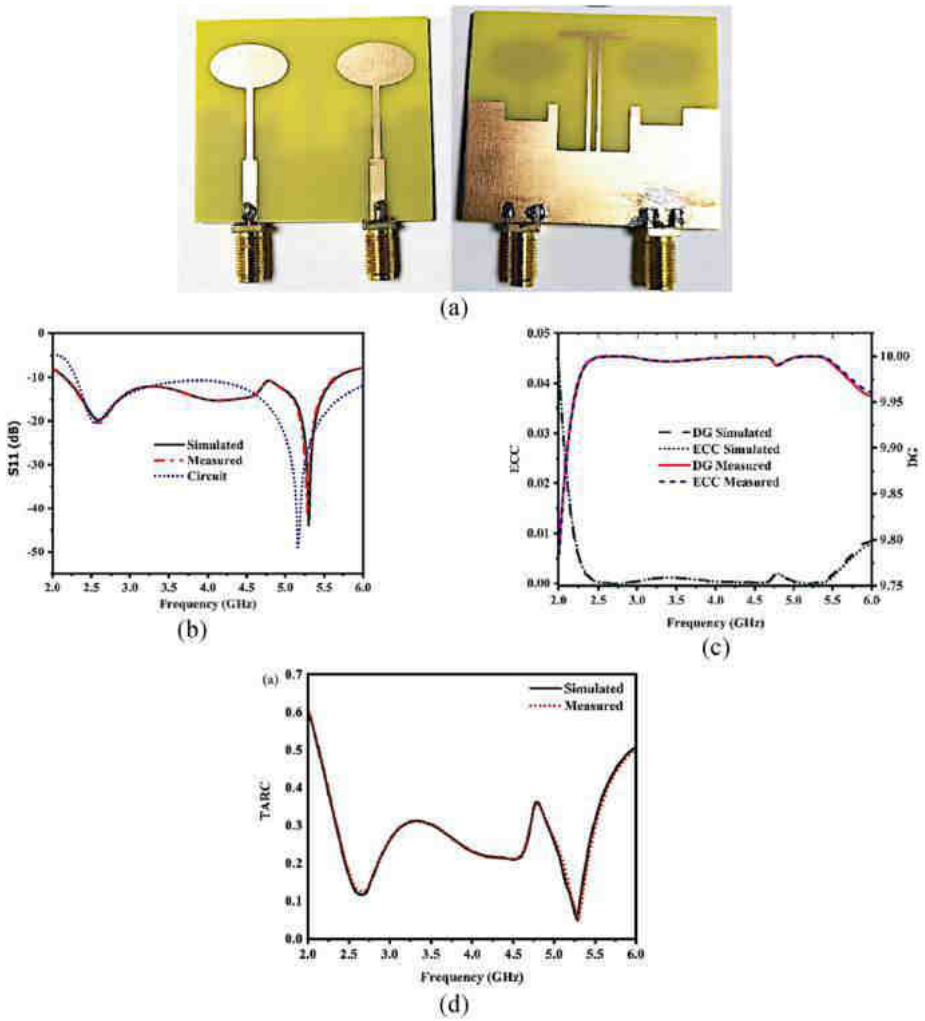

Fig. 10. (a) The geometry of the antenna, Measured and Simulated (b) Reflection coefficient, (c) Envelope correlation coefficients and Diversity gain and (d) TARC [127].

6. **World Health Organization (WHO)**: CENELEC and ANSI/IEEE [73] have established standards for regulated (controlled) and uncontrolled environments. Regulated settings involve knowledgeable individuals (e.g., workers), while uncontrolled environments expose individuals without their awareness or control (e.g., the general public).

3.5.2. Human head simulation model

The Standard Anthropomorphic Model (SAM) head is a simplified human model skull, comprising two main components: the liquid and the outer shell. The skull, hand, and mobile phone are three distinct elements in the SAM model, as illustrated in Fig. 8. This model is a systematic framework for simulating mobile phone systems, including specific absorption rate (SAR) evaluations, and is obtained from the CST component library. In order to satisfy the essential qualities across all relevant frequencies, the skull liquid and hand materials are broadband frequency-dependent substances [74,75].

Effect on the SAR with proximity of the human body.

1. SAR Distribution

Research indicates that the interaction between reactive near-field components and standing waves can elevate SAR levels when mobile devices are in close proximity to the human body. This underscores the importance of conducting a thorough SAR evaluation during compliance testing of mobile devices, as it leads to greater energy absorption in tissues compared to uniform models [76].

2. Proximity Sensors

The management of RF exposure is facilitated by integrating SAR proximity sensors, which detect the presence of a human body near a mobile device. These sensors mitigate the risk of excessive exposure by regulating the RF output to maintain SAR levels within safe limits [77, 78].

3. Distance Impact

Research has shown that SAR values fluctuate significantly depending on the distance from the human body. For instance, simulations have demonstrated that SAR decreases as distance from the body increases, emphasizing that maintaining greater separation can effectively reduce RF exposure [79].

4. Coupling effect of the antenna with human body in defected ground and partial ground antenna configurations

The coupling effect of the antenna with defected ground and partial ground configurations.

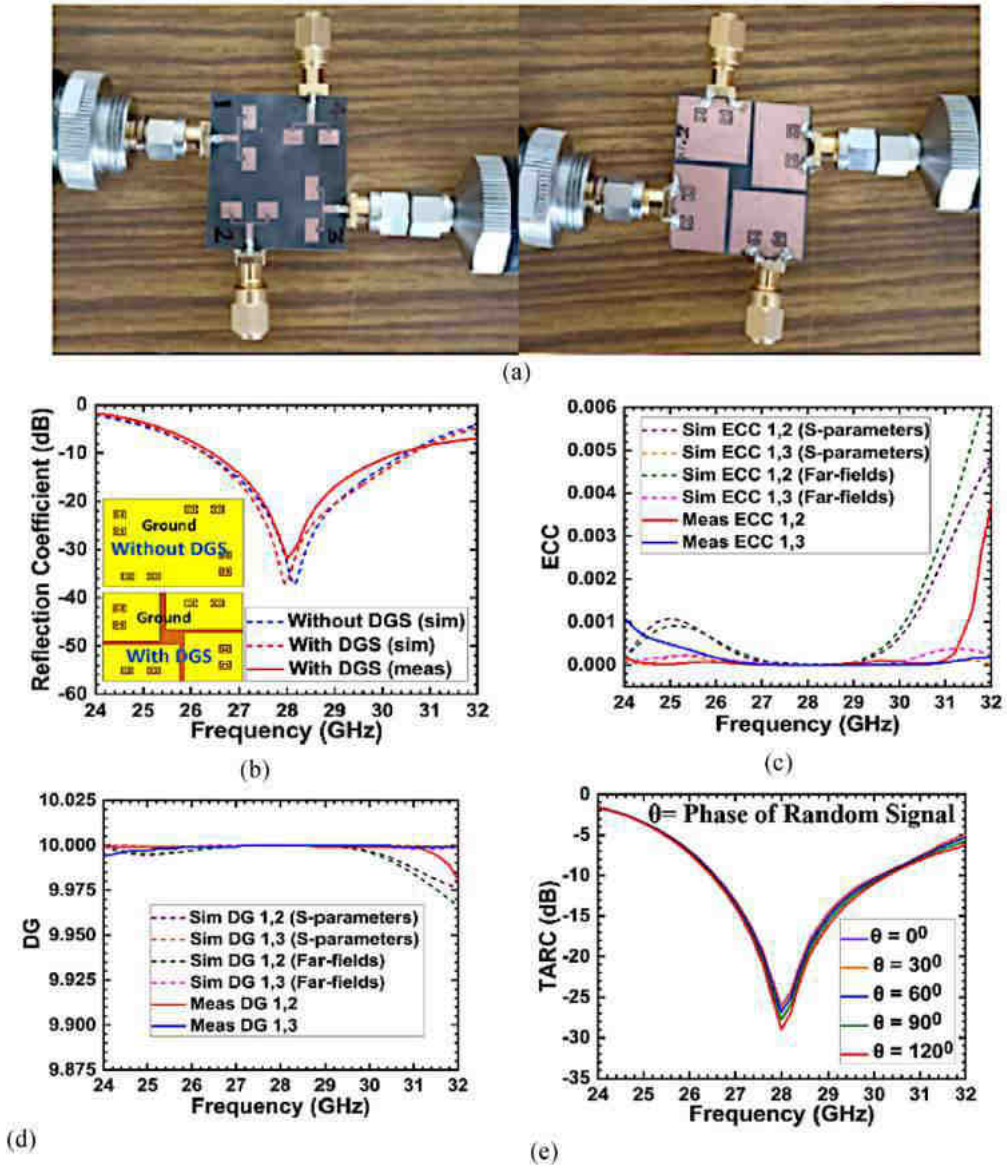

Fig. 11. (a) The geometry of the antenna and Measured and Simulated (b) S-parameter, (c) ECC, (d) DG and (e) TARC [128].

1. Radiation Characteristics

The presence of the human body significantly affects the radiation characteristics of antennas, including changes to input impedance, current distribution, and radiation patterns, potentially reducing overall performance. In configurations involving partial ground arrangements and defected ground structures (DGS), the coupling effect may lead to unintended changes in the antenna's efficiency and directionality [80, 81].

2. Design Issues

The interactions with the human body can considerably compromise the radiation characteristics of antennas that are designed to operate in close proximity to the body, such as those used in wearable technology. Consequently, the dielectric properties of human tissue, which absorb and scatter electromagnetic radiation, have an impact on the efficacy of antennas. Subsequently, these characteristics necessitate precise design considerations [80].

3. Defected Ground and Partial Ground Configurations

To enhance performance, antennas incorporating partial ground configurations or defected ground structures (DGS) are designed to modify the ground plane. However, the effectiveness of these designs can be significantly influenced by the proximity of the human body. The coupling effect may distort the intended benefits of such configurations, highlighting the importance of precise design and simulation to minimize adverse effects [80,81].

3.5.3. SAR testing process

Manufacturers are required to conduct SAR testing to verify compliance with safety standards. The SAR must not exceed 2 W/kg when averaged over 10 g of tissue. This test includes using a phantom model that replicates the human head and body. The smartphone is tested in various positions, including holding it at an angle away from the cheek and touching the ear while functioning at maximum power levels across all frequency bands. SAR testing is complicated by the introduction of 5G technology, which employs millimeter-wave frequencies and advanced antenna systems such as phased-array antennas and multiple-input multiple-output (MIMO). These technologies require more intricate testing arrangements to accurately measure SAR values, as they increase the number of antennas in devices [82,83].

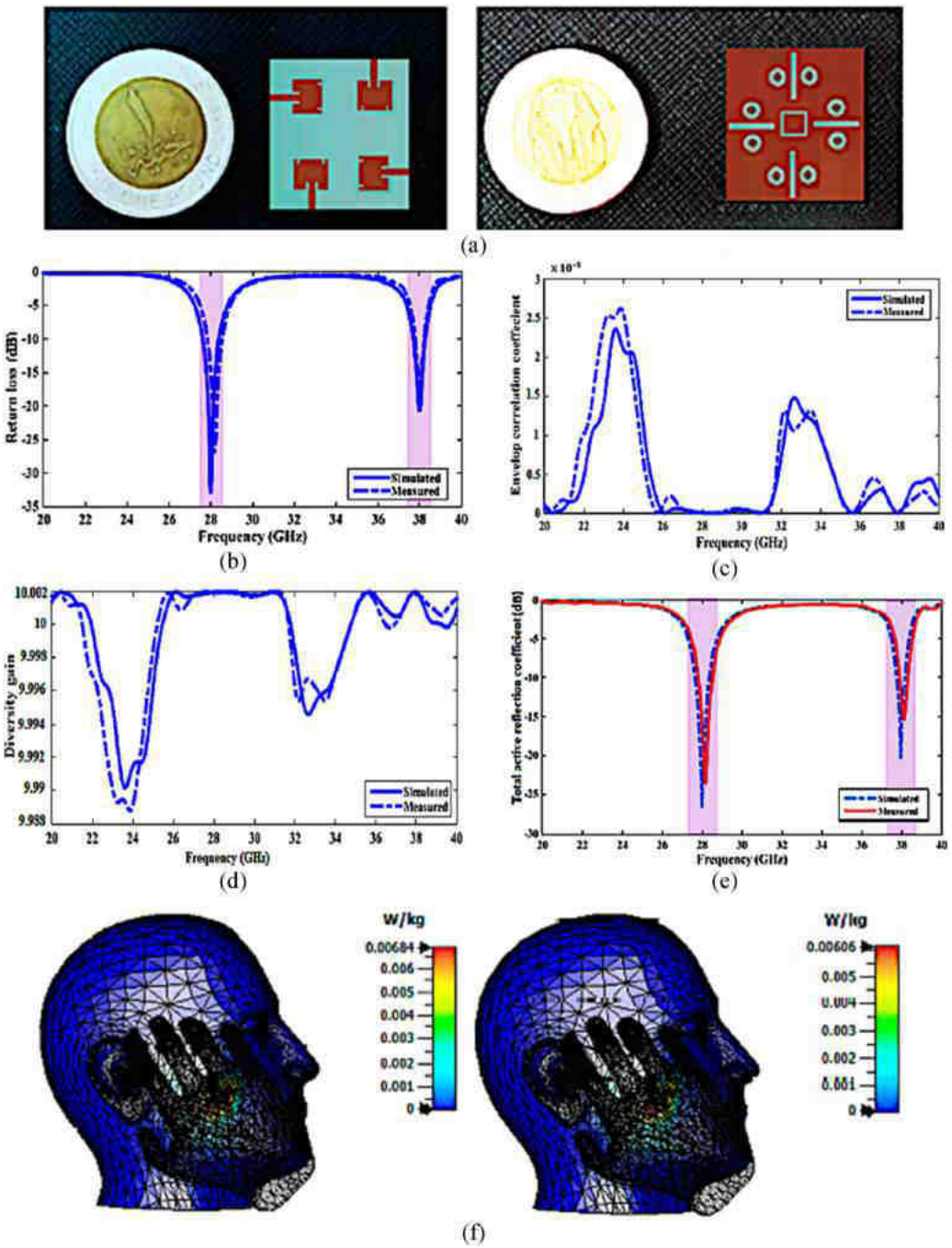

Fig. 12. (a) The geometry of the antenna, Measured and Simulated (b) Reflection coefficient, (c) Envelope correlation coefficients, (d) Diversity gain and (e) TARC and (d) Simulated SAR at 28 GHz & 38 GHz [129].

3.5.4. Recent innovations and case studies

Recent research has investigated the potential of metamaterials to reduce SAR values in 5G devices. These engineered materials can manipulate electromagnetic radiation in ways that conventional materials cannot. Studies have demonstrated that different metamaterial designs can substantially reduce SAR exposure by modifying the distribution of RF energy during the device's operation [84,85]. Research has also focused on the effect of the distance between the smartphone and the user's head, with results suggesting that a significant reduction in SAR values can be achieved by increasing this distance. The importance of user behavior in managing exposure was underscored by a study showing that moving the phone just 5 mm away from the skull could significantly reduce SAR [84,85]. Compliance with SAR regulations is enforced in Europe by the Radio Equipment Directive (RED). To market their devices, manufacturers must submit documentation demonstrating compliance with SAR limits. Regulatory bodies conduct periodic inspections to ensure ongoing compliance, particularly given the increased monitoring and testing introduced by 5G technology [86]. To assess the performance of 5G devices in real-world scenarios, over-the-air (OTA) testing has become an essential component of the SAR compliance procedure. This method considers the complexities introduced by the multiple antennas and signal processing techniques employed in 5G technology. OTA testing is implemented to guarantee that devices continue to comply with standard usage scenarios [82].

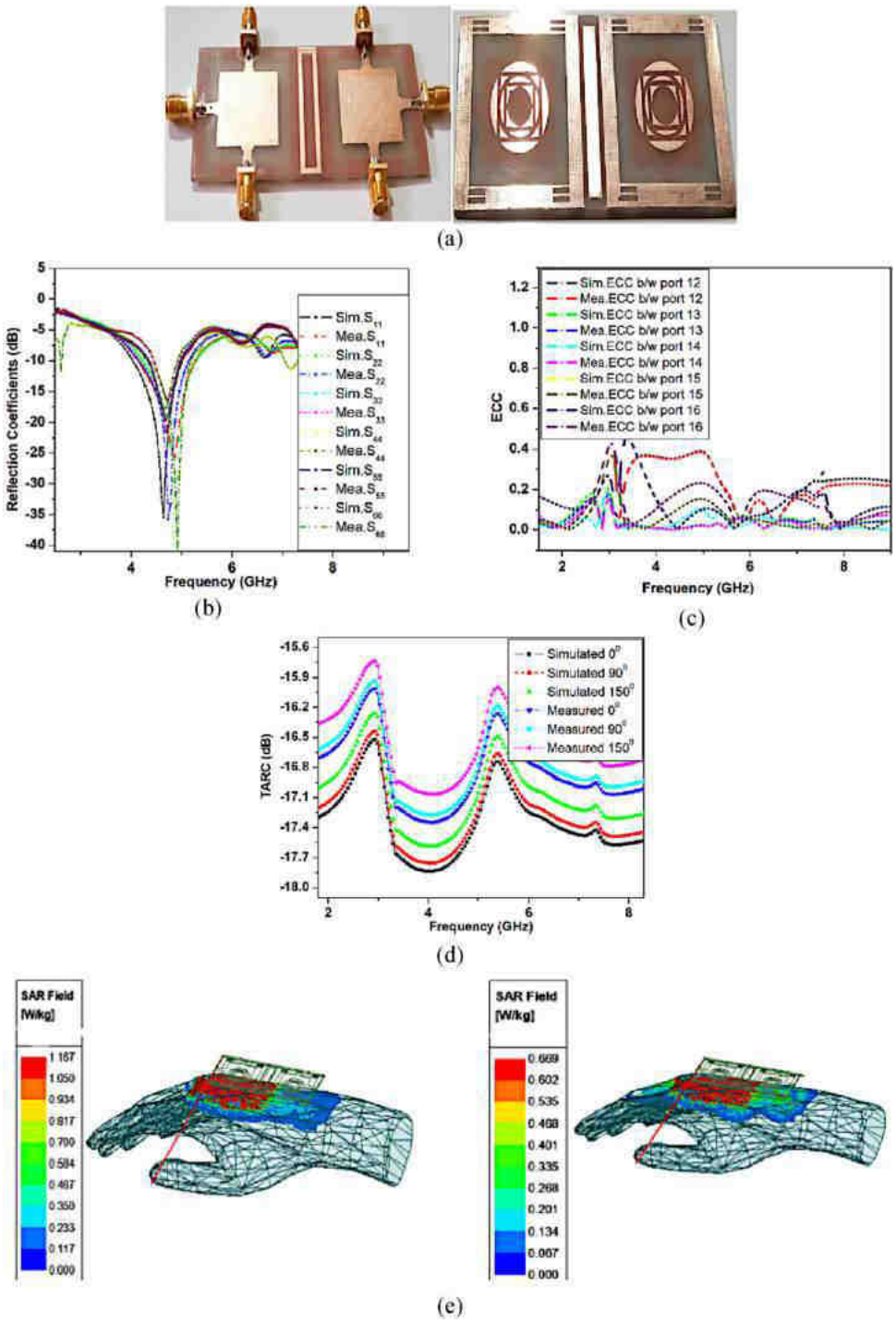

Fig. 13. (a) The geometry of the antenna, Measured and Simulated (b) Reflection coefficient, (c) Envelope correlation coefficients, (d) TARC and (e) Simulated SAR [130].

4. Mutual coupling reduction technique

The electromagnetic interaction among the distinct elements within an antenna array is referred to as mutual coupling in antennas, which influences its radiation pattern, efficiency, and overall performance. When antenna elements are situated in close proximity to one another, mutual coupling occurs, resulting in the transfer of energy from one element to another. This results in a decrease in the radiated power of the original element [87,88]. There are several key techniques for reducing mutual coupling in MIMO antennas. The graphical presentation of these techniques is shown in Fig. 9.

4.1. Metamaterials

Metamaterial decoupling techniques aim to reduce interference between antenna parts. This involves using metamaterials between nearby elements to improve isolation. By using metamaterials, antennas can be made smaller without losing effectiveness. However, challenges remain in achieving good performance over different frequencies. Researchers are working on new antenna designs to overcome these issues [89,90]. Metamaterial decoupling uses special materials to manage how electromagnetic waves behave, reducing unwanted antenna interactions. Adding these materials can greatly improve the separation between

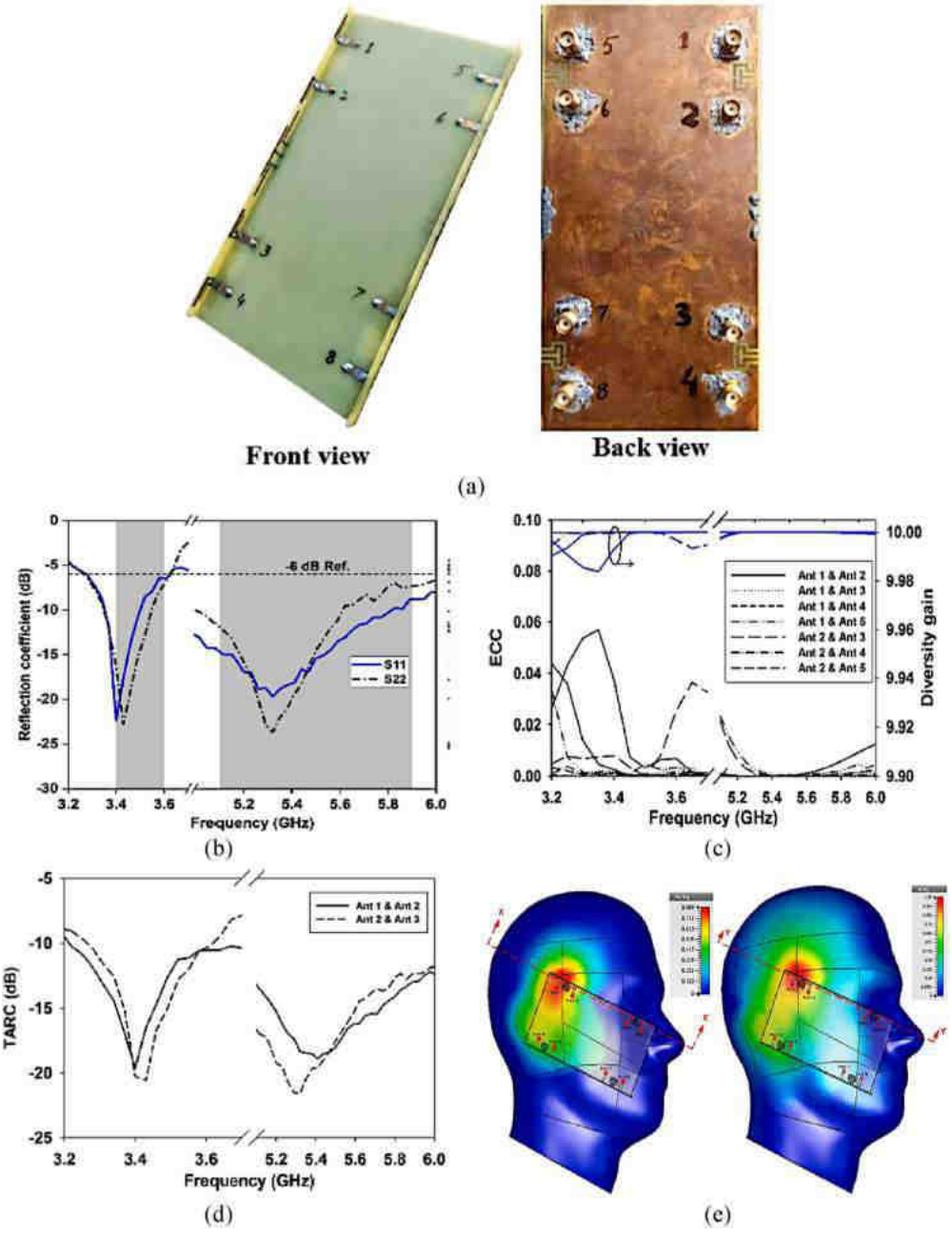

Fig. 14. (a) The geometry of the antenna, (b) Measured reflection coefficient, (c) Measured ECC, (d) Measured TARC and (e) Simulated SAR at 3.5 GHz & 5.5 GHz [131].

antennas, boosting how well antenna arrays work, especially in things like Massive MIMO systems. Using metasurfaces with certain properties allows for better separation and matching of signals, making them perfect for small, tightly packed arrays [90].

The metamaterial decoupling technique offers the significant advantage of achieving higher isolation between adjacent antenna elements compared to traditional methods. It is cost-effective and practical, requiring straightforward configurations that have a negligible impact on the antenna array's physical dimensions, radiation efficiency, gain, and bandwidth. Metamaterial is particularly advantageous in ultra-wideband (UWB) MIMO antennas, synthetic aperture radar (SAR) systems, and compact MIMO arrays that require multiple radiation patterns and polarizations. However, it may require additional surface current suppression to achieve optimal isolation. Careful design is essential to prevent any negative impacts on the MIMO array's radiation characteristics.

Application - Metamaterials effectively decouple closely-spaced antenna elements in MIMO systems, even when the inter-element spacing is less than $0.02\lambda_0$. This method is particularly promising for vast MIMO arrays with dozens or hundreds of elements, capitalizing on the periodic structure of metamaterials. Additionally, metamaterial-based decoupling improves antenna arrays' efficiency, gain, and reduces mutual coupling by leveraging its focusing capabilities [91,92].

Bandwidth - Metamaterial-based decoupling techniques provide wide decoupling and matching bandwidths, eliminating the necessity for supplementary matching measures. Integrating a metamaterial surface can significantly improve antenna arrays' envelope correlation coefficient (ECC), reducing it from 0.25 to below 0.08. This enhancement increases channel capacity and diversity gain. Unlike conventional methods, metamaterial-based decoupling does not jeopardize the

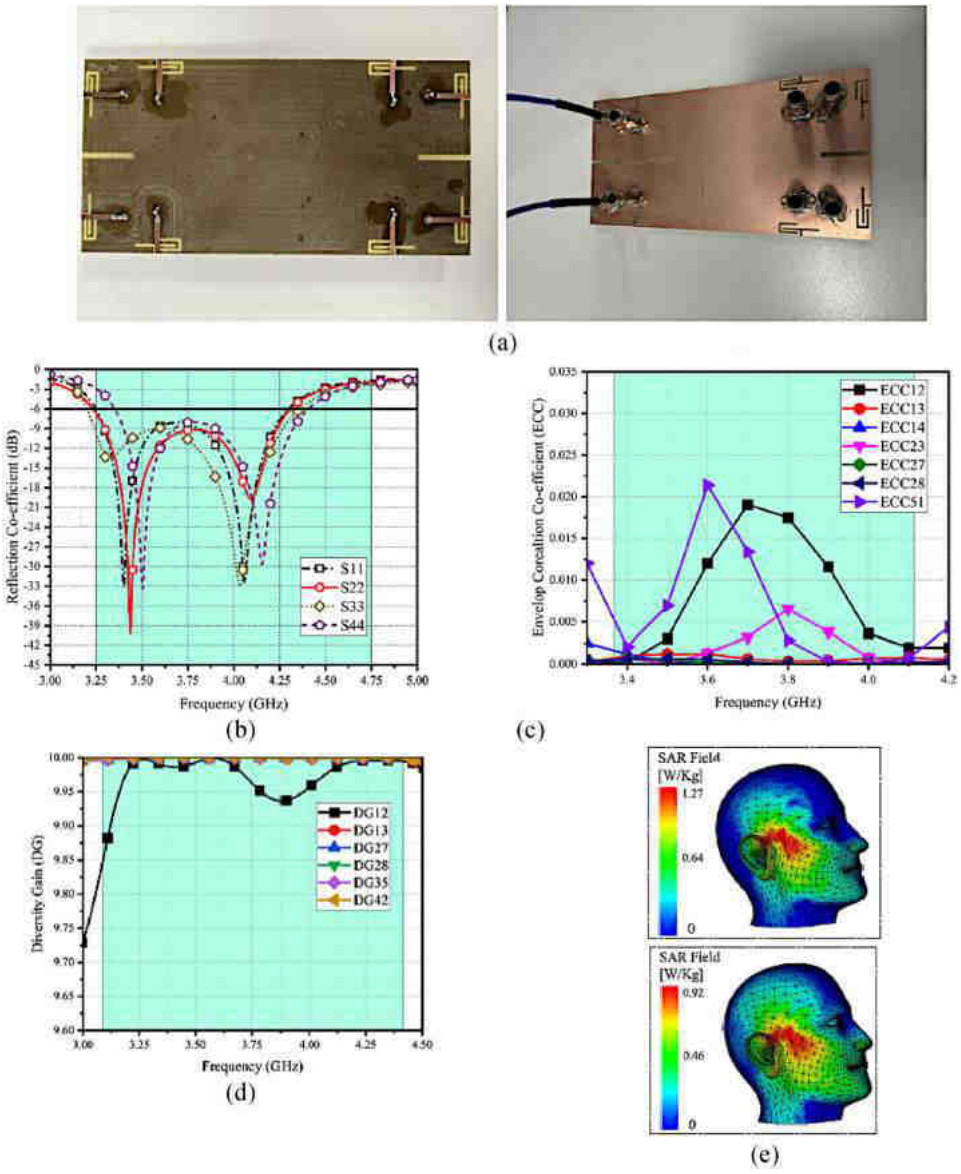

Fig. 15. (a) The geometry of the antenna, (b) Measured reflection coefficient, (c) Measured ECC, (d) Measured DG and (e) Simulated SAR at 3.5 GHz & 4.2 GHz [132].

matching bandwidth; instead, it has the potential to expand it even further [91–93].

4.1.1. Decoupling structure/defected ground structure (DGS)

Ground currents in the antenna arrays are effectively reduced by the periodic or non-periodic etched slots that are positioned properly on the antenna frame. By maximizing efficiency, decreasing mutual coupling, and expanding bandwidth, this technique methodically consolidates slots or openings in the ground plane, improving antenna performance. In a structured manner, the DGS is implemented to serves as a bandstop filter, separating nearby ports and assisting in the accurate adjustment of antenna performance parameters [94]. By incorporating a discrete element or transmission line, the cross-admittance of the decoupling network is optimized. This technique minimizes mutual coupling using a planar decoupling network that simulates a resonator.

Defected Ground Structures (DGS) substantially reduce mutual coupling, thereby improving MIMO performance. They provide design flexibility with various shapes and configurations, enhancing selectivity, gain, and bandwidth, particularly in compact wireless devices. However, designing DGS can be complex, necessitating precise optimization to prevent increased losses and unwanted resonances. While effective in enhancing isolation, their advantages may be restricted in wideband applications unless specifically designed. DGS is advantageous in microwave filters and amplifiers, wireless communication devices, and MIMO antenna arrays, as it regulates objectionable frequencies and reduces interference.

Defected Ground Structure (DGS) and partial ground planes are techniques used to improve antenna performance by altering the ground plane. DGS involves creating specific patterns or defects in the ground plane to enhance bandwidth, improve radiation patterns, and reduce unwanted back lobes. These defects can be shapes like slots or patches and are designed for better efficiency and size reduction, especially in microstrip antennas. On the other hand, a partial ground plane does not cover the entire area beneath the antenna and affects performance by changing impedance and radiation characteristics. This simpler design helps achieve specific bandwidths and gain levels without the intricate modifications of DGS. In summary, DGS uses specific defects for enhanced performance, while a partial ground plane simplifies the design by reducing the ground area.

Application - DGS-based decoupling techniques have proven

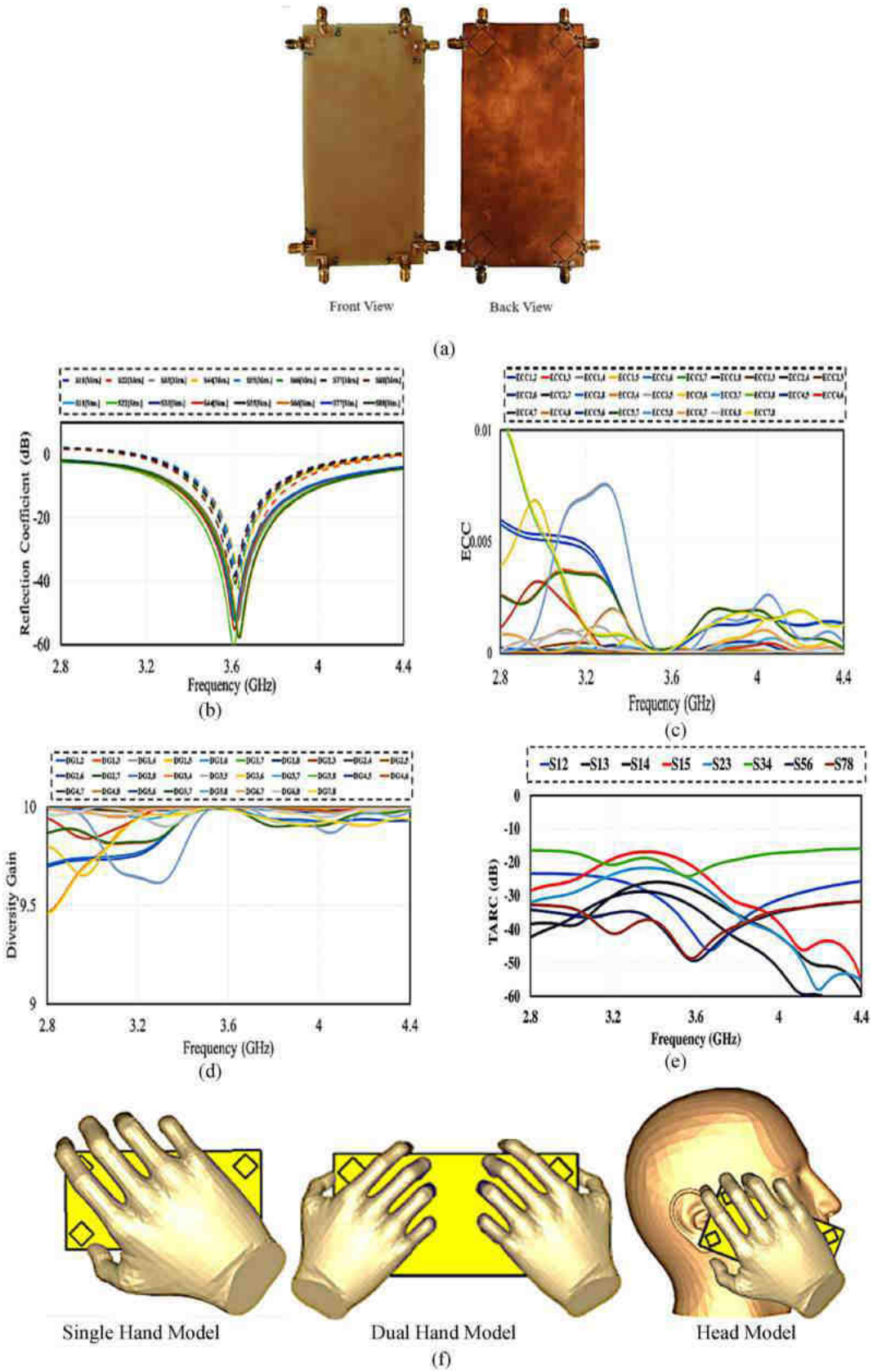

Fig. 16. Provides a comprehensive analysis of the antenna's performance, including multiple critical parameters. It includes: (a) the geometry of the antenna, showing both measured and simulated configurations; (b) the return loss, depicting the antenna's efficiency in reflecting signal power; (c) the Envelope Correlation Coefficient (ECC), indicating the level of correlation between the antenna elements; (d) the Diversity Gain (DG), measuring the improvement in signal reception due to diversity techniques; (e) the Total Active Reflection Coefficient (TARC), representing the overall reflection coefficient when all ports are active; and (f) the simulated Specific Absorption Rate (SAR), assessing the safety of the antenna in terms of electromagnetic exposure to the human body [133].

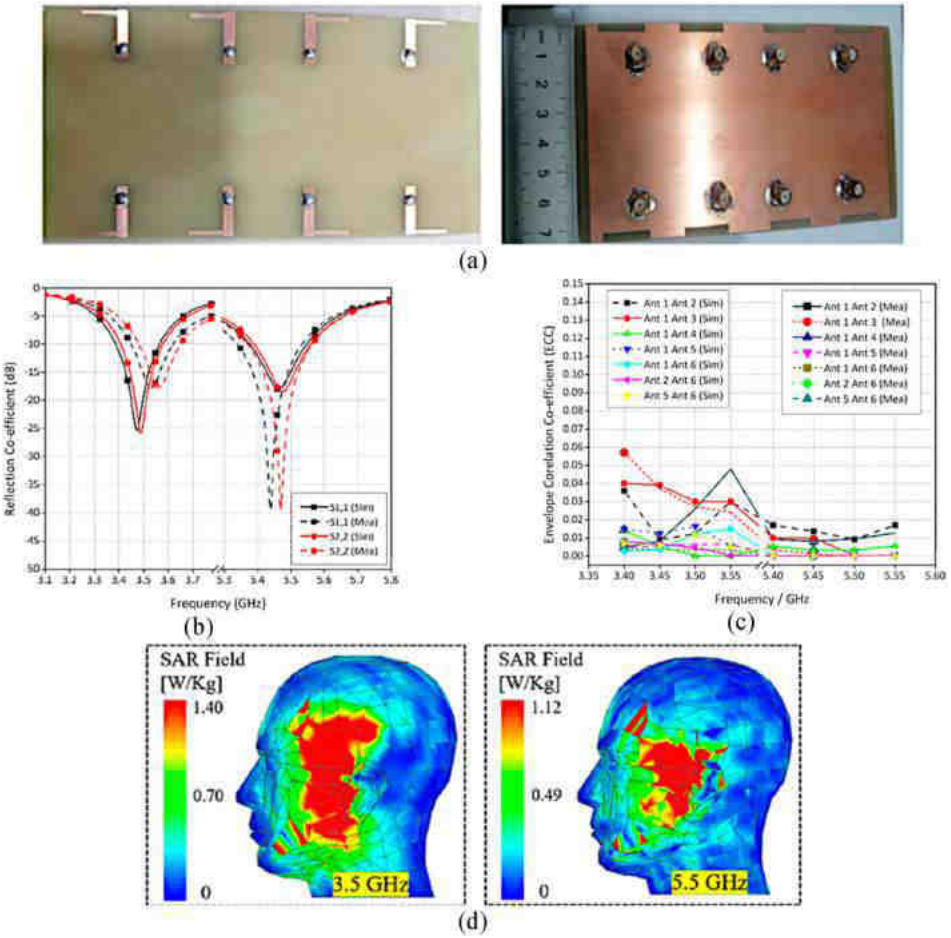

Fig. 17. (a) The geometry of the antenna, Measured and Simulated (b) Reflection coefficient, (c) Envelope correlation coefficients and (d) Simulated SAR [134].

effective across a broad frequency spectrum, ranging from 3 GHz to millimeter-wave frequencies of approximately 60–75 GHz. Various DGS structures, including circular, rectangular, dumbbell-shaped, and zigzag-shaped designs, have been implemented to facilitate MIMO antenna decoupling. Furthermore, DGS can be enhanced by synergistically combining techniques such as electromagnetic bandgap (EBG) structures and grounding branches to further improve overall decoupling performance [95,96].

Bandwidth - Decoupling based on DGS provides a wide decoupling and matching bandwidth, often exceeding 15–20 %. For instance, a rectangular DGS achieved >10.7 dB isolation in the 3.3–3.6 GHz and 4.8–5 GHz bands, while a circular DGS and CSRR provided >15 dB isolation in the 26.5–38.2 GHz band. Integrating DGS with techniques like hybrid EBG can increase the decoupling bandwidth to over 20 %. Importantly, the overall antenna matching bandwidth is not substantially compromised by the additional decoupling structures introduced by DGS [95].

A dual-port MIMO antenna has recently been developed by researchers operating across different frequencies, as evident in Refs. [97–104]. In Ref. [97], researchers describe a two band MIMO antenna that operates between 2 and 3.71 GHz and 5.9 and 7.54 GHz. The antenna has two isolated elements over 20 dB and has a maximal gain of 7.5 dBi. A novel dual-band 28/38 GHz MIMO antenna for 5G mobile applications is introduced in Ref. [98]. This antenna achieves a maximum gain of 7.581 dBi and an approximate 27 dB isolation. According to Ref. [99], an additional 2-element antenna intended for 28 GHz function to obtains a maximal gain of 9 dBi and 71.9 dB isolation. Furthermore, reference [100] introduces a circular patch MIMO antenna that is dual-band reconfigurable and equipped with EBG. This antenna can operate at 3.5 GHz and 5.2 GHz and is designed to serve industrial, scientific, and medicinal applications, as well as 5G. The dual-frequency band 3.5 GHz and 4.85 GHz slot MIMO antenna with dual port, which boasts an isolation of over 30.7 dB, is emphasized in Ref. [101]. A dual-band two-port antenna that operates at 2.32 GHz and 5.2 GHz, with a maximal gain of 1.21 dBi and 46 dB isolation, is described in Ref. [102]. Reference [103] illustrates a UWB antenna that operates within the frequency range of 1.5 GHz–12 GHz and achieves a maximal gain of 4.55 dBi. Finally [104], introduces a compact 28 GHz frequency spectrum antenna with a maximum gain of 4.2 dBi.

Notable studies have been made in the implementation of four-port MIMO antennas, as [105–118] indicates. In Ref. [105], researchers investigate a 4 elments antenna operate at 28 GHz. Additionally [106], introduces a dual-frequency 28/38 GHz MIMO antenna with four elements, achieving isolation greater than 30 dB. A 4-port dual-band 28/37 GHz antenna is reported in Ref. [107] with a maximal gain exceeding 13.7 dBi and more than 30 dB isolation. In Ref. [108], researchers effectively developed a four-patch MIMO antenna that operated at 26 GHz, attaining a predicted gain of 8.72 dBi and an isolation level of 23.2 dB. Reference [109] investigates four-patch MIMO/array antenna operating in ultra-wideband mode from 25 to 50 GHz, achieving high simulated isolation. Reference [110] presents a quad-port antenna designed for a wideband frequency range from 24.8 to 27.6 GHz, demonstrating maximal gain exceeding 9 dBi. Additionally [111], details a four port antenna, providing isolation of around 40 dB and a peak gain of 12 dBi, while [112] introduces a high-gain four elements MIMO antenna functioning at 2.02, 5.87, and 11.19 GHz. In Ref. [113], researchers successfully design a compact four-element dual-band MIMO antenna operating at 2.74 and 5.25 GHz, achieving isolation levels of 34

Table 1
Comparison with related works using DGS structures.

Ref.	Years	Size of MIMO Antenna (mm^3)	No. of Antenna Element	Operating Frequency (GHz)	Efficiency (%)	ECC	Isolation (dB)	Gain	DG (dB)	TARC (dB)	SAR (W/kg)
[97]	2024	126 × 63 × 1.52	2	2.1–3.6, 5.9–7.4	–	0.0002	20	7.5 dBi	9.991	−10	–
[102]	2024	56 × 48 × 1.6	2	2.32 5.2	–	<0.001	−21 −44.84	−1.21 dBi −1.15 dBi	9.99	–	–
[127]	2024	48 × 45 × 1.6	2	5.83	–	0.005	−59	–	9.97	<0.4	–
[100]	2022	26 × 31 × 1.6	2	3.5/5.2	–	0.015	> −25	3.5 dBi	9.992	–	–
[104]	2022	12.8 × 8.1 × 1.6	2	28	–	0.013	−25	4.2 dB	9.99	–	–
[99]	2021	34.7 × 31.1 × 1.31	2	28	81.9	0.00015	32.7	9 dBi	9.99	–	–
[101]	2021	38.6 × 56.4 × 1.524	2	3.5 4.85	–	0.005	29 41.4	2.45 dBi 4.56 dBi	–	–	–
[103]	2021	40 × 36.67 × 1.6	2	1.5–12	–	–	–	4.55 dBi	–	–	0.188 0.070
[98]	2019	55 × 110 × 0.508	2	28 38	89.89 88.25	1.36×10^{-5} 3.86×10^{-5}	−28.32 −26.27	7.88 dBi 9.49 dBi	–	–	–
[115]	2024	46 × 46 × 1.6	4	4.72–5.24	>60	<0.006	–	2.73 dB	10	–	–
[129]	2024	17.76 × 17.76 × 1.52	4	28 38	91	$<3 \times 10^{-5}$	< −39 < −60	9 dBi	9.9998	< −25	0.00684
[106]	2023	60 × 60 × 0.508	4	28 38	99.5 70	<0.0035	>30	8.14 dB 8.04 dB	>9.982		0.702 0.622
[108]	2023	25 × 25 × 0.787	4	26	–	<0.0015	23.2	8.72 dBi	8.3	−26	–
[109]	2023	33 × 33 × 0.233	4	25–50	80–92	<0.005	–	–	10	< −10	–
[112]	2023	78 × 50 × 1.6	4	2.02/5.87/11.19	–	0.05	–	10.03 dBi	10	−14	–
[114]	2023	80 × 0.25 mm^2	4	30	85	–	–	7.5 dBi	10	–	–
[117]	2023	22 × 22 × 0.79	4	28 39	–	<0.001	21.59	5.65 dB 5.53 dB	10	< −10	–
[118]	2023	40 × 40 × 1.6	4	3.33–3.66	–	<0.01	< −17.5	2.045 dB	>9.99	−10	–
[128]	2023	28.3 × 28.3 × 0.787	4	28	96	0.00001	40	11 dBi	9.999	−29	–
[107]	2022	43.611 × 43.611 × 0.4	4	28 38	–	$<2.5\times10^{-4}$	>20 >30	7.9 dB 13.7 dB	$<3.5 \times 10^{-4}$ >10	−15 −14	–
[111]	2022	30 × 35 × 0.787	4	28	85	<0.0003	>40	12 dBi	>9.9	–	–
[113]	2022	60 × 60 × 1.6	4	2.74 5.25	74 75	<0.05	34 26	2.8 dBi 4.91 dBi	–	–	–
[116]	2022	40 × 40 × 1.6	4	3.2–5.75	91	<0.05	22	9 dBi	>9.9	< −30	–
[110]	2021	23.75 × 42.5 × 0.508	4	26	87	<0.002	25	9 dBi	9.9	–	–
[105]	2020	30 × 35 × 0.76	4	28	80	<0.01	17	8.3 dB	>9.96	–	–
[130]	2023	$0.60\,\lambda_0 \times 1.32\lambda_0 \times 0.024\lambda_0$	6	4.8	86	<0.029	< −48.068	6.45 dB	9.89	–	1.167
[120]	2022	71 × 95 × 1.6	6	2.9–11	–	<0.075	>20	8 dBi	10	< −10	–
[119]	2021	134 × 75 × 0.8	6	3–5	86	<0.006	< −15	1.9 dB	10	< −7	<2
[122]	2024	150 × 75 × 0.8	8	3.29–6.61	52.9–85.7	<0.057	>16.6	4.53 dBi	>9.98	6	0.5
[124]	2024	150 × 75 × 0.8	8	3.4–3.6/4.8–5.8	40–60	0.04	18	5.8 dBi	–	–	1.31
[132]	2024	150 × 75 × 0.8	8	3.26–4.48	60–85	<0.03	>14.5	4.8 dBi	>9.95	–	1.27
[123]	2023	150 × 75 × 7	8	3.5/5.5	58–72	<0.024	>15	7.4 dB	9.99	<20	–
[126]	2023	116 × 60 × 6	8	3.45	57.23	0.01	17	3.5 dB	–	–	–
[131]	2023	140 × 70 × 6	8	3.5 5.5	68 78	0.018 0.001	20 23	2.8 dBi 3.2 dBi	9.9 9.9	−11 −18	0.809 1.05
[133]	2023	150 × 75 × 1.6	8	3.3–4.1	80–85	<0.001	>30	4.1 dB	>9.5	< −30	0.4 1.8
[121]	2021	75 × 37.5 × 0.8	8	3.3–5.95	47–78	<0.11	>15	–	–	–	–
[134]	2021	150 × 75 × 1.6	8	3.4–3.6 5.4–5.6	63–69 52–58	<0.1	14	3.1 dBi	–	–	1.4 1.12
[125]	2017	80 × 80 × 0.76	8	2.4	76.1	<0.1	>10	3.09 dBi	–	–	–

ECC - Envelope Correlation Coefficient DG – Diversity GainTARC - Total active reflection coefficientSAR - Specific Absorption Rate.

dB and 26 dB, respectively. Next [114], presents MIMO antenna that operates around 30 GHz four elements and predicted gain greater than 7.5 dBi. In Ref. [115], the author proposed a four rectangular elements antenna for WLAN, Wi-Fi, 5G, and Wi-Max applications, demonstrates a peak gain exceeding 2.73 dB. In Ref. [116], the author details a streamlined four-port MIMO antenna operating across frequencies from 3.2 to 5.75 GHz, providing 22 dB isolation and an average gain of 9 dBi. Reference [117] introduces a four-port MIMO antenna that operates at 28/39 GHz and is dual-band with isolation below 21.59 dB and a peak gain of 5.53 dB. Finally [118], presents an innovative compact vivaldi MIMO antenna with four elements, specifically engineered for 5G wireless devices., achieving a gain of 2.405 dB.

There are several research have been made in the implementation of six-port MIMO antennas as depicted in Refs. [119,120]. In Ref. [119], researchers explain a 6-element MIMO antenna frequency band from 3 to 5 GHz and reach the maximum isolation of 15 dB. In Ref. [120], the author introduced an Ultra-Wideband (UWB) MIMO antenna operating between 2.9 and 11 GHz, demonstrating a maximal gain of over 8 dBi

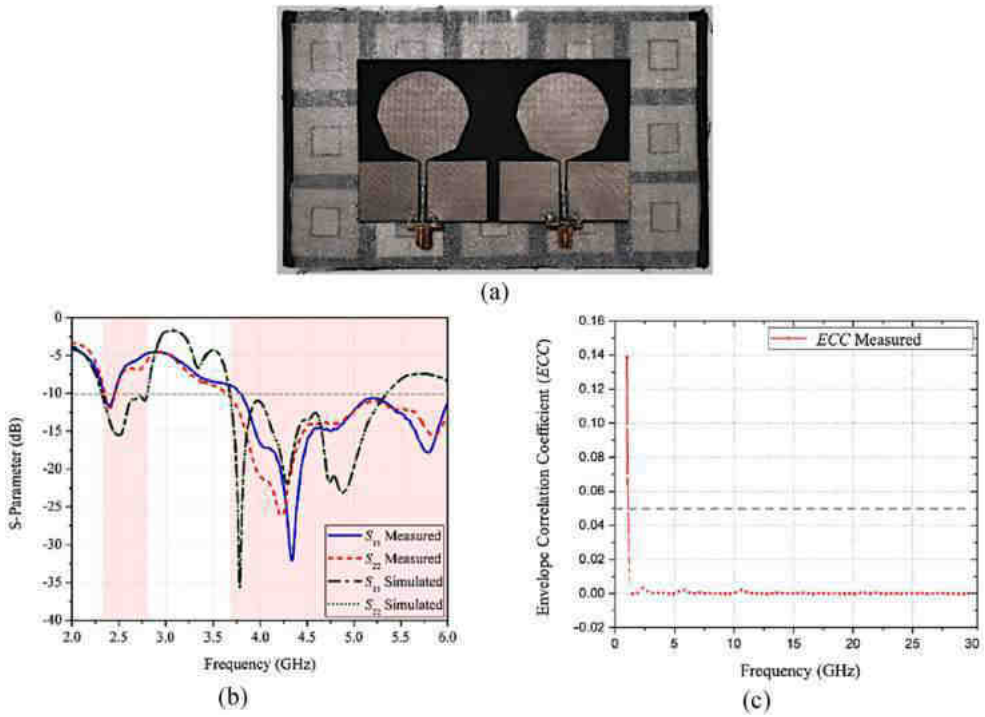

Fig. 18. (a) The antenna's design, (b) The measured reflection coefficient, and (c) The measured envelope correlation coefficients.

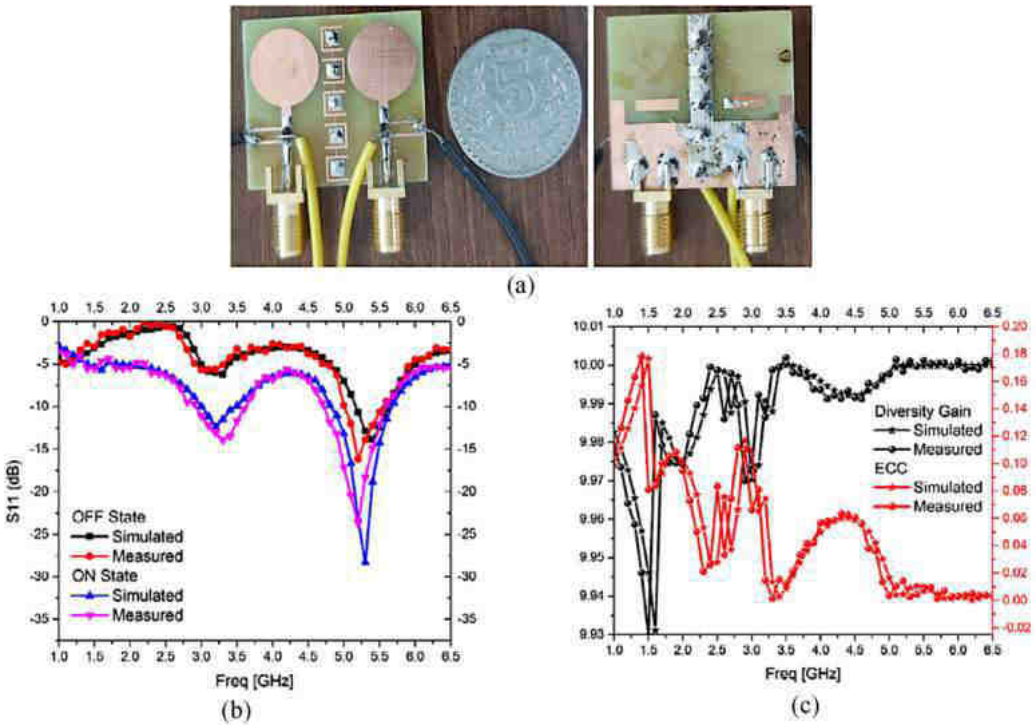

Fig. 19. (a) The geometry of the antenna, (b) Measured reflection coefficient and (c) Measured envelope correlation coefficients and diversity gain.

and an isolation level of approximately 20 dB.

Considerable research endeavors have also been focused on deploying 8-port MIMO antenna as documented in Refs. [121–126]. In Ref. [121], the authors present a MIMO antenna operating at 3.3–5.95 GHz, featuring 8 elements that achieve isolation surpassing 15 dB. Moreover [122], describes a MIMO antenna operating below 7 GHz with 8 ports, utilizing a differential-fed open-end slot antenna (OESA) method, achieving a peak gain exceeding 4.53 dBi. Additionally [123], introduces a dual-band 3.5/5.5 GHz antenna with 8 elements and an isolation of 15 dB. In Ref. [124], researchers have developed a compact eight ports MIMO antenna operating at 3.5 and 5.3 GHz, achieving 18 dB isolation and a peak gain of 5.8 dBi. Furthermore [125], presents a planar 8-port MIMO antenna operating at 2.4 GHz, achieving a maximum gain of 3.09 dBi. Lastly, reference [126] introduces a compact rectangular antenna array operating at 3.45 GHz, enhancing isolation up to 17 dB.

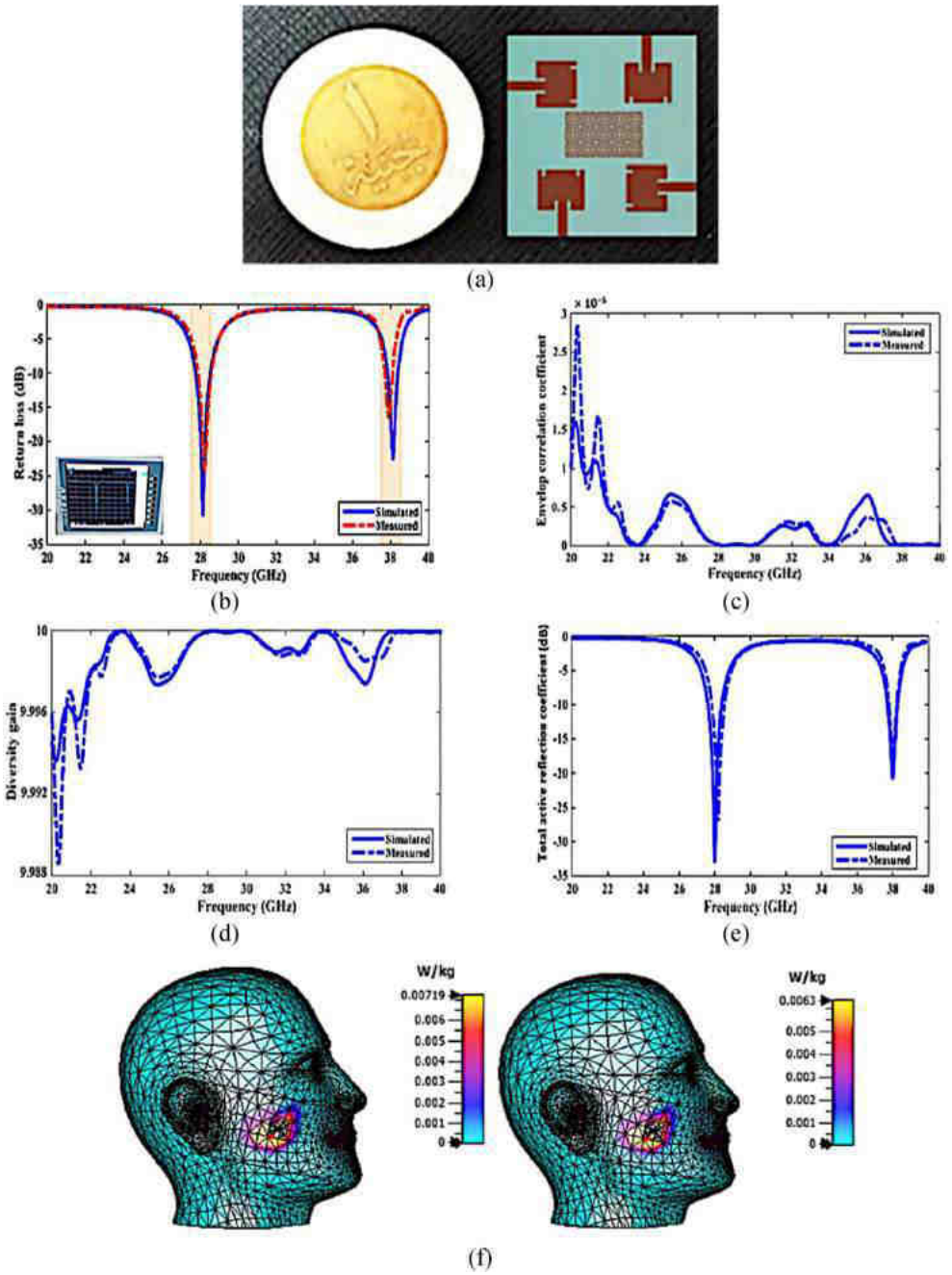

Fig. 20. (a) The geometry of the antenna, Measured and Simulated (b) S-parameter, (c) ECC, (d) DG and (e) TARC and (f) Simulated SAR at 28 GHz & 38 GHz [159].

In [127], Kumar et al. proposed compact, wideband MIMO antenna proposed for S-band applications aims to achieve significant isolation between closely spaced antenna elements. This is achieved through the implementation of a Defected Ground Structure (DGS) technique. To further reduce antenna size and improve isolation, researchers incorporated three rectangular openings and two L-shaped extensions to restrict surface wave propagation. The results, as shown in Fig. 10, are promising: Diversity Gain (DG) exceeds 9.97 dB, Envelope Correlation Coefficient (ECC) is below 0.05, Mean Effective Gain (MEG) is ≤ -3 dB, Total Active Reflection Coefficient (TARC) is below 0.4, and Channel Capacity Loss (CCL) is less than 0.3.

In [128], Ghosh et al. proposed a high-gain, four-port mm-wave broadband MIMO communication solution is designed for 5G applications. The antenna is compact and low-profile, featuring two quarter-wavelength square-shaped CSRRs on the ground plane interconnected via a corporate feed network. Additionally, the design incorporates two rectangular patches. The overall dimensions of the four-port orthogonal MIMO configuration are 28.3 mm $\times$ 28.3 mm $\times$ 0.508 mm. Operating within the 5G frequency range of 26.5 GHz–30.4 GHz, the antenna demonstrates exceptional diversity performance, supported by various metrics including an Envelope Correlation Coefficient (ECC) below 0.0001, DG exceeding 9.999 dB, CCL below 0.12 bits/s/Hz, TARC and MEG are both less than -3 dB, as illustrated in Fig. 11.

In [129], Rania & Ahmed proposed a highly compact, 4-port dual-band MIMO antenna with a defected ground structure (DGS) has been developed. This design effectively minimizes mutual coupling across a wide frequency spectrum. Fabricated on a Rogers TMM4 substrate measuring 17.76 $\times$ 17.76 mm^2, the antenna comprises four planar patch antennas are positioned perpendicularly at the corners. Each

Table 2
A comparative analysis of related works utilizing EBG structures.

Ref.	Years	Size of MIMO Antenna (mm^3)	No. of Antenna Element	Operating Frequency (GHz)	Efficiency (%)	ECC	Isolation (dB)	Gain	DG (dB)	TARC (dB)	SAR (W/kg)
[140]	2024	51 × 30 × 1.6	2	28/38	91	$<1.8 \times 10^{-4}$	90	11.5 dBi	10	< −30	–
[141]	2023	18 × 9.2 × 0.787	2	3.69–10.99	–	–	19	10.4 dBi	–	–	–
[157]	2023	185 × 111 × 4.21	2	2.34–2.46 3.66–6.00	–	<0.5	15	6.59 dBi 11.6 dBi	–	–	0.088 0.07
[158]	2022	31 × 26 × 1.6	2	3.5/5.2	–	–	25	2.51 dBi	10	–	–
[142]	2021	42.2 × 21.6 × 1.6	2	4.2–5.2	–	<0.025	50	–	10	< −10	–
[143]	2021	50 × 50 × 0.8	2	3.05 3.75	–	<0.03	–	–	–	–	–
[144]	2021	26 × 31 × 0.8	2	3.1–11	80	<0.01	>25	5.67 dB	>9.99	–	–
[145]	2021	23 × 18 × 0.35	2	26	61	–	–	8.65 dBi	–	–	0.096 0.32
[146]	2020	38.2 × 95.94 × 1.6	2	2.43–2.5	58.53	0.0087	24.67	4.68 dBi	9.995	–	–
[147]	2020	70 × 40 × 3	2	3.25	–	–	–	4.9 dBi	–	–	–
[148]	2020	50 × 50 × 1.6	2	2–11	–	<0.01	25	5.5 dBi	10	< −10	–
[149]	2019	95 × 49.7 × 1.6	2	3.45	–	<0.03	>26	4.83 dBi	>9.8	–	–
[159]	2024	17.76 × 17.76 × 1.52	4	28 38	93	$<3 \times 10^{-5}$	68 90	8.9 dBi	10	< −30	0.00576 0.00332
[150]	2024	64 × 64 × 1.6	4	3.5/4.65	63	0.01	42	5.6 dBi	–	–	0.94
[151]	2023	–	4	4.2	95	–	50	–	–	–	–
[152]	2023	48 × 48 × 1.6	4	3.3–3.7	77	0.0002	10.5	–	>9.99	<0.29	–
[153]	2022	40 × 40 × 1.6	4	3.2–5.75	91	<0.05	22	9 dBi	>9.9	< −20	–
[154]	2021	145 × 75 × 0.51	4	2.81–7.23	96	<0.0029	21.1	6.59 dBi	9.9853	–	0.887641
[155]	2022	134 × 75 × 0.8	6	3–5	86	<0.005	20	–	10	< −8	0.6
[156]	2023	27.2 × 27.2 × 1.6	8	21–34	–	<0.36	28	17 dB	9.9	−27.5	–

antenna operates at 28/38 GHz and incorporates four rectangular slots and a full ground plane. The patches are spaced 0.5 λo apart. The DGS further minimizes mutual coupling. Both simulations and measurements demonstrate a notable reduction in mutual coupling (−39 to −60 dB), enhancing ECC, TARC, MEG, and DG performance as depicted in Fig. 12.

In [130], Akhilesh et al. proposed a six-port MIMO antenna that is intended for mid-band operation at a resonant frequency of 4.8 GHz has dimensions of 0.60 $\lambda_0 \times 1.32\lambda_0 \times 0.024\lambda_0$, where λ_0 denotes the free space wavelength at 4.8 GHz. The antenna includes design elements such as a circular cutting ground plane, inset feeding, a slotted partial ring ground, a planar rectangular patch, and six-port electromagnetic wave components. To enhance isolation, I-shaped stumps and a slotted ring ground have been integrated. The antenna achieves an impedance bandwidth of −10 dB from 3.92 GHz to 5.2 GHz and exhibits isolation levels exceeding 15 dB between all terminals. Fig. 13 illustrates the performance metrics, including a peak gain of 6.45 dB, radiation efficiency of 86 %, envelope correlation coefficients below 0.002, diversity gain of 9.98, channel capacity loss below 0.014 bits/sec/Hz, and branch power ratio less than −1 dB.

In [101], Khan et al. introduced a dual-band 8 × 8 MIMO antenna designed to operate at 3.5 GHz and 5.5 GHz frequencies for 5G smartphone applications. A modified F-shaped radiator is present in each antenna element, positioned at the edge of a smartphone PCB measuring 140 × 70 mm^2. The dimensions of each element are 4.5 × 11 mm^2 ($0.05\lambda_o \times 0.16\lambda_o$, with λ_o being the free-space wavelength at 3.5 GHz). The design achieves mutual couplings below −20 dB at the lower band and −22 dB at the higher band. The envelope correlation coefficient for all antenna elements is under 0.11 as presented in Fig. 14.

In [132], Kiani et al. proposed an eight-element slotted wideband MIMO antenna system is designed specifically for the N77 (3.2–4.2 GHz) frequency band. Printed on a 0.8-mm-thick FR-4 substrate measuring 150 × 75 mm^2, these MIMO antennas enhance signal reception by providing pattern and polarization diversity across multiple device orientations. Utilizing an inverted C-slotted stub and a T-slot enables wideband coverage from 3.25 to 4.49 GHz. The antennas exhibit radiation and total efficiencies exceeding 60 % for all elements. To enhance isolation between elements positioned along the width of the PCB, a slit is implemented, achieving 14.5 dB isolation. This results in a diversity gain (DG) exceeding 9.95 dB and an envelope correlation coefficient (ECC) below 0.025. Compliance with safety standards is confirmed through SAR analysis when the antenna system is used near humans, as depicted in Fig. 15.

In [133], Yasir et al. proposed a high-performance, dual-polarized, eight-element MIMO antenna has been developed for 5G smartphones, incorporating four dual-polarized microstrip diamond-ring slot antennas positioned at the corners of the PCB. The use of a defected ground structure offers advantages such as simplified fabrication, compact dimensions, and improved efficiency compared to other techniques. The design achieves MC of less than 30 dB and an impedance bandwidth of −10 dB spanning 700 MHz for all radiating elements, covering frequencies from 3.3 GHz to 4.1 GHz. Each dual-polarized element attains an average gain of over 3.8 dBi and an average radiation efficiency of over 80 %. The antenna provides complete radiation coverage on all sides. Key MIMO antenna characteristics such as DG, ECC, TARC, and channel capacity have been calculated and meet the required standards, as depicted in Fig. 16.

In [134], Haider et al. proposed a new dual-band antenna has been developed for operation within 5G frequency ranges. The antenna integrates inverted L-shaped sensors and a rectangular defected ground structure, effectively covering the 3.4–3.6 GHz and 5.4–5.6 GHz bands.

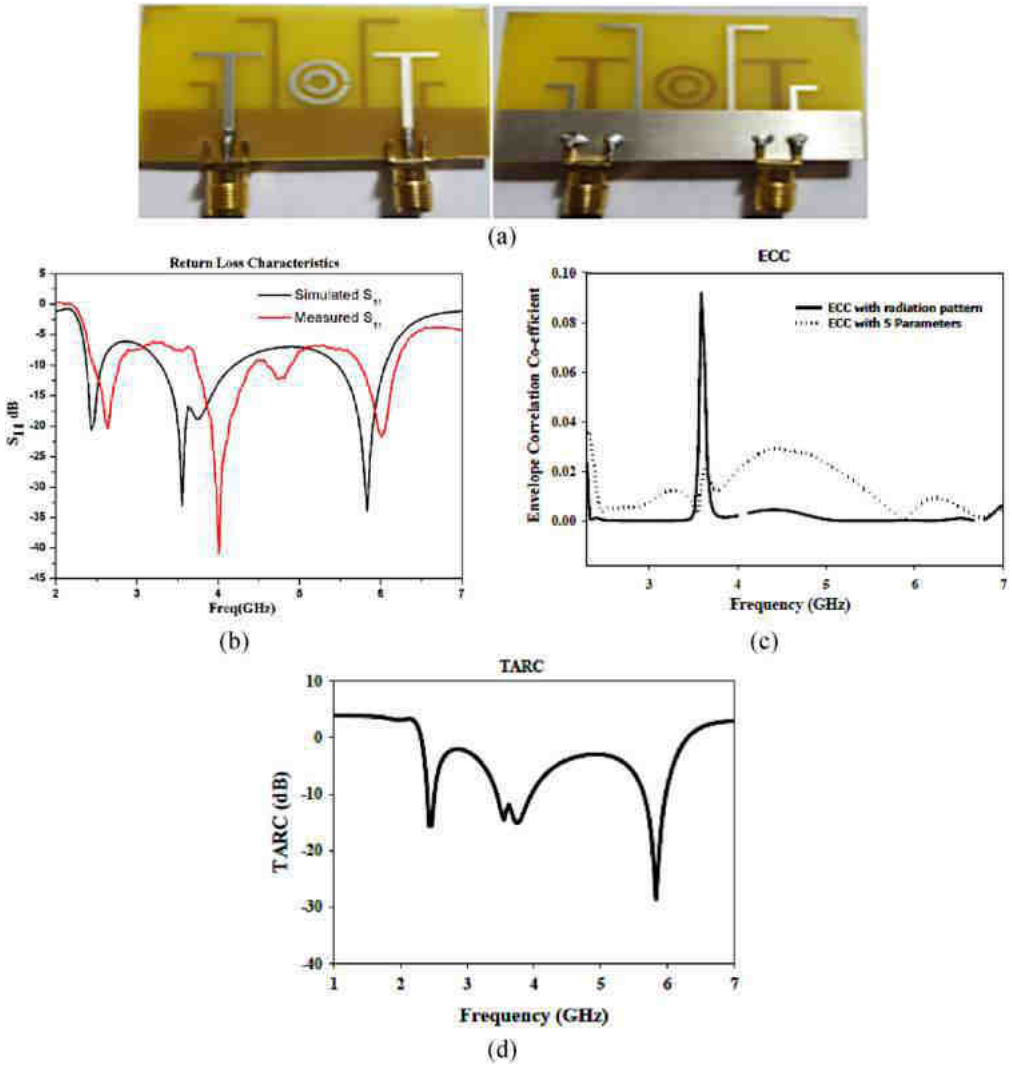

Fig. 21. (a) The geometry of the antenna, (b) Measured and simulated S11, (c) Measured envelope correlation coefficients and (d) Calculated TARC [177].

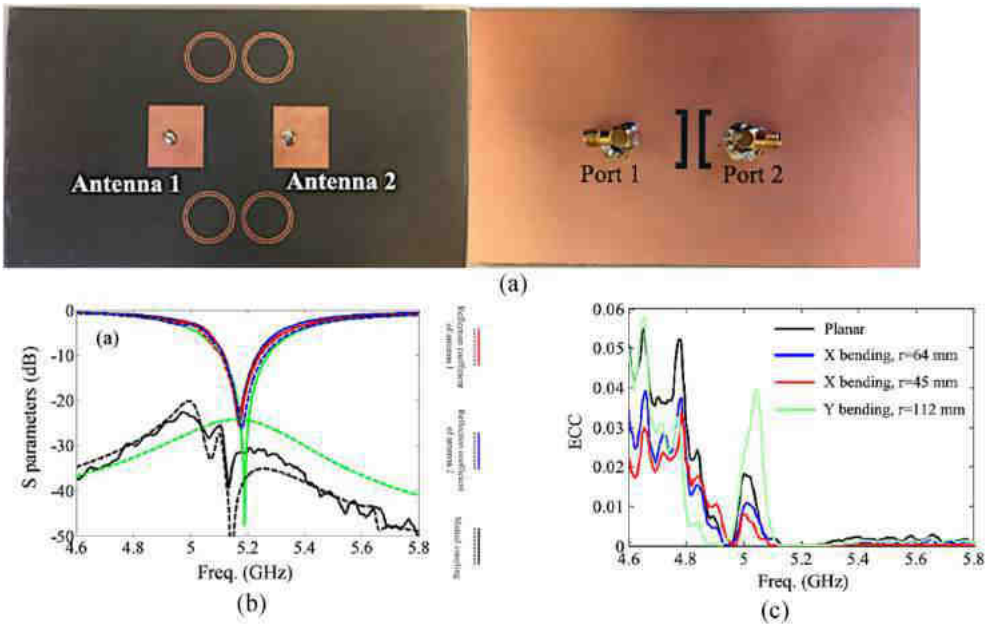

Fig. 22. (a) The geometry of the antenna, (b) Measured and simulated reflection coefficient and (c) Measured envelope correlation coefficients [178].

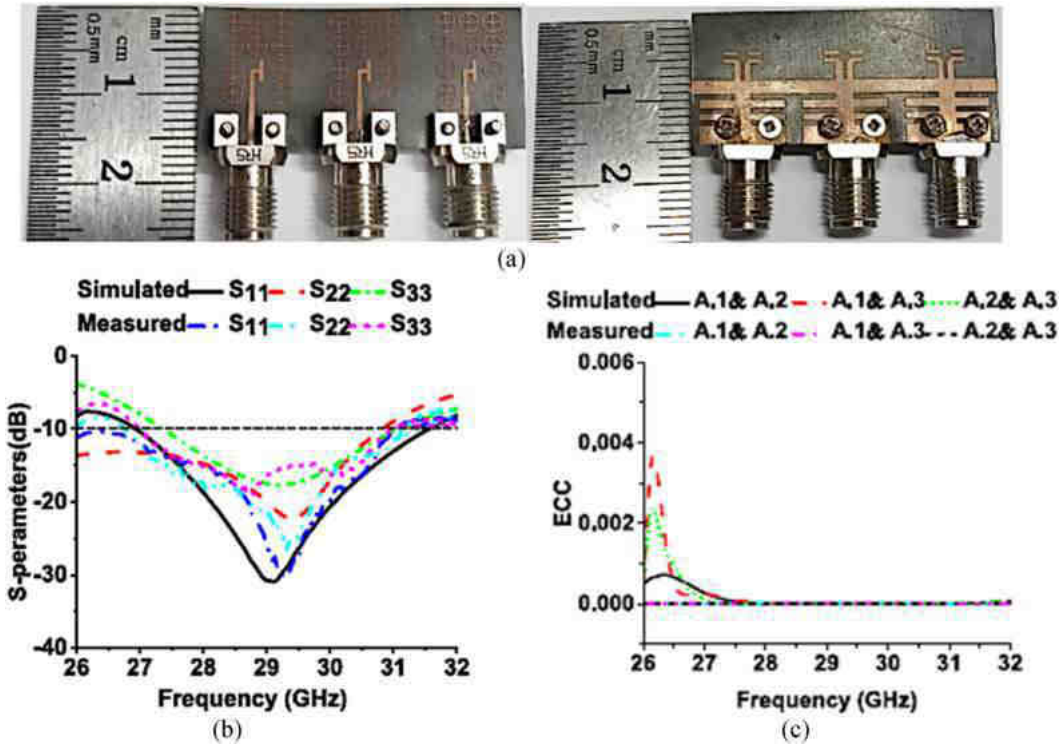

Fig. 23. (a) The antenna's geometry, (b) Simulated and measured return loss, and (c) Simulated and measured envelope correlation coefficients [144].

In the proposed MIMO system, the antenna achieves a maximum gain of 3.1 dBi and efficiency ranging from 52 % to 69 %. The system ensures a minimum isolation of 13 dB and an envelope correlation coefficient (ECC) of less than 0.05 between radiating elements. Furthermore, the channel capacity is 38 and 39.5 at both resonant bands with a 20 dB signal-to-noise ratio (SNR), and the mean practical gains and diversity meet acceptable parameters. The radiation characteristics demonstrate exceptional diversity performance, and SAR values confirm user safety, as depicted in Fig. 17.

Table 1 compares MIMO antennas with DGS structures, highlighting their size diversity ranging from 17.76 × 17.76 mm^2 to 150 × 75 mm^2, element counts of 2–8, and operating frequencies from 2 GHz to over 11 GHz. They typically exhibit low ECC below 0.01, high efficiencies up to 91 %, isolation above 15 dB, gains up to 8.72 dBi, negative TARC indicating good performance, and a consistent DG around 10 dB. SAR values are within safety limits, with figures like 0.702 W/kg. However, challenges include missing SAR and efficiency data, along with gaps in ECC and isolation metrics, which complicate consistent safety and performance assessments. Variability in gain and operating frequencies impacts design consistency and application versatility, while differences in size and element counts further complicate direct comparisons.

4.1.2. Electromagnetic band gap (EBG)

In the field of antenna engineering, EBG structures are essential for decreasing the amount of surface waves and optimizing antenna performance. Periodic structures known as Electromagnetic Band Gap (EBG) structures feature a band gap that prevents the propagation of electromagnetic radiation within a specific frequency range. Higher antenna effectiveness and gain can be achieved by utilizing them as ground planes or reflectors to reduce surface waves. To achieve optimal performance, it is essential to ensure that the EBG unit cell parameters and the spacing between the antenna and EBG are designed correctly. EBGs enable antennas to be positioned closer to the ground plane to facilitate more compact designs. However, designing EBGs with practical capacities for lower microwave frequencies and achieving wideband performance continues to take work [135–137].

The ability of Electromagnetic Bandgap (EBG) structures to achieve high isolation levels, frequently exceeding 25 dB, is a significant advantage. This capability reduces interference and improves overall performance. Additionally, EBG structures can enhance radiation patterns and be customized in size and shape to suit specific applications, making them suitable for compact devices such as smartphones and IoT products. However, developing effective EBG structures can be time-consuming and complex, with the potential for increased losses and bandwidth limitations. EBG is especially advantageous in MIMO systems, wireless communication devices, medical imaging, and satellite communication, where high isolation and reliable performance are crucial.

Application - EBG-based decoupling techniques have been implemented across a wide frequency range, from sub-6 GHz to millimeter-wave frequencies, typically ranging from 28 to 38 GHz. Various EBG designs such as mushroom-type, corrugated, and strip-type have been employed for MIMO antenna decoupling. Additionally, EBG can complement other techniques like defected ground structures (DGS) to enhance overall decoupling performance [95,138,139].

Bandwidth - The decoupling and matching bandwidths of EBG-based techniques typically exceed 15–20 %. For example, a mushroom-type EBG achieved >10 dB isolation across the 3.3–3.6 GHz and 4.8–5 GHz ranges, while combining EBG with DGS demonstrated >20 dB isolation in the 4.5–8 GHz range. Optimizing the size and number of EBG unit cells allows precise control over the decoupling bandwidth. Importantly, integrating the EBG structure does not significantly reduce the overall antenna matching bandwidth, which is crucial [95,138].

Recent research has focused on a dual-port MIMO antenna designed to operate across multiple frequencies, as indicated by a series of studies [140–149]. A high-isolation Orthogonal Printed Elliptical Slot Antenna (OPESA) array with MIMO is introduced in a study [140]. This antenna has a maximal gain exceeding 11.51 dBi and an isolation level of approximately 90 dB. A planar MIMO antenna using a modified EBG structure to increase bandwidth is presented in another study [141], which achieves a maximal gain of 10.4 dBi. Furthermore, researchers [142] have developed a MIMO CPW-Fed slot antenna for sub-6 GHz 5G

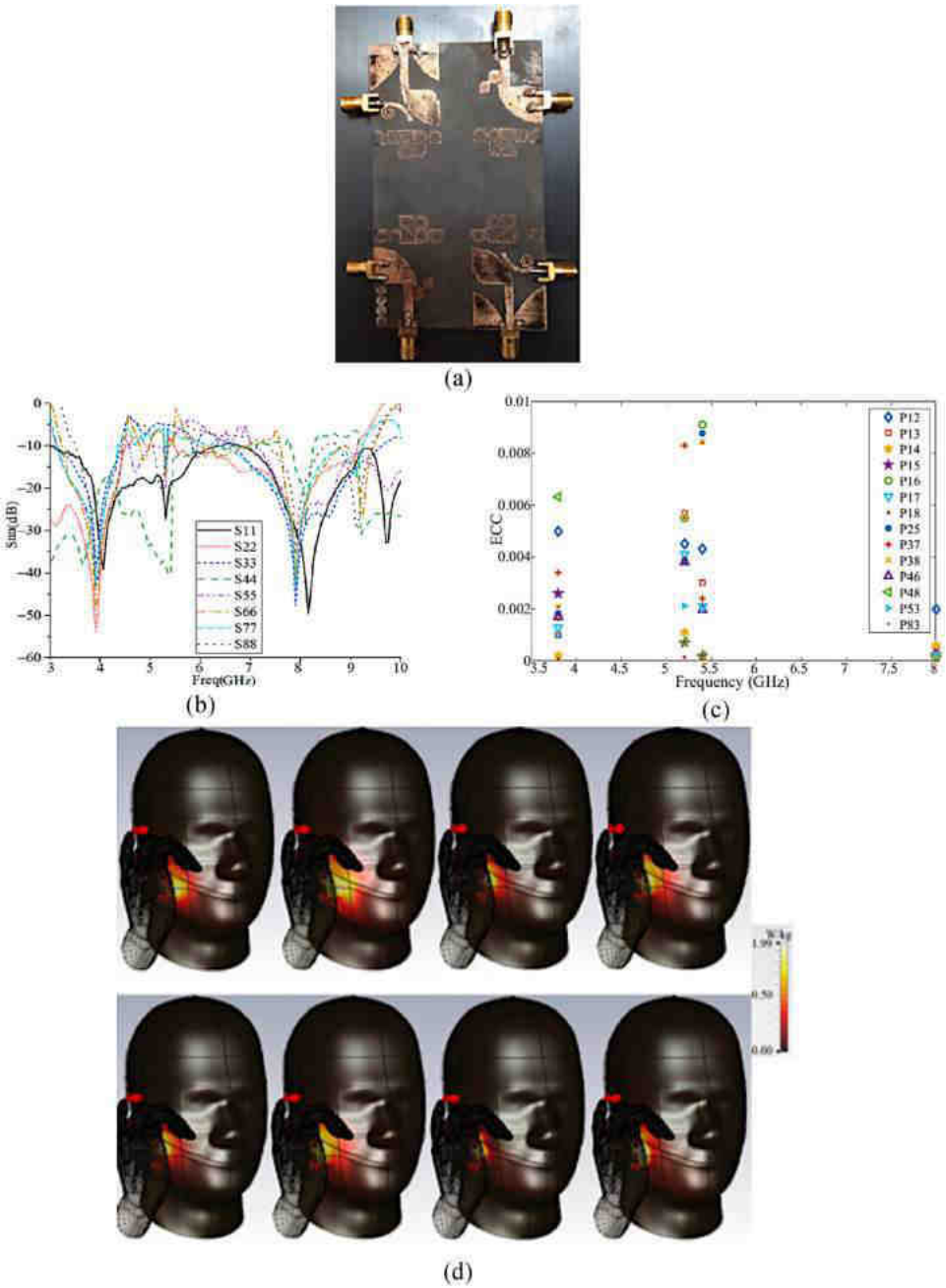

Fig. 24. (a) The geometry of the antenna, (b) Measured S11, (c) Measured envelope correlation coefficients and (d) Simulated SAR [179].

applications that achieves an isolation level of 50 dB. Next, a study [143] describes a novel variable band gap center frequency and dual band gap stacked electromagnetic band gap structure for MIMO antenna system that achieves an isolation of over 16.16 dB. Another innovative design [144] demonstrates a 25 dB isolation and includes a compact, uni-planer wide band MIMO antenna. In addition, a 5G MIMO antenna [145] that operates at 26 GHz is described, boasting a maximal gain of 8.65 dBi. A compact and high-isolation MIMO antenna system demonstrates a maximal gain of 4.68 dBi and an isolation of 24.67 dB discuss in Ref. [146] that operate at 2.43–2.5 GHz. Consequently, a MIMO antenna [147] that operates at a frequency of approximately 3.25 GHz generates a gain that surpasses 4.9 dBi. In another study [148], a cognitive radio (CR) based MIMO antenna is engineered to operate at 2–11 GHz, resulting in a 25 dB isolation level. Lastly, a wideband circularly polarized (CP) MIMO dielectric resonator antenna [149] that operates at 3.3–3.8 GHz based on a two-element MIMO antenna boasts a maximal gain of 4.83 dBi.

As demonstrated by numerous studies [150–154], significant research has been focused on the development of four-port MIMO antennas. A reconfigurable Multiple-Input Multiple-Output (MIMO) antenna array optimized for 5G portable devices is proposed in one investigation [150]. Another study focuses on a MIMO antenna with four elements and more than 50 dB isolation [151]. Additionally, a report details a compact four-port MIMO antenna featuring a G slot, achieving a peak gain exceeding 2.5 dB and an isolation exceeding 10.5 dB [152]. Researchers in a separate study have developed a compact four-port MIMO antenna operating from 3.2 to 5.75 GHz, with a gain of 9 dBi and isolation of 65 dB [153]. Finally, a four port MIMO antenna specifically designed for 5G devices operates within a wideband frequency range of 2.81–7.23 GHz, achieving a peak gain exceeding 6.59 dBi and an isolation level of approximately 21.1 dB [154].

There are also researches on six and eight port MIMO antenna. For

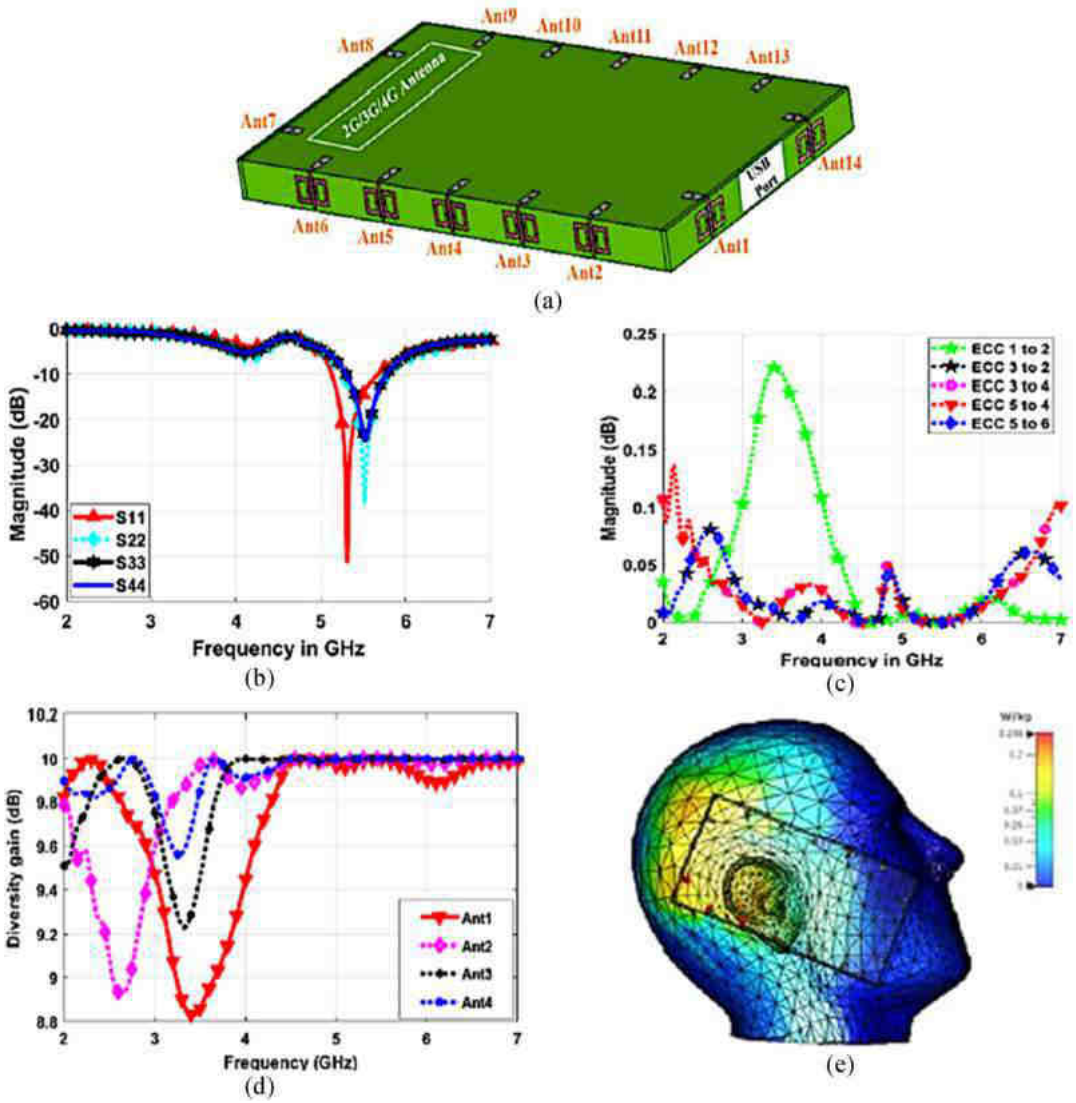

Fig. 25. (a) The geometry of the antenna, (b) Simulated return loss, (c) Simulated ECC, (d) Simulated DG and (e) Simulated SAR [180].

six port, reference [155] presents a novel EBG structure MIMO antenna with an isolation level of 28 dB. Lastly, reference [156] presents a compact MIMO antenna with high gain achieves a peak gain of 2.73 dBi and an isolation level of 20 dB.

In [157], Kumkhet et al. proposed a wearable ultra-wideband MIMO antenna, crafted from conductor and polyester fiber fabrics, measures $115 \times 70\ mm^2$. Its flexibility allows installation on curved surfaces. With a frequency range from 2 GHz to 30 GHz, it offers an average gain of 3.75 dBi and a correlation coefficient of 0.5, suitable for 5G (2.6 GHz and 26 GHz) and WBAN (2.4 GHz, 5.2 GHz, and 3.1 GHz–10.6 GHz) applications. Researchers developed an electromagnetic band gap (EBG) structure, reducing specific absorption rates (SAR) to 0.088 W/kg at 2.4 GHz and 0.070 W/kg at 5.2 GHz. This design, with gains of 6.59 dBi and 11.6 dBi respectively, exceeds the conventional SAR limit of 2.0 W/kg at 10 g as shown in Fig. 18.

In [158], Nikam et al. presented a dual-band multiple-input-multiple-output (MIMO) antenna (RDMA) that can be reconfigured has been created for fifth-generation (5G) networks. This antenna operates at 3.5 GHz and in the industrial, scientific, and medical (ISM) bands at 5.2 GHz. In order to facilitate dual-band functionality, this antenna implements the partial ground plane DGS technique and pin diode integrated branch lines. By modifying the design parameters of the DGS and BLs, the antenna can be tailored to operate at alternative frequencies. Reconfigurable antennas offer several key advantages, including the ability to switch between multiple frequency bands, adjust their radiation patterns dynamically, and adapt their polarization, making them suitable for various wireless applications and reducing the need for multiple antennas in a device. As wireless technologies evolve, reconfigurable antennas can be adapted to meet new requirements, making them suitable for emerging applications in areas like IoT and 5G. Furthermore, a dispersion diagram has been employed to design and characterise a novel dual-band electronics bandgap structure inspired by mushrooms. As illustrated in Fig. 19, to obtain isolation greater than −25 dB between closely spaced antenna elements (at λ5G/17.14), this EBG structure is positioned between RDMA elements.

In [159], Elabd and Ahmed presented a metamaterial-inspired EBG approach is integrated into a highly compact 4-port dual-band MIMO antenna. This innovative design effectively reduces MC across a wide frequency range. The antenna measures $17.76 \times 17.76\ mm^2$ and is fabricated on a Rogers TMM4 substrate. Each antenna element features a rectangular patch with four slots and a complete ground plane, operating in multi band mode at 28/38 GHz. An EBG structure is placed to further minimize MC between elements, with a spacing of 0.5λo. This enhancement significantly improves metrics such as ECC, TARC, MEG, and DG. The antenna's radiation efficiency is validated through comprehensive time-domain analysis. Furthermore, Fig. 20 illustrates

Table 3
A comparative review of related studies using SRR structures.

Ref.	Years	Size of MIMO Antenna (mm^3)	No. of Antenna Element	Operating Frequency (GHz)	Efficiency (%)	ECC	Isolation (dB)	Gain	DG (dB)	TARC (dB)	SAR (W/kg)
[166]	2024	10 × 5 × 0.4	2	23.2–30.64 37.5–43.75	>89	<0.01	>20	6.97 dB	9.999	–	–
[167]	2024	18 × 9.2 × 0.787	2	28 38	–	0.0001	30 28	7.8 dB 6 dB	9.99	–	–
[177]	2024	50 × 30 × 0.8	2	2.4 3.5 5.8	–	<0.01	25 18 32	1.02 dB 1.89 dB 1.43 dB	–	< −10	–
[168]	2023	18 × 38 × 0.8	2	28	88	<0.005	64	8.75 dB	>9.9	<0.4	0.409
[169]	2023	26 × 14.5 × 0.508	2	28 38	–	0.0001	−39 −38	5.2 dB 5.5 dB	9.99	−22	–
[170]	2021	50 × 40 × 1.6	2	3.4–3.8	–	–	>18	4.1 dB	–	–	–
[171]	2021	48 × 35 × 1.6	2	2–18	89	<0.07	27	8 dBi	>9	–	–
[178]	2020	150 × 85 × 1.57	2	5.2	95	<0.06	30	7 dBi	–	–	1.07
[172]	2023	70 × 70 × 1.6	4	2.5, 3.3, 3.5, 4.7, 5.2	–	<0.5	>28	1.74 dB	10	< −10	–
[173]	2022	42 × 42 × 0.787	4	2.5–4	–	0.03	38	2.2 dB	–	< −10	–
[174]	2021	40 × 40 × 1.6	4	2.4	–	–	14	–	–	–	–
[175]	2023	12 × 45.6 × 0.254	8	25–29.5	75	–	−20	20.5 dBi	0.9999	–	–
[176]	2023	150 × 75 × 7	8	3.3–5	40–82	<0.12	>12	6 dB	–	–	–
[145]	2021	100 × 60 × 0.254	8	3.8 5.2 8	94	0.009	<40	13.5 dBi	–	–	0.391 1.121 1.991
[180]	2024	150 × 80 × 7.5	14	5.2–5.8	70–90	<0.01	–	–	10	–	<0.288

the antenna's suitability for 5G cellular devices, confirmed by specific absorption rate (SAR) analysis.

Table 2 summarizes the comparison of MIMO antennas using EBG structures. Antennas vary in size from 18 × 9.2 × 0.787 $mm^3/\mu m^2$ to 185 × 111 × 4.21 $mm^3/\mu m^2$, with 2–8 elements operating from 2.34 GHz to 21.34 GHz. Efficiency ranges from 53 % to 95 %, and ECC is predominantly below 0.05, with isolation often exceeding 15 dB (up to 50 dB). Gains range from 2.51 dBi to 17.9 dBi, and Diversity Gain (DG) is typically around 10 dB. TARC values are negative, indicating good performance, and SAR values are mostly within safety limits, e.g., 0.088 and 0.94 W/kg. Challenges include missing SAR data critical for safety assessments, varying ECC and isolation metrics hindering interference comparisons, and inconsistent performance across designs due to frequency range limitations.

4.1.3. Split ring resonator (SRR)/complementary SRR

Split Ring Resonators (SRRs) are essential components of antenna engineering, as they enable the development of practical yet compact antenna configurations. By generating a resonant effect, they facilitate precise frequency calibration and increase the performance of the antenna. SRRs find applications in various antenna designs due to their magnetic resonance properties and unique interaction with electromagnetic radiation. Fabrication is typically completed using printed circuit board methodologies, and critical design considerations include parameters such as ring width, gap size, and substrate material selection. In scenarios where spatial constraints are present, the utilization of SRRs results in antennas distinguished by their expanded multiband capabilities, improved operational performance, and reduced footprint. This is an invaluable quality. Nevertheless, the resonant frequency may exhibit sensitivity to environmental factors, and their design intricacies and fabrication procedures can present challenges [160–163].

One of the primary advantages of SRRs is their ability to provide substantial isolation between closely spaced antennas, which is crucial for reducing mutual coupling and improving MIMO system efficiency. They can also be tailored to specific frequencies, allowing for customized performance across various applications, and can be integrated into compact designs without significantly enlarging the footprint. However, SRR technology has some drawbacks. The design and production of SRRs can be complex and require precise manufacturing techniques, such as laser cutting or CNC machining, which may lead to higher production costs and longer lead times. Additionally, while SRRs offer excellent isolation, their effectiveness may be limited to certain frequency bands, which can restrict their use in wideband applications. SRRs are particularly advantageous in wireless communication systems, where they enhance signal integrity and reduce interference, thereby improving overall antenna performance.

Application - To optimize wireless communication performance across a broad frequency spectrum, from sub-6 GHz to millimeter-wave frequencies (28–38 GHz), employing SRR and CSRR decoupling techniques is essential. These techniques reduce mutual coupling between closely spaced antenna elements in MIMO systems. In MIMO antennas, these structures are widely applied, achieving mutual coupling of less than −18 dB across frequencies such as 2.4/5.8 GHz WLAN, LTE, and 3.5 GHz 5G. Additionally, SRR structures enable the development of compact antenna designs without compromising performance, exemplified by a symmetrical antenna operating at 5.0 GHz with −27 dB return loss [164,165].

Bandwidth - SRR and CSRR structures provide wide decoupling bandwidths, often exceeding 15–20 %. For example, in the 4.5–8 GHz range, a combination of SRR and CSRR achieved over 20 dB isolation. Importantly, integrating SRR and CSRR structures does not compromise the overall antenna matching bandwidth, crucial for maintaining antenna performance across a wide frequency range [164,165].

In recent times, researchers have developed a two elements MIMO antenna capable of operating across various frequencies, as evidenced in Refs. [166–171]. Reference [166] illustrates a multi-band MIMO antenna operating within the frequency ranges of 23.2–30.64 GHz and 37.5–43.75 GHz. The antenna features two elements with isolation levels exceeding 20 dB. In Ref. [167], the author details a two band 5G MIMO antenna operates at 28 and 38 GHz, achieving a peak gain of 7.8 dB and 30 dB isolation. Reference [168] describes a two-port MIMO antenna system operating within the 27–29 GHz frequency band. Reference [169] introduces a dual-band MIMO antenna with high isolation for 5G millimeter-wave networks, achieving a maximum gain

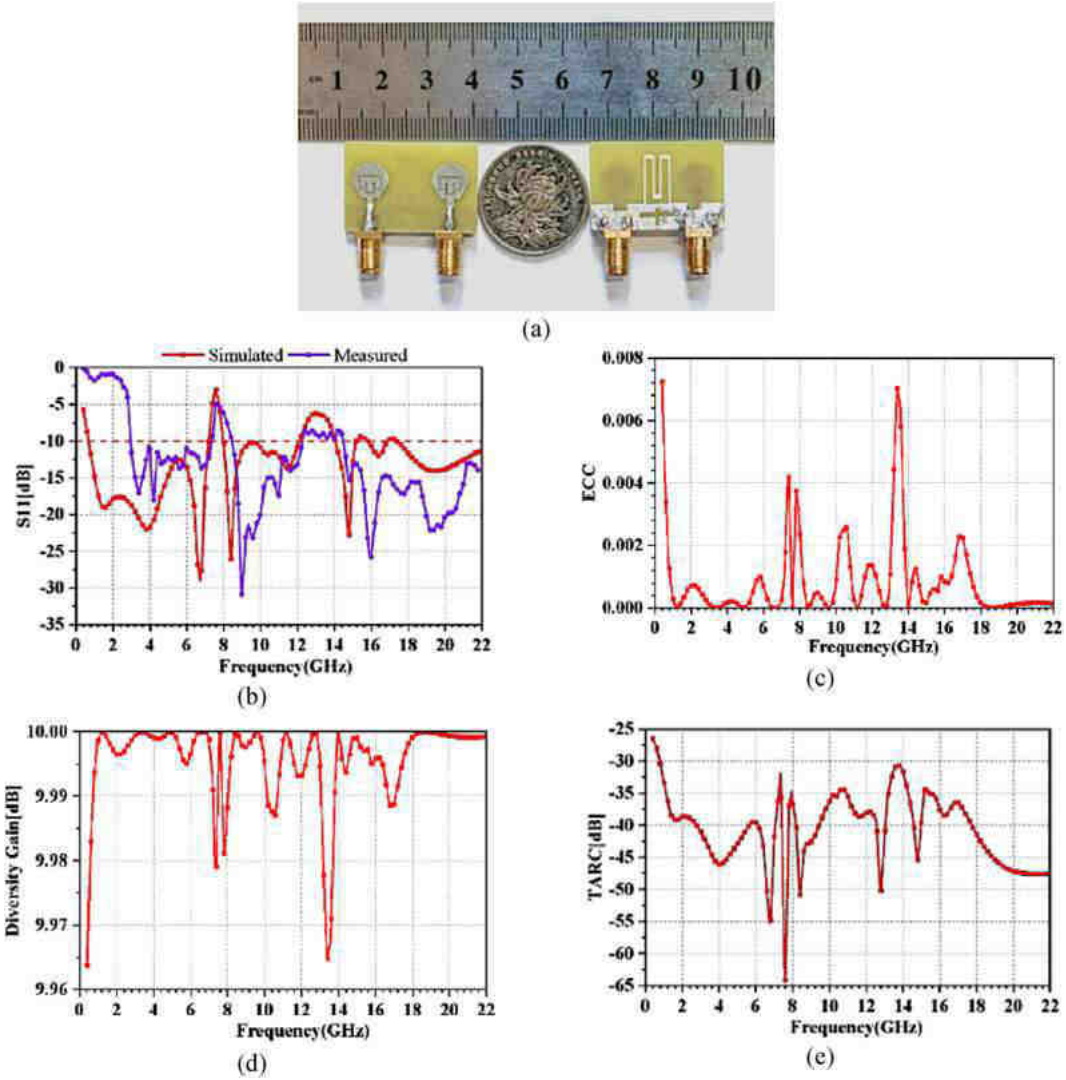

Fig. 26. (a) The geometry of the antenna, (b) Measured and Simulated reflection coefficient, (c) Calculated envelope correlation coefficients, (d) Calculated diversity gain and (e) Calculated TARC [188].

of 5.5 dB and isolation of 38 dB. Reference [170] discusses a straightforward MIMO antenna operating within the frequency from 3.4 to 3.8 GHz, with a peak gain over 4.1 dBi and isolation of approximately 39 dB. Lastly, reference [171] presents a two-element ultra-wideband (UWB) MIMO antenna designed for optimal performance and miniaturization with antennas placed very close together.

Considerable research has focused on the utilization of four-port MIMO antennas, as indicated by Refs. [172–174]. Firstly, reference [172] introduced frequency reconfigurable multiband MIMO antenna for 5G communication systems and exhibits a maximal gain of over 1.74 dB and an isolation of over 28 dB. In Ref. [173], the author discusses a four-port antenna functioning from 2.5 to 4 GHz, achieving 38 dB isolation and a peak gain of 2.2 dB. Reference [174] discuss a multiband MIMO antenna with four elements shows additional resonance at 5.1 GHz and achieves an isolation level of 14 dB.

Significant investigation has been directed towards the usage of eight-port MIMO antennas, as suggested by the citations provided in Refs. [175,176]. In Ref. [175], the author presents an eight-element UWB MIMO antenna operates from 3.1 to 10.6 GHz, exhibiting a 20 dB isolation level and a maximum gain of 7 dBi. In Ref. [176], the author describes a miniature eight-port MIMO antenna array 5G sub-6 GHz handset applications operating within the range of 3.3–5 GHz, achieving a maximal gain of 3 dB and exhibiting an isolation of 12 dB.

In [177], Christina et al. proposed a method to reduce MC between two tri-band antennas designed for LTE, WLAN, and 5G applications involves several steps. Initially, a monopole is optimized for operation at 3.5 GHz, with modifications made to the partial ground plane to achieve resonance at the other two frequencies. This approach establishes a MIMO antenna system using two tri-band monopoles. Low-band resonators are strategically placed to minimize mutual coupling in the higher frequency bands by attenuating surface wave propagation. Additional reduction in coupling at the low band is achieved using aSRR. The resulting MIMO antenna covers WLAN, 5G, and LTE frequencies spanning the 2.4, 3.5, and 5.8 GHz bands. It exhibits maximum return loss values of −22 dB, −35 dB, and −38 dB respectively, with mutual coupling levels of −25 dB, −18 dB, and −32 dB. Additionally, the envelope correlation coefficient is less than 0.01, and the total active reflection coefficient is below −10 dB, as depicted in Fig. 21, meeting acceptable standards.

In [178], Zhang et al. proposed a compact wearable multi-antenna system designed to function effectively under bending conditions is examined. Two conventional methods for passive mutual coupling suppression, utilizing electromagnetic bandgap structures and defected ground structures (DGS), are evaluated for their performance when subjected to bending or deformation. The introduction of a novel isolator inspired by metamaterials is essential to overcome the

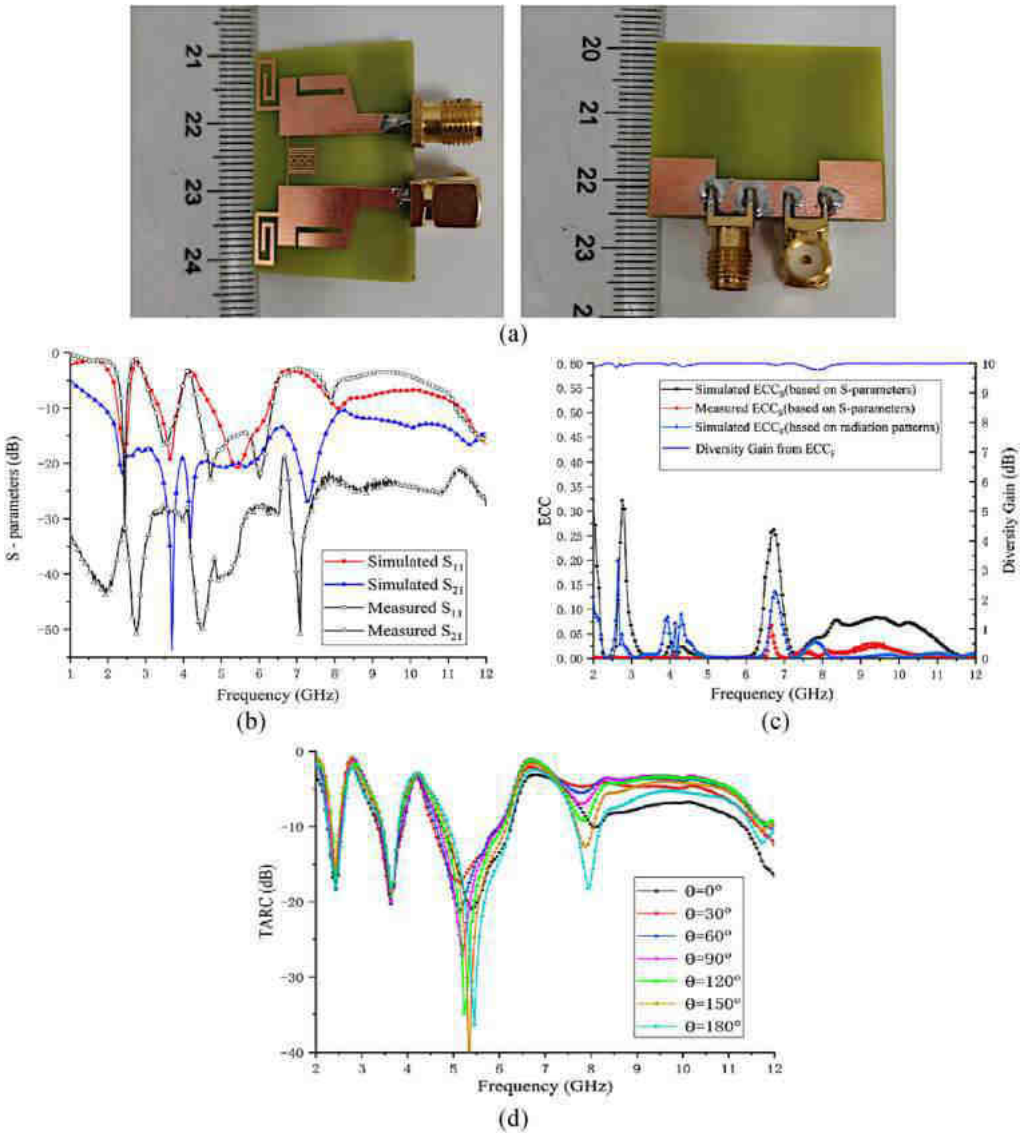

Fig. 27. (a) Antenna geometry, (b) Measured and simulated S11, (c) Measured and simulated envelope correlation coefficients and diversity gain, (d) Measured TARC [173].

limitations of conventional isolators in on-body applications. This innovative design integrates DGS with modified split ring resonators (SRR) to ensure consistent isolation performance and broad coverage, as depicted in Fig. 22, even under challenging bending conditions. Importantly, it maintains the compact structure of a linear array. Implementing this isolator ensures a low envelope correlation coefficient between the two on-body antennas, which is critical for enhancing transmission efficiency in MIMO systems.

In [144], Lutful et al. introduced a MIMO antenna system optimized for 5G applications, inspired by metamaterials (MMs), is developed with radiation pattern deflection capability. The MM structure enhances gain and provides broad angular coverage to minimize attenuation in electromagnetic wave propagation. Strong isolation within the MIMO antenna system is ensured. Across all three deflection configurations, the antenna increases gain by 2–3 dBi and achieves a −10 dB impedance bandwidth of 3.4 GHz (27.5–30.9 GHz). As depicted in Fig. 23, this deflection mechanism significantly improves isolation between MIMO elements to below −10 dB and augments gain within the 27.5–30.9 GHz operating frequency range.

In [179], Saeidi et al. proposed a high-isolation, compact dual-polarized MIMO antenna has been developed to meet the specifications of sub-6 GHz 5G and X-band communications in devices. Capable of operating within three frequency bands—3.8 GHz, 5.2 GHz, and 8.0 GHz—the antenna achieves isolation levels exceeding 20 dB without additional decoupling techniques, thanks to the incorporation of metamaterial elements. The proposed triple-band antenna boasts an impressive radiation efficiency of 98 % at 3.8 GHz, a bandwidth of 1.6 GHz (2.9 GHz–4.5 GHz), and a gain of 13.5 dBi. Fig. 24 illustrates that performance evaluation encompasses the analysis of S parameters, radiation characteristics, ECC, and SAR.

In [146], Ennajih et al. introduced a fourteen-element massive MIMO compact antenna system with a low SAR designed for 5G and future terminals. The antennas target the sub-6 GHz LTE-band 46 (5.1–5.8 GHz) for long-term evolution 5G wireless communication. The antenna system, constructed on an FR-4 substrate with a dielectric constant of 4.3, comprises a main board and four sideboards, with overall dimensions of 150 × 80 × 7.5 mm^3. The results show excellent impedance matching, isolation among antennas, and good gain. Furthermore, SAR analysis at the 5.5 GHz operating frequency indicates that the antenna system complies with safety standards for human exposure, as depicted in Fig. 25.

Table 3 compares MIMO antennas with SRR structures, highlighting

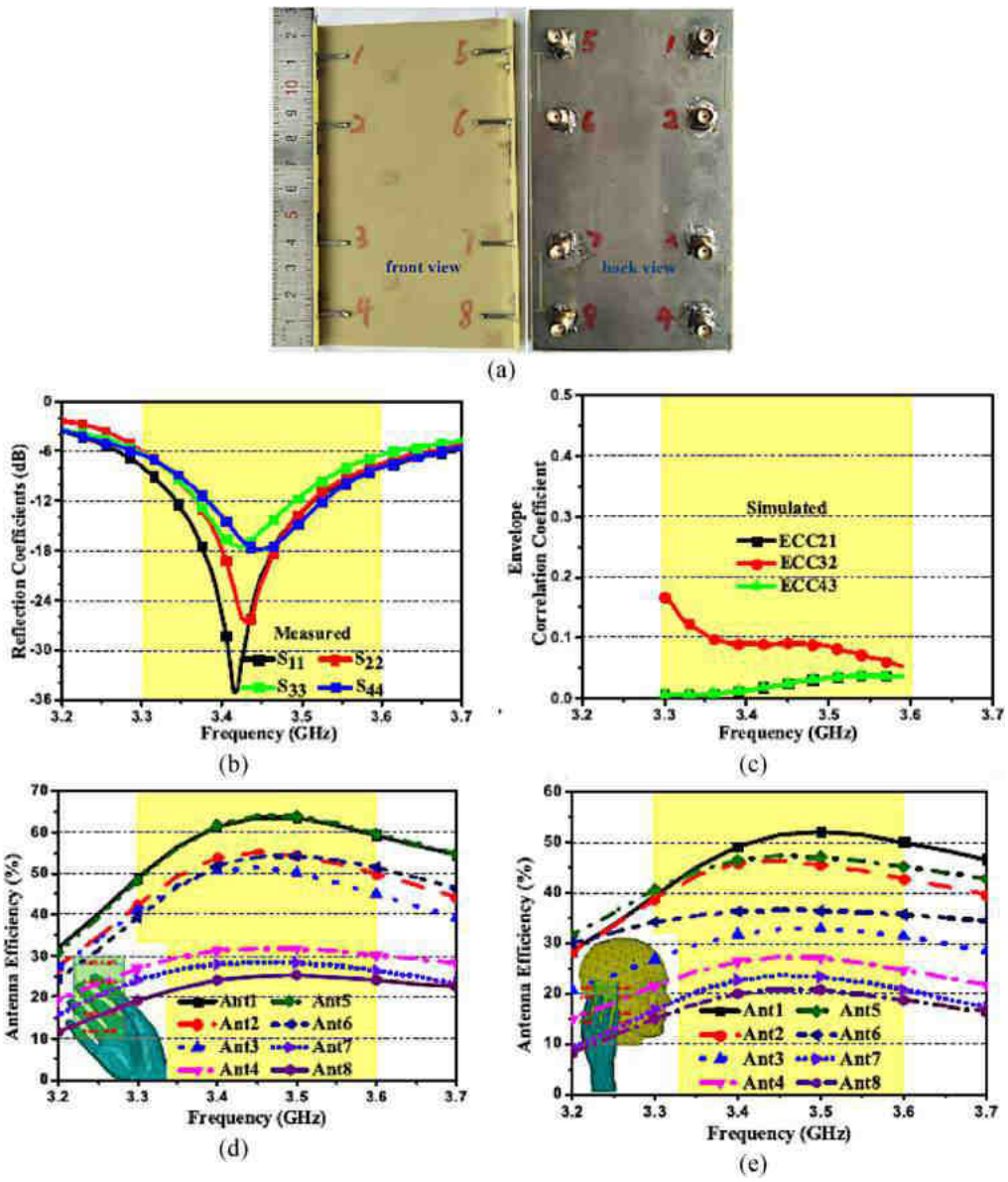

Fig. 28. (a) The geometry of the antenna, (b) Measured simulated reflection coefficient, (c) Simulated envelope correlation coefficients, (d) the antenna efficiencies of the MIMO array with a single hand model as well as (e) the antenna efficiencies of the MIMO array with a single hand and head model [210].

size variations from 10 × 5 × 0.4 mm^2 to 150 × 80 × 7.5 mm^2 and element counts from 2 to 14. These antennas achieve up to 90 % efficiency, operate from 2.3 GHz to 58 GHz, and have low ECC values under 0.01, suggesting minimal correlation. Gains range from 1.89 dBi to 13.5 dBi, isolation from 9 dB to over 40 dB, TARC values below 0 dB, and DG around 9–10 dB, with SAR within safe limits of 0.288 W/kg to 1.991 W/kg. However, more efficiency and SAR data are needed to ensure safety and performance assessments. Gain variability indicates inconsistent performance, while gaps in ECC and isolation data challenge comprehensive comparisons. Uniform DG values imply limited innovation, frequency range limitations affect versatility, and size and element count variations complicate direct performance comparisons.

4.2. Neutralization lines

The method of neutralization lines involves incorporating metallic slits or lumped elements, such as capacitors and inductors to establish a supplementary route for electromagnetic waves between antenna elements. This added pathway effectively mitigates mutual coupling, enhancing the isolation between antennas. Fine-tuning the position or characteristics of these neutralization lines enables precise control over the impedance and bandwidth of the MIMO antenna system. This adaptability facilitates the optimization of performance tailored to the requirements of specific applications [181,182].

Its primary advantages are cost-effectiveness and simplicity, allowing for easy integration into existing antenna designs without requiring significant space. Furthermore, NLs offer comprehensive efficacy across various frequencies. However, optimizing their design can be complex and may not substantially improve other performance metrics, such as radiation patterns. NLs are a valuable asset in modern antenna design, with typical applications including MIMO antenna arrays, wireless communication devices, miniaturized antennas for wearables, and tri-band systems.

Application - Using the neutralization line structure in compact MIMO systems with element spacing of no more than one wavelength helps conserve space. Acting as band-stop filters, neutralization lines enhance diversity gain, reduce mutual coupling, and lower the envelope correlation coefficient, thereby improving MIMO performance overall.

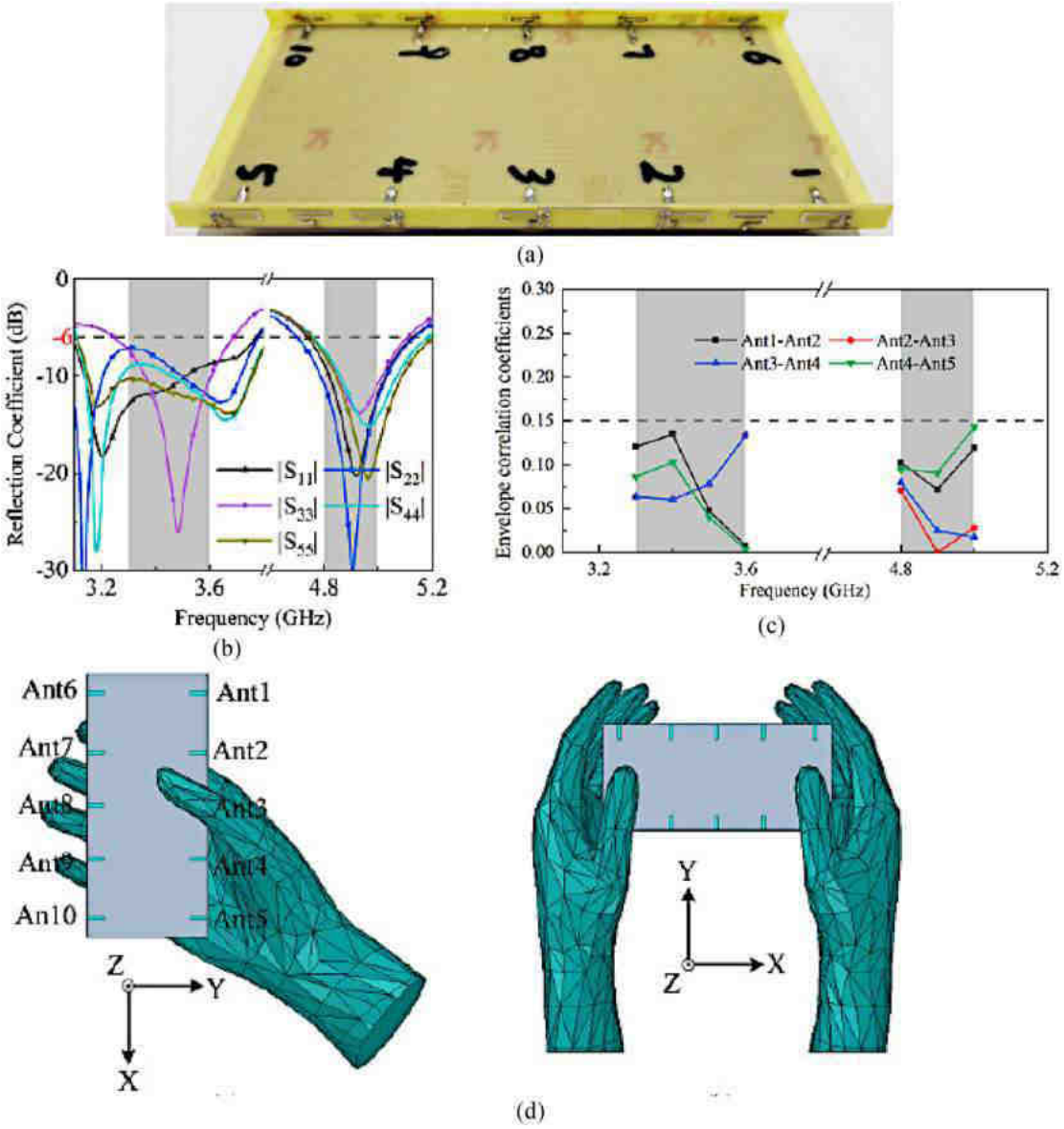

Fig. 29. (a) The geometry of the antenna, (b) Measured simulated reflection coefficient, (c) Simulated envelope correlation coefficients and (d) single hand and double hands operation [211].

Additionally, they enhance isolation at specific frequencies [95,183].

Bandwidth - Neutralization lines provide extensive decoupling bandwidths. For example, a wideband neutralization line effectively reduced mutual coupling across an ultra-wideband (UWB) frequency range. The design of neutralization lines can be optimized to achieve either a reduced antenna separation distance or a broader decoupling bandwidth, while maintaining low design complexity. In tri-band MIMO antennas, symmetrical distribution layouts and U-shaped neutralization lines have been implemented to decouple various frequency bands, including low, intermediate, and high frequencies [183,184].

As described in a number of references [185–199], recent research has produced a dual-port MIMO antenna that is capable of operating across a variety of frequencies. A compact CoPlanar Waveguide MIMO antenna that was specifically designed for Ultra-Wideband (UWB) applications was introduced in Ref. [185], it has an isolation level of approximately 16.5 dB A co-axial feed, a compact antenna with dual-band operating bands covering 5G is described in Ref. [186], which achieves a maximal gain of 3 dB and an isolation level of 15 dB. The metamaterial-inspired antenna was devised in Ref. [187] for dual-band, with an isolation level that exceeds 22 dB. A two-port, compact, and multiband MIMO antenna is detailed in Ref. [188]. This antenna features a maximal gain exceeding 6.2 dBi and an isolation greater than 18 dB. Additionally, reference [189] introduces a dual-port, high-isolation MIMO antenna designed in the shape of a trident for 5G applications, achieving 25 dB isolation. Reference [190] describes a MIMO antenna with circular polarization operating at 3.25 GHz, boasting a maximal gain of 3.3 dB and 22 dB isolation. A single-band, two-element MIMO antenna for future 5G wireless applications at 5 GHz is detailed in Ref. [191], with a maximal gain of 1.95 dBi and 21.3 dB isolation. Reference [192] discusses a Fractal H-Vicsek MIMO antenna developed for 5G applications in the 3.3–3.7 GHz band, achieving over 16 dB isolation. In Ref. [193] a compact CPW-fed triple-band MIMO antenna is designed, attaining 16 dB isolation and a maximum gain of 4.5 dB. Reference [194] introduces a semi-circular MIMO antenna with an isolation level surpassing 40 dB. Lastly, reference [195] escribes a low-profile dual-band MIMO antenna operating at 2.4 GHz, 5.2 GHz, and 5.8 GHz for WLAN applications, achieving isolation levels of 15 dB. A novel wideband decoupling technique to improve the performance of MIMO antenna is described in Ref. [196]. This antenna boasts an isolation level of approximately 15 dB. A pair of tri-band MIMO

Table 4
A comparative analysis of prior research utilizing the Neutralization Lines technique.

Ref.	Years	Size of MIMO Antenna (mm^3)	No. of Antenna Element	Operating Frequency (GHz)	Efficiency (%)	ECC	Isolation (dB)	Gain	DG (dB)	TARC (dB)	SAR (W/kg)
[185]	2023	46 × 46 × 1.6	2	3.1–11.7	59	<0.057	16.5	–	>9.78	< −10	–
[186]	2023	30 × 30 × 0.8	2	3.7–3.9 5.6–5.9	78	<0.4	13	3 dB	10	< −10	–
[187]	2023	30 × 35 × 0.8	2	3.82–4 5.62–5.92	80	<0.02	22 15.5	–	10	< −10	–
[188]	2022	30 × 20 × 1.6	2	0.67–7.29 8.07–12.11 14.07–15.41 16.04–22	70–93	<0.008	>18	3.62 dBi	10	< −30	–
[189]	2022	62 × 25.6 × 1.524	2	2.99–3.61 4.53–4.92	80.24 84.64	<0.002	< −16	3.14 dBi 3.84 dBi	10	< −10	–
[190]	2022	100 × 50 × 0.8	2	3.25	95	<0.001	>22	2.5 dB	>9.9	–	–
[191]	2022	30 × 6.75 × 0.254	2	4.9–5.06	79.5	<0.05	−21.3	1.95 dBi	10	–	–
[209]	2022	26 × 32 × 1.5	2	2.35–2.5 3.25–3.85 4.4–6.2	76	<0.35	< −27	1.26 dBi	–	–	–
[192]	2021	12.5 × 37 × 0.8	2	3.3–3.7	>40	0.009	>16	–	>10	–	–
[193]	2021	56 × 30 × 1.6	2	2.38–2.52 3.28–3.63 5.05–6.77		<0.005	18.2 16.3 17.1	4.5 dB	>9.99	< −10	–
[194]	2021	50 × 25 mm^2	2	3–10	98	<0.02	< −40	4.4 dBi	10	–	–
[195]	2020	36 × 33.5 × 1.6	2	2.4–2.7 4.4–6.7		<0.1	>15	–	>9.99	< −10	–
[196]	2020	32 × 36 × 0.5	2	3.5–6	–	–	15	–	–	–	–
[197]	2020	48 × 49 ×	2	2.3 3.5 5.7	–	<0.02	18.2 32.4 24.3	–	10	–	–
[198]	2019	35 × 33 × 0.8	2	3–6.5	–	–	–	3.8 dB	–	–	–
[199]	2019	135 × 67 × 0.8	2	4–5.95	–	<0.04	34	–	–	–	–
[200]	2022	64 × 64 × 1.5	4	5.05–5.43	>70	0.14	25	7.93 dBi	–	–	–
[201]	2022	13.75 × 13.75 × 0.787	4	35	85	<0.5	30	5 dB	9.6	< −10	–
[202]	2021	150 × 75 × 0.8	4	3.6	40	<0.1	18.5	–	–	< −5	–
[203]	2020	100 × 100 mm^2	4	1.88–3.15	65	<0.04	>30	6 dB	–	–	–
[204]	2020	120 × 60 × 0.8	4	3.4–3.6	–	–	16	–	–	< −5	–
[205]	2019	48 × 34 × 1.6	4	3.52–10.08	79.87	<0.039	23	2.91 dB	9.59	–	–
[206]	2019	18 × 30 × 0.5	4	3.36–3.68	52	<0.025	>20	2.8 dB	–	–	–
[207]	2020	150 × 73 × 0.8	8	3.3–5.6	80	0.1	15	–	–	–	–
[208]	2020	150 × 70 × 0.8	8	3.1–6	75	<0.039	12.5	–	–	–	0.852
[210]	2019	124 × 74 × 6	8	3.3–3.6	60	<0.15	>15	4.8 dBi	–	–	–
[211]	2019	150 × 70 × 0.8	10	3.3–3.6 4.8–5.0	>45	<0.15	>12	–	–	–	–

antennas with high isolation and projecting an isolation level of 11.5 dB is the subject of reference [197]. A UWB MIMO antenna modified with a wideband neutralization line is described in Ref. [198] and achieves a maximal gain of 3.8 dB. Finally [199], introduces MIMO array with T-shaped neutralization line and is based on a two-element MIMO antenna, it has an isolation level of approximately 20 dB.

The applicability of four-port MIMO antennas has been the subject of significant research study, as demonstrated by the citations [200–206]. The authors provide further details a miniaturized MIMO antenna that operates within the frequency range of 5.05–5.43 GHz in Ref. [200]. This antenna, which consists of four elements, obtains a maximal gain of 10.09 dBi and an isolation that exceeds 19.2 dB. A low-profile planar MIMO antenna with a peak gain exceeding 5 dB and a notable isolation level at a centre frequency of 35 GHz is introduced in Ref. [201]. This array is specifically designed for 5G mobile applications. As specified in Ref. [202], a four-element MIMO antenna that is intended for 3.5 GHz operation achieves an 18.5 dB isolation. Furthermore, reference [203] illustrates an antenna array formed by four PIFA elements that operates at 1.88–3.15 GHz and is designed for accesss-point MIMO systems. Next, reference [204] introduces a novel compact MIMO antenna at 3.4–3.6 GHz with an isolation of over 16 dB. A compact and small size MIMO antenna designed for ultra-wideband applications with a maximal gain of 2.91 dB is described in Ref. [205] for operation within the frequency range of 3.52–10.08 GHz. Consequently, reference [206] introduces a 4x4 inverted L-monopole antenna that operates at 3.36–3.68 GHz and has a maximal gain of 2.8 dB.

There are several researches have been made in the implementation of eight port MIMO antennas as depicted in Refs. [207,208]. In Ref. [207], researchers explain an eight-element ultra-wideband MIMO antenna frequency band from 3.3 to 5.6 GHz and reach the maximum isolation of 15 dB. In Ref. [208], the author proposed a dual-band MIMO antenna that functioning at the range of 3.1–6 GHz exhibits an isolation level of approximately 12.5 dB.

In [188], Wang et al. proposed a compact, multiband two-port MIMO antenna is designed for diverse wireless transmission networks, featuring an overall size of just 30 × 20 × 1.6 mm^3. This MIMO antenna design features two radiating patches, each composed of a semicircle and a semi-regular hexagon, with surface-etched C-slots and U-slots to optimize the antenna's return loss characteristics. A cross-shaped aperture is positioned at the center of the ground to further enhance the isolation between the radiation elements, while a neutralization line is integrated to restrict current transmission across the ground plane. The

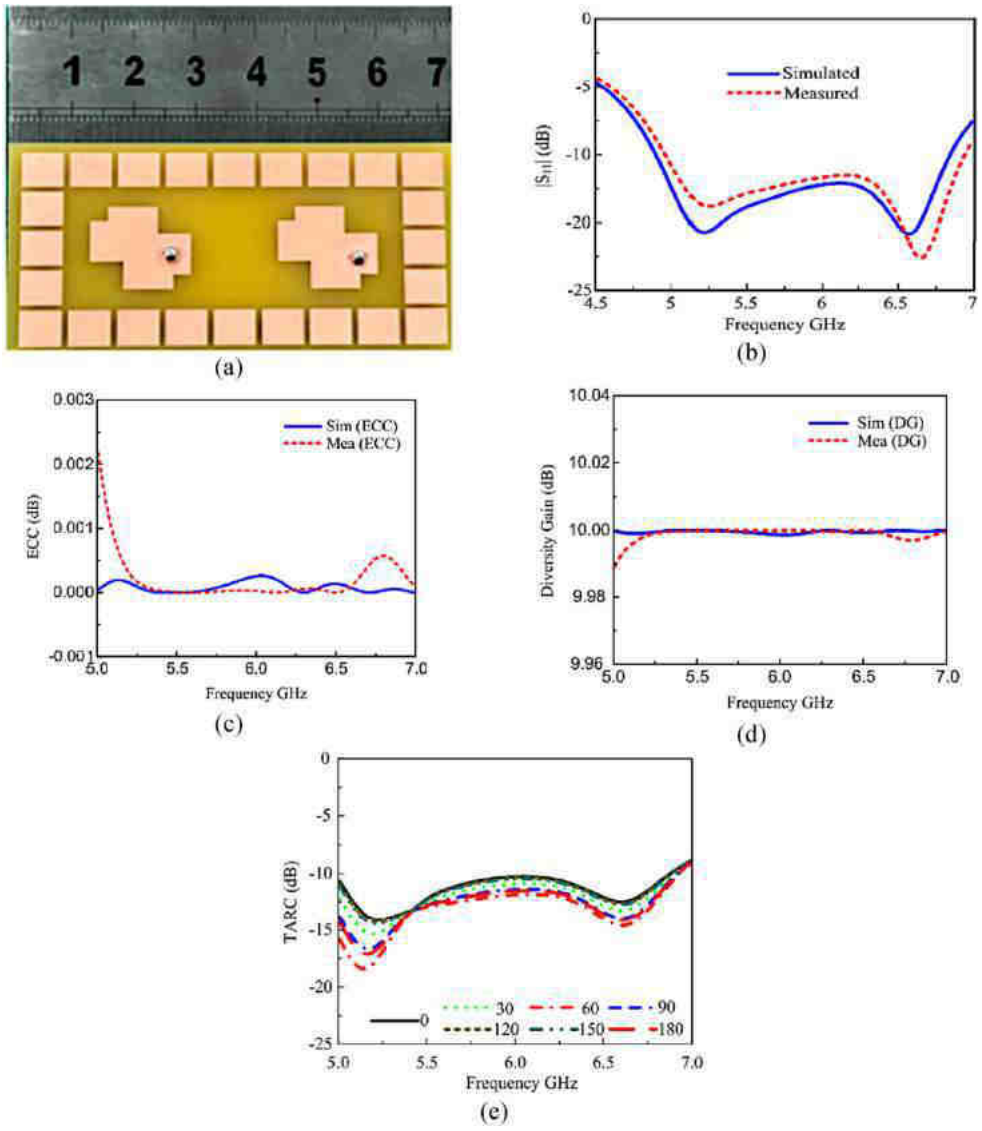

Fig. 30. (a) The geometry of the antenna, (b) Simulated and measured S11, (c) Simulated and measured ECC, (d) Simulated and measured DG and (e) Simulated TARC [255].

results indicate that the antenna operates effectively across various frequency ranges: 0.67–7.29 GHz, 8.07–12.11 GHz, 14.07–15.41 GHz, and 16.04–22 GHz (with S11<−10 dB). Additionally, the antenna achieves an RF isolation of more than 18 dB between its two terminals. Finally, Fig. 26 illustrates that the diversity metrics, including ECC, DG, TARC, CCL, and MEG, all show satisfactory performance.

In [209], Cao et al. proposed a tri-band MIMO antenna is meticulously designed using characteristic mode analysis as a guiding principle. The design process begins by incorporating rectangular spiral-shaped segments and L-shaped openings at strategic points to modify the characteristic modes of a basic rectangular microstrip antenna, resulting in a tri-band antenna unit. Subsequent analysis of modal significance and current distributions identifies the mode responsible for mutual coupling in the initial two-port MIMO antenna configuration. This insight guides the development of a meandering neutralization line connecting two adjacent edges and a rectangular opening at the center of the shared ground plane, serving as decoupling mechanisms. These enhancements successfully increase isolation to over 18 dB between two units spaced 7.4 mm apart. Empirical validation supports the effectiveness and feasibility of this systematic design approach for the MIMO antenna. The final design is notably compact (32 mm × 26 mm), achieves a peak gain exceeding 1.26 dBi, an ECC below 0.35, and a radiation efficiency exceeding 76 % across all three targeted frequency bands (0.15 GHz, 0.6 GHz, and 1.8 GHz), as depicted in Fig. 27.

In [210], Jiang et al. proposed a novel eight-element MIMO array is proposed for 5G smartphone systems that operate within the 3.45-GHz band (3.3–3.6 GHz). The array is strategically distributed symmetrically within the smartphone frame and consists of two kinds of four-antenna arrays: U-shaped and L-shaped coupled-fed loop elements. The frequency band from 3.3 to 3.6 GHz is effectively covered by all components, as demonstrated through simulation, prototype fabrication, and testing, achieving a −6 dB impedance bandwidth. The integration of inverted-I ground positions and a neutralization line (NL) structure significantly enhances isolation to 15 dB. Additionally, the envelope correlation coefficient (ECC) between any pair of elements is below 0.15, as shown in Fig. 28, indicating independent elements with favorable far-field radiation characteristics. The measured efficiencies of the elements within the operational frequency band exceed 40 %. Moreover, using the correlation matrix method and assuming a 20 dB signal-to-noise ratio, the ergodic channel capacity of the array is estimated to be approximately 35 bps/Hz.

In [211], Wei et al. dual-mode inverted-F antennas (IFAs) are

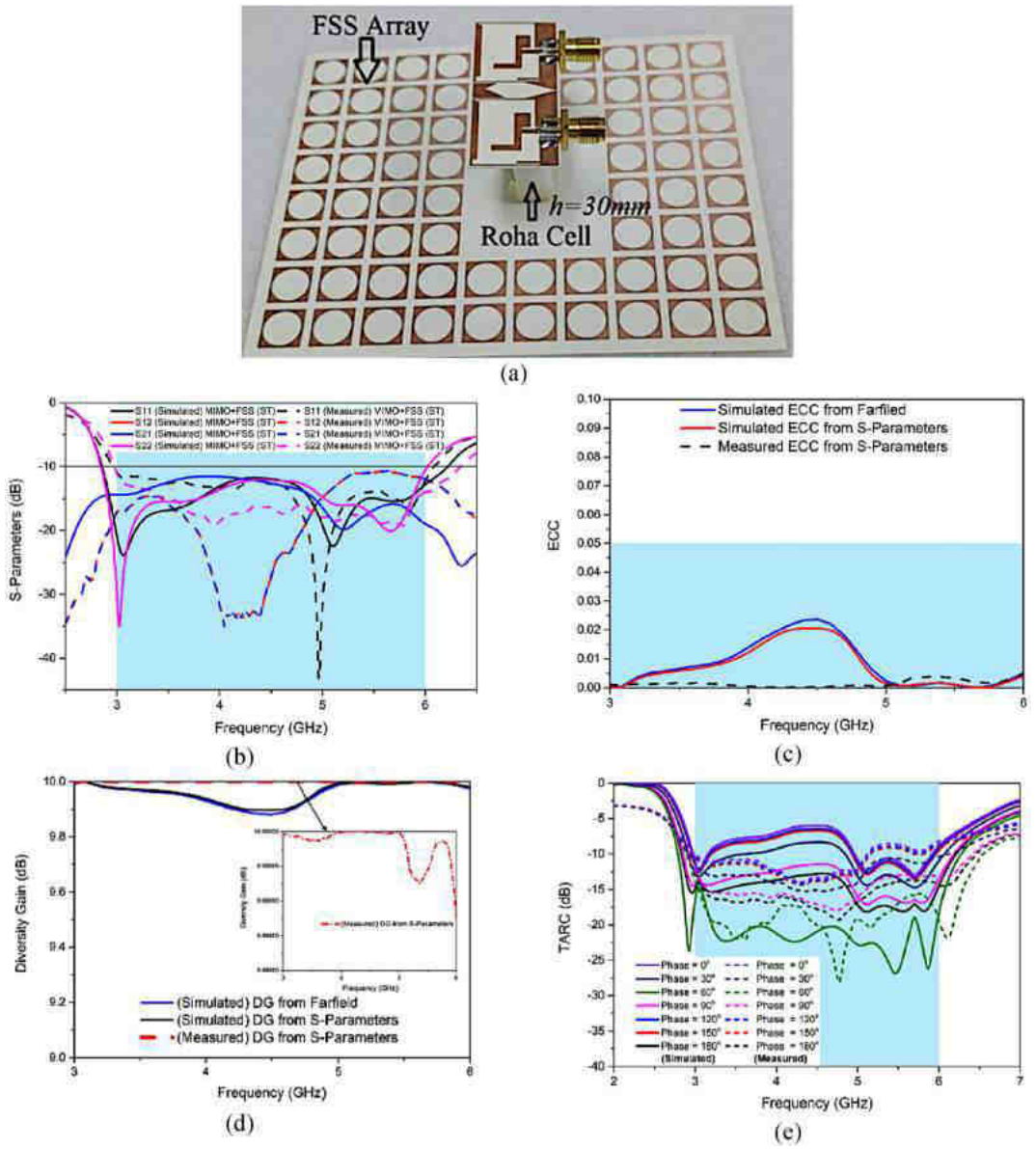

Fig. 31. (a) Antenna geometry, (b) Simulated and measured reflection coefficients, (c) Simulated and measured envelope correlation coefficients, (d) Simulated and measured diversity gain, and (e) Simulated and measured TARC [[256].

integrated into a ten-element MIMO array designed for 5G terminal applications to enhance dual-band functionality. The innovative dual-mode IFA design features two radiators positioned on the exterior and interior of the side border frame. The inner radiator activates a second one-quarter-wavelength mode at 4.9 GHz, while the outer radiator initiates a low-order mode at 3.5 GHz. Neutralization line architectures and decoupling branches are skillfully incorporated into the design to achieve superior isolation between components. To validate the design concept, a ten-element MIMO array prototype was meticulously developed, constructed, and subjected to rigorous testing. Fig. 29 illustrates empirical measurements confirming the antenna's capability to cover the 3.3–3.6 GHz and 4.8–5.0 GHz bands with exceptional efficiency and commendable isolation.

Table 4 contrasts MIMO antennas with a Neutralization Lines structure. The antennas vary from very small (12.5 x 37 × 0.8 mm^3) to larger (120 x 60 × 1.6 mm^3) designs, mostly with 2 or 4 elements. Efficiency ranges from 40 % to 98 %, and operating frequencies span 0.67–9.99 GHz. ECC values are typically low, indicating good signal correlation. Antenna gains range from 1.26 dBi to 7.93 dBi, while isolation ranges from 8.5 dB to over 22 dB. DG values, when specified, are around 10 dB. Not all studies provide TARC values, but those that do show values below 0. Only a few studies report SAR values, all below the safety limit. The table highlights several limitations: inconsistent reporting, significant efficiency variability, narrow focus on specific frequency bands, isolation variations, and a wide range of antenna gains. Many studies do not report TARC and SAR values, which are crucial for understanding overall performance and safety.

4.3. Parasitic elements or slots

In MIMO systems, parasitic elements are strategically placed to improve antenna characteristics such as gain, directivity, and impedance matching. It enhances the impedance bandwidth by employing coupling mechanisms in the ground plane or the radiation patch. The slot antenna offers wide bandwidth, high gain, increased efficiency, and substantial mutual coupling values.

This technique achieves high isolation levels, often surpassing 20 dB, by strategically placing parasitic elements or openings near active

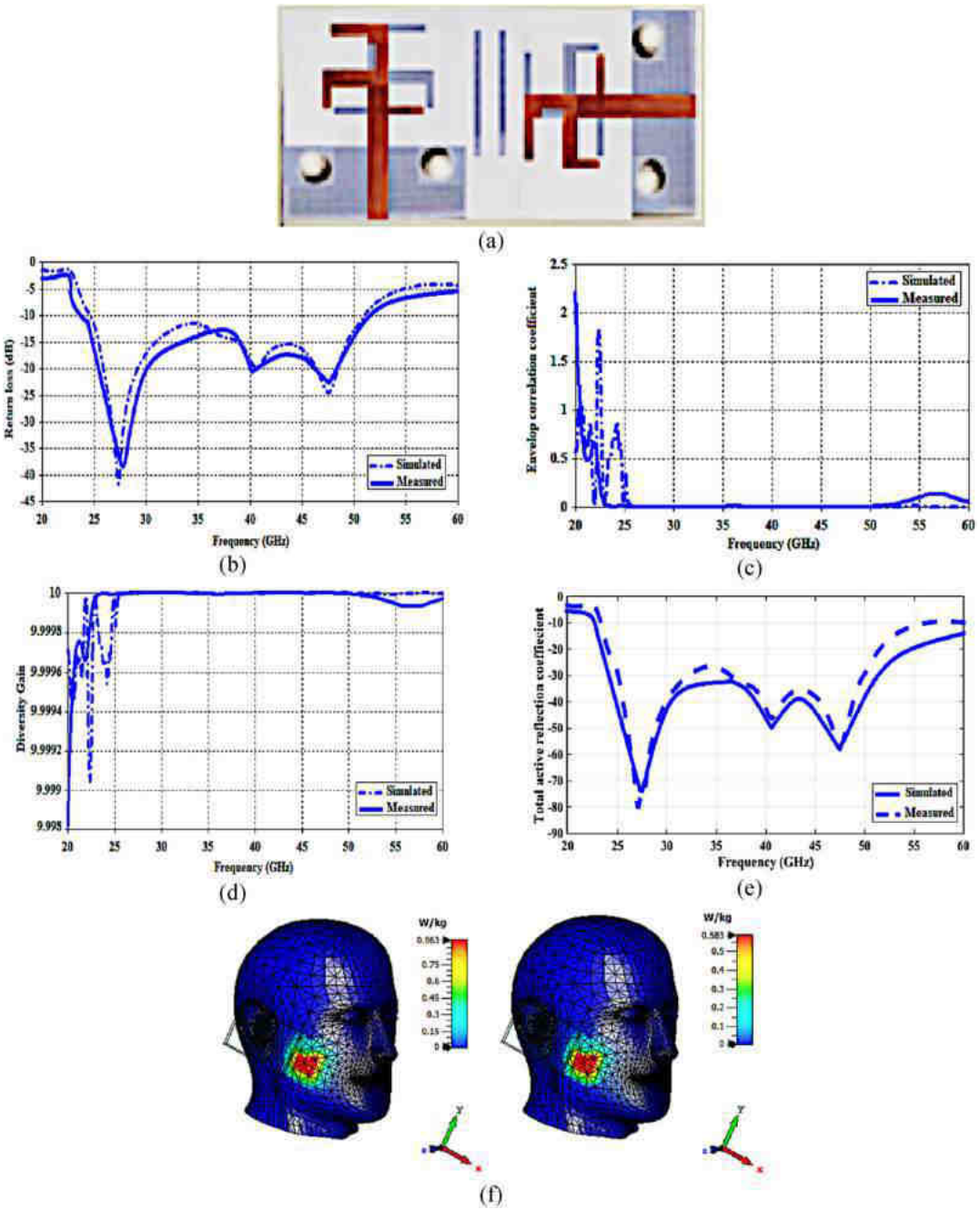

Fig. 32. (a) The geometry of the antenna, Measured and Simulated (b) Return loss, (c) ECC, (d) DG and (e) TARC and (f) Simulated SAR at 28 GHz & 38 GHz [257].

antennas. Its simple design can be easily integrated into existing structures without requiring significant additional space. Moreover, it is versatile and effective across a broad range of frequencies. However, optimizing the size and placement of the parasitic elements can be challenging, and it may not significantly enhance other performance metrics, such as gain or radiation patterns, despite improving isolation. This approach is commonly used in slot antennas, wireless communication devices, MIMO antenna arrays, and compact designs for wearable technology, highlighting its importance in modern antenna engineering.

Application - Parasitic elements are versatile in antenna design, used to compensate for resistive and reactive components, thereby improving impedance matching and reducing mutual coupling. Rectangular openings in the patch enable multi-band operation, functioning similarly to a bandpass filter. This method facilitates antenna miniaturization while maintaining effectiveness. For example, a compact and symmetrical antenna utilizing parasitic elements achieved a −27 dB return loss at 5.0 GHz [212–214].

Bandwidth - The parasitic element-based decoupling technique has been employed to achieve mutual coupling reduction across an ultra-wideband (UWB) frequency range, showcasing its capability to provide wide decoupling bandwidths. Optimization of the parasitic elements' design allows for reducing antenna separation distances or expanding decoupling bandwidths, all while maintaining a low level of design complexity. In tri-band MIMO antennas, symmetrical distribution layouts further enhance decoupling performance across various frequency bands, including low, intermediate, and high frequencies [212–214].

Researchers have recently made advancements in the design of a dual-port MIMO antenna capable of functioning at multiple frequencies, as illustrated in Refs. [215–233]. A concise, multiband MIMO antenna

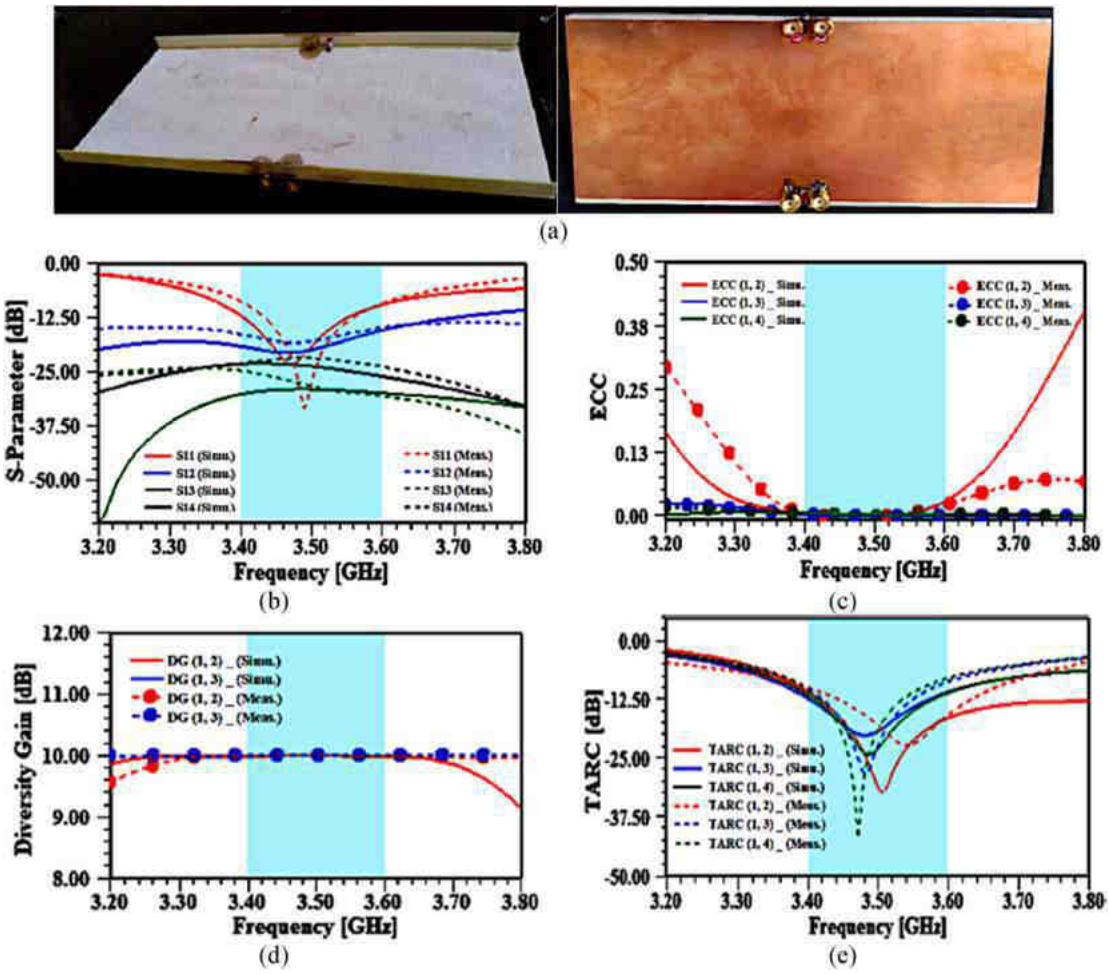

Fig. 33. (a) The geometry of the antenna, Measured and Simulated (b) S11, (c) ECC, (d) DG and (e) TARC [258].

design is introduced in the specified reference [215] for WLAN applications. This antenna achieves a maximum gain exceeding 3.1 dBi and an isolation level of approximately 27 dB. The dual-band MIMO antenna with low mutual coupling described in Ref. [216] provides effective isolation for 5G millimeter-wave networks, attaining a maximal gain of 2.65 dBi and an isolation of 15 dB. The manuscript in Ref. [217] represents the exceptional 1 × 2 MIMO antenna structure, which has a maximal gain exceeding 8.72 dBi. Documented in Ref. [218] is a compact MIMO UWB antenna that exhibits a peak gain exceeding 4.93 dBi. For 5G Antenna-in-Package Design at Millimeter-Wave Frequencies, reference [219] describes a two-element antenna that achieves 11.5 dBi of peak gain. A C-shaped parasitic structure MIMO antenna with a maximal gain of 7.69 dBi and 30 dB isolation is described in Ref. [220]. A compact, high-gain MIMO antenna operates at 4.5 GHz for Unmanned Aerial Vehicle (UAV) band, achieves an isolation of 10.7 dB and a maximal gain of 6 dBi, as described in Ref. [221]. [222] describes a UWB MIMO antenna consisting of two elements that function in the frequency range of 2.3–17.8 GHz, with a demonstrated gain exceeding 6.5 dBi. In Ref. [223], a compact coradiator annular ring diversity antenna with 20 dB isolation and a maximum gain of 8 dBi is described for various wireless applications in super wideband. A multiple-input–multiple-output (MIMO) antenna is reported for 5G frequency range-2 (FR-2), 28 GHz bands with isolation exceeding 25 dB is described in Ref. [224]. 18 dB isolation is achieved by a compact dual-polarized MIMO antenna functioning at 3.5 GHz, as described in Ref. [225]. At frequencies between 3.2 and 4 GHz, a dipole MIMO antenna [226] achieving a maximum gain of over 9.2 dBi [227]. presents a compact high-isolation UWB MIMO antenna that functions at a frequency of 3.1–17.5 GHz and achieves a gain exceeding 14 dBi. A miniaturized MIMO antenna described in Ref. [228] achieves 28 dB isolation when operating at 3–5 GHz. Next, reference [229] describes two-element MIMO antenna that operates at dual frequency and has a maximum gain of 5.4 dBi. The dual-band 28 and 38 GHz antenna described in Ref. [230] attains a maximum gain of 6.6 dBi. The paper [231] describes a novel design of high-isolation dual-band antenna that functions at 3.5 and 4.85 GHz, it boasts an isolation of 41.4 dB and a maximal gain of 4.56 dBi. A low-profile dual-band MIMO patch antenna described in Ref. [232] comprises two elements that function at the frequency of 2.6/3.6 GHz and exhibit an isolation of 13 dB. Lastly [233], describes a compact fractal MIMO antenna that operates between 4.7 and 5 GHz and features 18.5 dB isolation.

Significant academic research has focused on enhancing four-port MIMO antennas, as evidenced by the sources cited [234–245]. An examination of a quad-port MIMO antenna intended for operation at 27.6 GHz is detailed in Ref. [234]. Reference [235] describes a MIMO antenna with four elements, operating in the ultra-wideband (UWB) spectrum from 3.1 to 10.6 GHz, and achieving an isolation exceeding 20 dB. In Ref. [236] a 4-port, multi-band antenna is described, with a maximal gain exceeding 6.2 dBi and an isolation exceeding 20 dB. A Quad-Port Dual-Band MIMO antenna functioning at 3.5 & 5 GHz was accomplished by the researchers in Ref. [237] and the antenna achieved an isolation of 16.5 dB. a dual-band 4 port MIMO antenna operating in the dual frequency band range of 2.47–3.38 GHz and 4.94–7.24 GHz and exhibiting high simulated isolation is described in Ref. [238]. A four elements sub-6 GHz MIMO antenna to operate within a frequency range of 1.6–4.4 GHz obtains a maximal gain in excess of 5.62 dBi and an

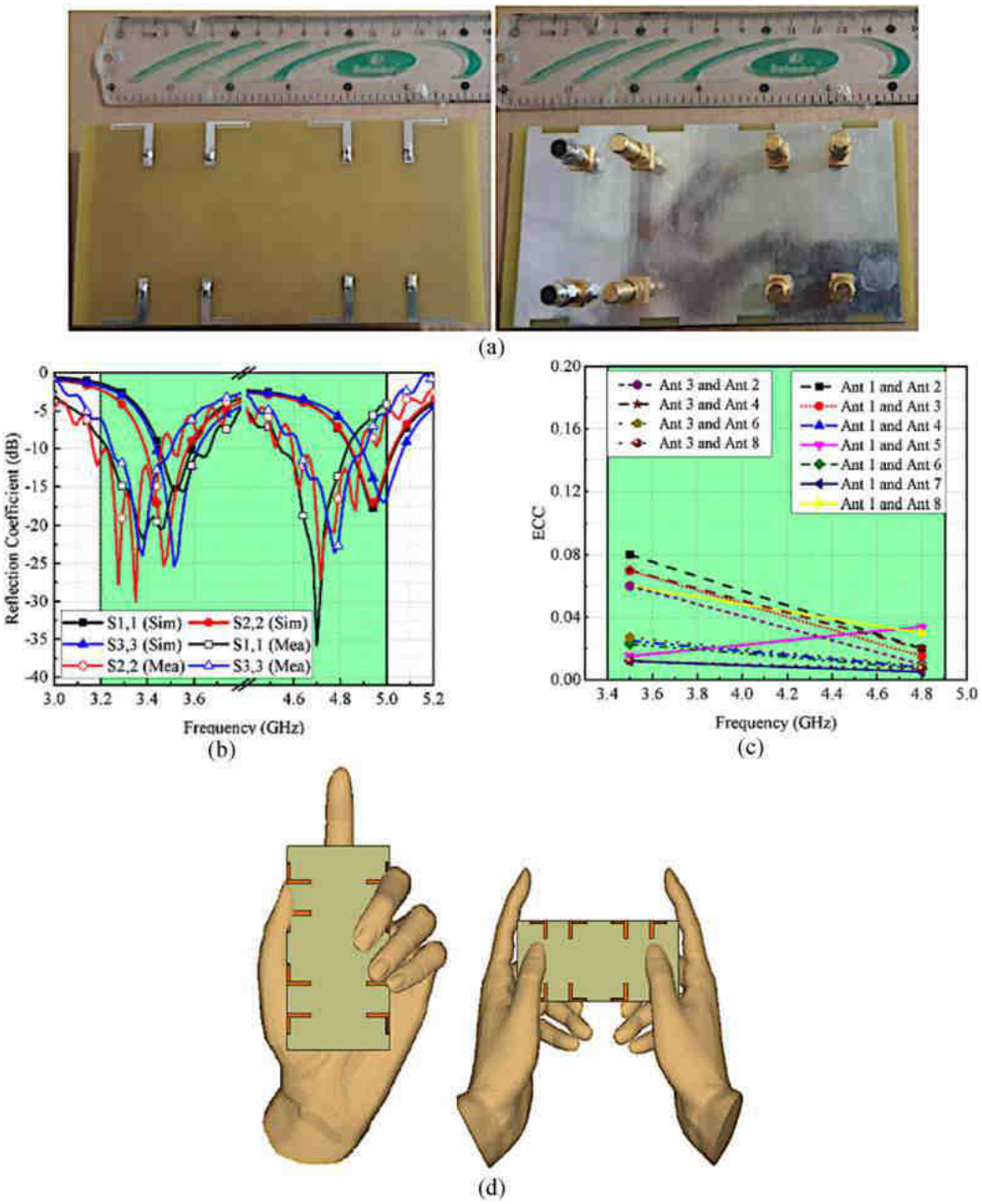

Fig. 34. (a) The geometry of the antenna, Measured and Simulated (b) Reflection coefficient, (c) Envelope correlation coefficients and (d) Single hand mode & dual hand mode [259].

isolation of approximately 40 dB, as described in Ref. [239]. Antenna reference [240] describes a wideband MIMO antenna with four elements and enhanced isolation, designed for 5G smartphone applications, covering the frequency range from 1.9 GHz to 5.2 GHz with a maximum gain in excess of 6.1 dB. The maximal gain of a four-port MIMO antenna described in Ref. [241] is 4.4 dBi when operating at dual-band frequencies. For 3.1–11.8 GHz, researchers in Ref. [242] devised a UWB MIMO antenna that achieved isolation levels of 20 dB. Reference [243] describes an inset-fed planar MIMO antenna operating at around 28/38 GHz, featuring four elements and an anticipated gain surpassing 5.5 dBi. Reference [244] demonstrates that a dual-band, compact, high-gain antenna with a simple geometry achieves a maximum gain exceeding 9.5 dBi and 11.5 dBi. Reference [245] describes a 4-port circularly polarized (CP) MIMO antenna operating at 5.9 GHz with a maximum gain of 7.68 dBi and an isolation of less than 34 dB.

As references [246–254] illustrate, considerably of research goes into the production of 8-port MIMO antennas [246]. presents a Semi-Circular Arc MIMO antenna with 8 components that achieves isolation above 15 dB while operating at 2.84–11 GHz. A sub-6 GHz antenna with 8 terminals and an isolation of 14.5 dB is presented in Ref. [247] by the 8 × 8 High-Isolation Broadband MIMO antenna. Furthermore [248], provides details on an eight-port/four-resonator slot antenna array with a dual-polarized function for MIMO with isolation of more than 25 dB. Achieving 25 dB isolation and a peak gain of 6.32 dBi, researchers successfully developed an eight-element MIMO antenna in Ref. [249] that operated at 14–18 GHz. An inverted L-shaped monopole eight elements MIMO antenna in Ref. [250] has a maximal gain of 4 dBi and operates at 3.5 GHz. Next [251], presents an 8-element MIMO antenna implemented for Chipless-RFID Tags (CRT) that that operates around 3.5–10.5 GHz and predicted gain greater than 5 dB. In

Table 5
A systematic review of previous investigations that have applied the Parasitic Elements method.

Ref.	Years	Size of MIMO Antenna (mm^3/μm^3)	No. of Antenna Element	Operating Frequency (GHz)	Efficiency (%)	ECC	Isolation (dB)	Gain	DG (dB)	TARC (dB)	SAR (W/kg)
[218]	2024	40 × 23 × 1.6	2	3.28–17.8	95.34	0.003	< −20	4.93 dBi	9.997	–	–
[221]	2024	50 × 27 × 1.6	2	4.5	–	0.02	40	6 dBi	10	–	–
[222]	2024	55 × 33 × 1.52	2	2.1–18	90	0.0001	>45	6.5 dBi	9.99	–	0.72
[223]	2024	29 × 29 × 0.8	2	3–50	80–95	<0.002	<20	8 dBi	>9.995	–	–
[229]	2024	6.2 × 13 × 0.25	2	18 28	90	<0.22	20	3.5 dBi 5.4 dBi	>9.6	< −10	–
[256]	2024	117.5 × 94.9 × 0.508	2	3–6	97	0.004	>13	7.96 dBi	>9.99	< −8	–
[216]	2023	45 × 30 × 1.6	2	2.5 4.5	70	0.02	15	2.65 dBi	9.98	–	–
[217]	2023	50 × 39 × 1.6	2	5.653	–	<0.1	50	21 dBi	10	−9.7	–
[219]	2023	8.16 × 8.16 × 3.8	2	28/39	–	–	−16	11.5 dBi	–	–	–
[255]	2023	70 × 40 × 1.6	2	4.89–6.85	84	<0.002	64	6.45 dBi	10	< −10	–
[257]	2023	14.76 × 8.38 × 0.203	2	28 38	95	$<2.5 \times 10^{-5}$	−35 75	6 dBi 10 dBi	9.998	< −10	1.57 1.36
[224]	2022	10.8 × 19.64 × 1.6	2	28	–	0.01	< −25	4.8 dBi	9.99	–	–
[225]	2022	25 × 25 × 1.57	2	3.5 5.35	86 80	<0.06 <0.11	>19.8 >16.75	–	>9.994 >9.971	< −4	–
[228]	2022	50 × 30 × 1.6	2	3–5	80	<0.00005	>28	–	>9.999	–	–
[230]	2022	7.5 × 8.8 × 0.25	2	28 38	–	0.04	< −20	6.6 dBi 5.86 dBi	>9.8	–	–
[220]	2021	15 × 26 × 1.57	2	16	–	0.14	> −30	6.43 dB	9.89	–	–
[232]	2020	18 × 23 × 1.6	2	2.6/3.6	–	0.015	13	–	–	−20	–
[215]	2019	50 × 30 × 1.59	2	2.45/5.2/5.8	63.8	<0.027	27	3.1dBi	–	–	–
[226]	2019	150 × 150 × 0.8	2	3.6	–	<0.002	>25	8 dBi	–	–	–
[227]	2019	65 × 65 × 1.62	2	3.1–17.5	–	<0.007	< −20	–	>9.99	−1.4	–
[233]	2019	21 × 24 × 0.8	2	4.7–5	–	0.002	−18.5	–	–	–	–
[241]	2024	62 × 62 × 0.6	4	2.8–8.9	82.4	<0.014	>33	4.4 dBi	9.9993	−5.4	–
[234]	2023	32 × 32 × 0.787	4	24.6–30.6	92	0.0002	>27	12.4 dBi	9.99	–	–
[236]	2023	30 × 40 × 1.67	4	2–3, 3.4–3.9, 4.4–5.2	–	0.01	20	6.3 dBi	10	< −20	–
[238]	2023	50 × 50 × 0.8	4	2.47–3.38 4.94–7.24	80	<0.064	15	2.28 dBi 5.21 dBi	9.95	–	–
[239]	2023	40 × 40 × 1.6	4	1.6–4.4	53	<0.001	−40	5.62 dBi	>9.9	–	–
[242]	2023	54 × 54 × 1.52	4	3.1–11.8		0.001	20	6.35 dBi	10	–	–
[244]	2022	28 × 28 × 0.79	4	28 38	–	<0.001	−50	9.5 dBi 11.5 dBi	9.99	–	–
[245]	2022	1.46 × 1.46 × 0.029	4	5.9	94	<0.001	−65	7.68 dBi	9.99	–	–
[237]	2021	150 × 75 × 6.2	4	3.5 5	85 82	0.01	16.5	4.7 dBi 5 dBi	–	–	–
[240]	2021	54 × 120 × 13	4	1.9–5.2	65–92	<0.05	> −16	6.1 dB	–	–	–
[243]	2021	41.5 × 8 × 0.787	4	28/38	84	0.005	25	5.5 dBi	>9.96	–	–
[258]	2021	150 × 75 × 6	4	3.4–3.6	78.5–87	<0.03	>16.5	5.7 dBi	>9.995	< −11	–
[235]	2019	40 × 43 × 1	4	3.1–10.6	92	<0.2	20	4 dBi	>9.5	−8	–
[247]	2023	12.7 × 6.1 × 0.8	8	3.28–5.05	82	<0.01	>14.5	–	–	–	–
[249]	2023	60 × 60 × 1.6	8	14–18	–	<0.008	>25	6.32 dBi	9.96	< −10	–
[251]	2022	62.2 × 124.4 × 1.6	8	3.5–10.5	92.7	<0.008	>18	5 dB	–	–	–
[259]	2022	150 × 75 × 0.8	8	3.5 4.8	55 72	<0.08	>12	>2 dBi	–	–	–
[246]	2021	0.61λ × 0.61λ × 1.6	8	2.84–11	–	<0.02	>15	7.2 dBi	–	–	–
[250]	2021	136 × 68 × 0.8	8	3.5	50–75	<0.1	>15	4 dBi	–	–	1.36
[253]	2021	150 × 75 × 0.8	8	3.5	76–83	<0.05	> −17.5	5 dB	10	–	–
[254]	2021	75 × 37.5 × 0.8	8	3.3–5.95	47–78	<0.11	>15	–	–	–	–
[248]	2019	75 × 150 × 1.6	8	3.6	60	<0.01	25	5 dB	–	–	–
[252]	2019	18.6 × 7 × 0.8 (single)	8	3.3–4.2 4.8–5	53.8–76.5 62.6–79.1	<0.1 <0.2	15	–	–	–	–

Ref. [252], the author proposed an 8-element dual-band MIMO antenna, designed for operation in both the 5G New Radio band n77 (3300–4200 MHz) and the 5 GHz band (4800–5000 MHz), achieves an isolation exceeding 12.5 dB. In Ref. [253], the author describes a compact 8-port MIMO antenna array operate in the 3.5 GHz band, offering isolation of 17.5 dB and a peak gain of 5 dB. Finally, a wideband dual-antenna for 5G mobile applications is described in Ref. [254], which improves isolation by up to 15 dB.

In [216], Khan et al. proposed A circularly polarized wideband MIMO antenna with high isolation features a square-cut square patch design, two ports with square cuts at each corner, and parasitic elements consisting of 9x5 periodic square metallic plates. The antenna uses an FR4 substrate with a height of 1.6 mm and measures 40 × 70 mm^2. The parasitic elements surrounding the antenna are strategically positioned to minimize MC and enhance circular polarization (CP). The proposed antenna demonstrates superior performance in terms of efficiency, ECC, DG, CCL, and TARC, as illustrated in Fig. 30.

In [256], Zeain et al. introduced a novel compact MIMO antenna shaped like a chair, featuring two radiating elements and a single layer of frequency-selective surface (FSS) tailored for 5G Sub-6GHz communication systems. The 1 × 2 MIMO antenna utilizes coplanar waveguide (CPW) feeding. Additionally, an FSS array structure comprising 68 Square-shaped structures with Circular Slot (SCS) shaped cells is implemented using a novel Surround Technique to bolster gain and isolation between the MIMO antenna elements. Fabricated on a Rogers 4350B substrate with a thickness of 0.508 mm, the antenna undergoes thorough evaluation based on S-parameters, radiation properties, and MIMO characteristics. Operating within the Sub 6-GHz 5G band (3–6 GHz), the proposed MIMO antenna demonstrates exceptional performance metrics, including ECC = 0.004, DG = 9.99 dB, CCL = 0.2 bit/s/Hz, MEG = −3.13 dBi, and TARC = > 0 dB, showcasing its advantageous antenna attributes as shown in Fig. 31.

In [257] Elabd and Ahmed introduced a two-element MIMO antenna array that is wideband and specifically designed for mmWave 5G mobile devices, covering the 28/38 GHz frequency bands. This antenna array features significant improvements in isolation and gain, utilizing dual-mode planar dipole antennas. The design is implemented on a Rogers RT 4003 substrate with dimensions of 14.76 × 8.38 mm^2 and a dielectric constant of 3.55, developed using CST Microwave Studio 2019. To improve ECC and enhance isolation between the MIMO antenna elements, the element spacing, including the parasitic element (PE), is precisely set to 0.5λ_0. Additionally, improvements are noted in TARC, MEG, and DG. The proposed design boasts a radiation efficiency of nearly 95 %, with measured gains ranging from 6 dBi across the entire band to 10 dBi at 40 GHz. The antenna demonstrates robust performance in simulations with both human head and handset models. The study reports a safe SAR value, with a low SAR10g of approximately 0.963 W/kg at 28 GHz and 0.583 W/kg at 38 GHz, as illustrated in Fig. 32.

In [258], Abi and Nesasudha introduced a handheld device-specific self-decoupled four port MIMO antenna pair operates within the 3.5 GHz midband of the 5G spectrum. The previously described configuration features a T-shaped parasitic structure, two monopole antennas spaced 7 mm apart, and a segment connecting the ground plane at the rear. Throughout the entire frequency range of 3.4–3.6 GHz, the antenna pair achieves isolation levels exceeding −16.5 dB. Within this bandwidth, every antenna demonstrates a maximal gain of no less than 5 dB and a total efficiency surpassing 78 %. The envelope correlation coefficient (ECC) among the elements of the antenna is substantially lower than the ideal value of 0.5, falling below the worst-case value of 0.03. The calculations and analyses of additional MIMO diversity parameters were conducted, encompassing Mean Effective Gain (MEG), Total Active Reflection Coefficient (TARC), Diversity Gain (DG), and Channel Capacity Loss (CCL). The outcomes of these analyses are illustrated in Fig. 33.

In [259], Kiani et al. proposed a MIMO antenna system comprising eight elements has been specifically engineered to enable 5G mobile communication, the antenna elements are composed of a ground plane with a rectangular aperture, an L-shaped parasitic element, and an L-shaped radiating component. This configuration allows the system to operate within two distinct frequency ranges, 4.67–5.08 GHz and 3.34–3.7 GHz, corresponding to bandwidths of 360 MHz and 410 MHz, respectively. Positioning the radiating elements on opposite sides of a 0.8 mm thick FR-4 substrate maintains a minimum isolation of 12 dB between any two elements. Various MIMO performance parameters, such as MEG, channel capacity, ECC, realized gain, far-field characteristics, and efficiency, were evaluated, as displayed in Fig. 34.

A systematic review of previous investigations applying the Parasitic Elements method to MIMO antennas is presented in Table 5. Antenna sizes vary from extremely small (e.g., 0.61 x 0.61 × 0.16 mm^3) to larger dimensions (e.g., 117.5 x 94.9 × 0.508 mm^3), with designs incorporating 2 to 8 elements. Their efficacy ranges from 50 % to 95.34 %, and operating frequencies range from 0.88 to 39 GHz. ECC values are generally extremely low, suggesting a strong correlation between signals. Antenna gains range from 2.61 dBi to 11.65 dBi, and isolation ranges from −65 dB to 21 dB. DG values are consistently maintained at approximately 10 dB. However, not all studies provide TARC values; those that do demonstrate values below 0. SAR is reported in only a handful of studies, all within the safety limit. Several limitations are emphasized in the table, including inconsistent reporting, significant efficiency variability, limited frequency bands despite broad coverage, and variations in isolation and antenna gains. Furthermore, many studies fail to report TARC and SAR values, which are essential for comprehending overall performance and safety.

5. Challenges and future directions

Several challenges have been linked to the development of MIMO antennas for 5G devices. Reducing MC between antenna elements is one of the primary challenges in achieving high isolation and efficient radiation patterns. In addition, the limited space available in mobile phones requires that MIMO antennas be efficient and compact, affecting design considerations regarding overall performance and radiation patterns. Another significant challenge is to ensure that compact MIMO antennas comply with the Specific Absorption Rate (SAR) safety limits. In addition, to facilitate a variety of 5G applications, MIMO antennas must be capable of accommodating a wide range of frequency bands, such as FR1 and FR2, necessitating complex design methods and materials. In order to enhance the functionality of MIMO antennas, it is crucial to optimize parameters such as isolation, efficiency, and gain to achieve low latency and high data rates.

Advanced materials and innovative structures should be the primary focus of future MIMO antenna designs to improve SAR compliance, reduce size, and enhance performance. The utilization of metamaterials and nanomaterials to develop antennas that are more compact and efficient is among the most significant areas. The antennas should be compatible with both mmWave and FR1 frequencies to support various 5G applications and function effectively with other technologies, such as IoT and V2X communications. Additionally, MIMO antennas should be adaptable to multiple smartphone designs and environments, including foldable and wearable options, as well as being compact and flexible. Their efficacy should be adjusted to correspond with user activity and the environment by implementing adaptive technologies. Optimal operation and compliance with standards should be ensured by implementing real-time performance monitoring systems. Finally, future research should aim to create technologies that enable real-time direct SAR measurements, surpassing the limitations of current simulation methods.

6. Conclusions

This comprehensive review provides an in-depth analysis of MIMO

antennas for 5G smartphones, focusing on mutual coupling techniques, performance comparisons, SAR analysis, and future directions. The review identifies critical challenges that MIMO antenna designers face, including mitigating mutual coupling, achieving compactness, ensuring SAR compliance, covering a wide range of frequency bands, and enhancing overall performance. Future MIMO antennas should be designed to seamlessly integrate with other technologies, be compact and flexible, and incorporate real-time performance monitoring. This review highlights the importance of assessing multiple performance metrics, including far-field gain, DG, ECC, TARC, and mean effective gain, in the evaluation of MIMO antennas. It also emphasizes the critical importance of SAR compliance, stressing the need to consider SAR in antenna design. This review provides a valuable resource for researchers and engineers engaged in MIMO antenna design for 5G smartphones. It highlights the key challenges and future directions in this field, offering insights into advanced solutions and design strategies necessary for developing efficient and compliant MIMO antennas in next-generation mobile devices.

CRediT authorship contribution statement

Nazrin Haziq Jemaludin: Writing – original draft. **Ahmed Jamal Abdullah Al-Gburi:** Supervision, Conceptualization. **Rania Hamdy Elabd:** Formal analysis. **Tale Saeidi:** Validation. **Muhammad Firdaus Akbar:** Writing – review & editing. **Imran Mohd Ibrahim:** Validation. **Zahriladha Zakaria:** Project administration.

Declaration of competing interest

The authors declare that they have no known competing financial interests or personal relationships that could have appeared to influence the work reported in this paper.

Data availability

The data that has been used is confidential.

Acknowledgments

The authors express their thank and acknowledge the support from Universiti Teknikal Malaysia Melaka (UTeM), the Centre for Research and Innovation Management (CRIM), and the Ministry of Higher Education of Malaysia (MOHE).

References

[1] S. Kumar, A.S. Dixit, R.R. Malekar, H.D. Raut, L.K. Shevada, Fifth generation antennas: a comprehensive review of design and performance enhancement techniques, IEEE Access 8 (2020) 163568–163593, https://doi.org/10.1109/ACCESS.2020.3020952.

[2] S. Mendonça, B. Damásio, L. Charlita de Freitas, L. Oliveira, M. Cichy, A. Nicita, The rise of 5G technologies and systems: a quantitative analysis of knowledge production, Telecomm Policy 46 (4) (May 2022) 102327, https://doi.org/10.1016/J.TELPOL.2022.102327.

[3] R. Dangi, P. Lalwani, G. Choudhary, I. You, G. Pau, Study and investigation on 5G technology: a systematic review, Sensors 22 (1) (Dec. 2021) 26, https://doi.org/10.3390/s22010026.

[4] R. Mittra, Challenges in Antenna Designs and Some Novel Techniques for Meeting Them, Jun. 2007, pp. 1–4, https://doi.org/10.1109/LAPC.2007.367420.

[5] D. Guha, Challenges and Innovations in Modern Antenna Technology, Jun. 2015, pp. 1–2, https://doi.org/10.1109/ICMAP.2015.7408724.

[6] P. Kumar, et al., A quad port dual band notch UWB MIMO antenna using hybrid decoupling structure, Results in Engineering 23 (Sep) (2024), https://doi.org/10.1016/j.rineng.2024.102551.

[7] U. Patel, et al., Split ring resonator geometry inspired crossed flower shaped fractal antenna for satellite and 5G communication applications, Results in Engineering 22 (Jun) (2024), https://doi.org/10.1016/j.rineng.2024.102110.

[8] O. Elalaouy, M. EL Ghzaoui, J. Foshi, A high-isolated wideband two-port MIMO antenna for 5G millimeter-wave applications, Results in Engineering 23 (Sep) (2024), https://doi.org/10.1016/j.rineng.2024.102466.

[9] T. Raj, R. Mishra, P. Kumar, A. Kapoor, Advances in MIMO Antenna Design for 5G: A Comprehensive Review, Multidisciplinary Digital Publishing Institute (MDPI), Jul. 01, 2023, https://doi.org/10.3390/s23146329.

[10] "How many people have smartphones worldwide (2024).". https://www.bankmycell.com/blog/how-many-phones-are-in-the-world. (Accessed 13 June 2024).

[11] Malaysia: 4G LTE population coverage 2023 | Statista. https://www.statista.com/statistics/1051191/malaysia-4g-lte-population-coverage/. (Accessed 13 June 2024).

[12] B.R. Binti, H. Arai, B-1-181 enhancing 4x4 MIMO Channel Capacity by dual polarized directional antenna, Proceedings of the IEICE General Conference 2016 (1) (Mar. 2016) 181 [Online]. Available: https://cir.nii.ac.jp/crid/1573105977318732032.bib?lang=en. (Accessed 14 June 2024).

[13] I. Nadeem, D.-Y. Choi, Study on mutual coupling reduction technique for MIMO antennas, IEEE Access 7 (Jun. 2019) 563–586, https://doi.org/10.1109/ACCESS.2018.2885558.

[14] S. Roy, S. Ghosh, U. Chakarborty, Compact dual wide-band four/eight elements MIMO antenna for WLAN applications, Int. J. RF Microw. Computer-Aided Eng. 29 (7) (2019) e21749, https://doi.org/10.1002/mmce.21749.

[15] S. Kumar, A.S. Dixit, Wideband antipodal vivaldi antenna using metamaterial for micrometer and millimeter wave applications, J. Infrared, Millim. Terahertz Waves 42 (9–10) (2021) 974–985, https://doi.org/10.1007/s10762-021-00799-2.

[16] M. Seyyedesfahlan, A. Uzun, A.K. Skrivervik, I. Tekin, Wideband multiport antennas, Sensors 20 (23) (2020), https://doi.org/10.3390/s20236960.

[17] P. Mattheijssen, M.H.A.J. Herben, G. Dolmans, L. Leyten, Antenna-pattern diversity versus space diversity for use at handhelds, IEEE Trans. Veh. Technol. 53 (4) (Jul. 2004) 1035–1042, https://doi.org/10.1109/TVT.2004.830156.

[18] R.G. Vaughan, J.B. Andersen, Antenna diversity in mobile communications, IEEE Trans. Veh. Technol. 36 (4) (Nov. 1987) 149–172, https://doi.org/10.1109/T-VT.1987.24115.

[19] N. Bayat-Makou, K. Wu, A. Kishk, Single-layer substrate-integrated broadside leaky long-slot array antennas with embedded reflectors for 5G systems, IEEE Trans. Antenn. Propag. (Jun. 2019) 1, https://doi.org/10.1109/TAP.2019.2930134.

[20] H. Liu, W. Yang, A. Zhang, S. Zhu, Z. Wang, T. Huang, A miniaturized gain-enhanced antipodal vivaldi antenna and its array for 5G communication applications, IEEE Access PP (Jun. 2018) 1, https://doi.org/10.1109/ACCESS.2018.2882914.

[21] A.S. Dixit, S. Kumar, A miniaturized antipodal vivaldi antenna for 5G communication applications, in: 2020 7th International Conference on Signal Processing and Integrated Networks (SPIN), Feb. 2020, pp. 800–803, https://doi.org/10.1109/SPIN48934.2020.9071075.

[22] N. Sheriff, S. Kamal Abdul Rahim, H. Tariq Chattha, T. Kim Geok, Multiport Single Element Mimo Antenna Systems: A Review, MDPI, Jan. 01, 2023, https://doi.org/10.3390/s23020747.

[23] I. Elmutasim, A brief review of massive MIMO technology for the next generation, Int. Arab J. Inf. Technol. 20 (2) (Mar. 2023) 262–269, https://doi.org/10.34028/iajit/20/2/13.

[24] P.L. Iturri, et al., Impact of high power interference sources in planning and deployment of Wireless Sensor Networks and devices in the 2.4 GHz frequency band in heterogeneous environments, Sensors 12 (11) (Nov. 2012) 15689–15708, https://doi.org/10.3390/s121115689.

[25] M.N.I. Mohd Yusoff, X. Peng, Impacts of Channel Loss and Electromagnetic Interference on Intra-vehicle Wireless Communications, Jun. 2020, pp. 1–5, https://doi.org/10.1109/VTC2020-Spring48590.2020.9128861.

[26] T. He, J. Huang, J. Lu, X. Shi, G. Liu, Eight-element dual-band multiple-input multiple-output mobile phone antenna for 5G and wireless local area network applications, Micromachines 14 (12) (Dec. 2023), https://doi.org/10.3390/mi14122200.

[27] R.D. Fabianczyk, S. Alkaraki, M. Aslam, Q. Abbasi, A. Evans, S.F. Jilani, Millimetre-wave multiple-input-multiple-output antenna frontend for beyond 5G applications, in: 2023 17th European Conference on Antennas and Propagation, EuCAP), Mar. 2023, pp. 1–4, https://doi.org/10.23919/EuCAP57121.2023.10133719.

[28] M. Abdullah, et al., High-performance multiple-input multiple-output antenna system for 5G mobile terminals, Electronics (Basel) 8 (10) (2019), https://doi.org/10.3390/electronics8101090.

[29] R. Khan, A.A. Al-Hadi, P.J. Soh, M.R. Kamarudin, M.T. Ali, Owais, User Influence on Mobile Terminal Antennas: A Review of Challenges and Potential Solution for 5G Antennas, Institute of Electrical and Electronics Engineers Inc, 2018, https://doi.org/10.1109/ACCESS.2018.2883788.

[30] R. Gomez-Villanueva, H. Jardon-Aguilar, Compact UWB uniplanar four-port MIMO antenna array with rejecting band, IEEE Antennas Wirel Propag Lett 18 (12) (Dec. 2019) 2543–2547, https://doi.org/10.1109/LAWP.2019.2942827.

[31] S. V Vinodhini, R. Darwin, Review on isolation enhancement techniques for MIMO antennas [Online]. Available: https://api.semanticscholar.org/CorpusID:212575024, 2018.

[32] R.S. Bakale, A.B. Nandgaonkar, S.B. Deosarkar, Isolation enhancement techniques for MIMO antenna: a review, in: 2020 International Conference on Smart Innovations in Design, Environment, Management, Planning and Computing (ICSIDEMPC), IEEE, Oct. 2020, pp. 57–62, https://doi.org/10.1109/ICSIDEMPC49020.2020.9299655.

[33] I. Nadeem, D.Y. Choi, Study on mutual coupling reduction technique for MIMO antennas, IEEE Access 7 (2019) 563–586, https://doi.org/10.1109/ACCESS.2018.2885558.

[34] What is 5G? Everything you need to know — a definition. https://www.sdxcentral.com/5g/definitions/what-is-5g/. (Accessed 10 June 2024).
[35] "What is 5G? | IBM." Accessed: June. 10, 2024. [Online]. Available: https://www.ibm.com/topics/5g.
[36] What is 5G? | definition from TechTarget. https://www.techtarget.com/searchnetworking/definition/5G. (Accessed 10 June 2024).
[37] The 5G advanced, an evolution towards 6G - ericsson. https://www.ericsson.com/en/reports-and-papers/white-papers/5g-advanced-evolution-towards-6g. (Accessed 10 June 2024).
[38] T. Raj, R. Mishra, P. Kumar, A. Kapoor, Advances in MIMO Antenna Design for 5G: A Comprehensive Review, Multidisciplinary Digital Publishing Institute (MDPI), Jul. 01, 2023, https://doi.org/10.3390/s23146329.
[39] S.K.K. Dash, Q.S. Cheng, T. Khan, M.V. Yadav, L. Wang, 5G millimeter-wave MIMO DRAs with reduced mutual coupling, Microw. Opt. Technol. Lett. 66 (1) (2024) e33982, https://doi.org/10.1002/mop.33982.
[40] Y. Pan, X. Qin, Y.-X. Sun, S. Zheng, A simple decoupling method for 5G millimeter-wave MIMO dielectric resonator antennas, IEEE Trans. Antenn. Propag. (1) (Jul. 2019), https://doi.org/10.1109/TAP.2019.2891456.
[41] Y.-M. Zhang, M. Yao, S. Zhang, Wideband decoupled millimeter-wave antenna array for massive MIMO systems, IEEE Antennas Wirel Propag Lett 22 (11) (Nov. 2023) 2680–2684, https://doi.org/10.1109/LAWP.2023.3291175.
[42] S. Luo, Y. Zhang, P. Mei, G.F. Pedersen, S. Zhang, Decoupling for millimeter-wave array antennas using near-field shrinking dielectric superstrate, IEEE Open Journal of Antennas and Propagation 4 (Jul. 2023) 1187–1194, https://doi.org/10.1109/OJAP.2023.3328813.
[43] What is 5G? Benefits of 5G network technology explained about verizon. https://www.verizon.com/about/our-company/5g/what-5g. (Accessed 13 June 2024).
[44] What is 5G? - how does 5G network technology work - cisco. https://www.cisco.com/c/en/us/solutions/what-is-5g.html. (Accessed 13 June 2024).
[45] What is 5G technology and how does it work? - twi. https://www.twi-global.com/technical-knowledge/faqs/what-is-5g. (Accessed 13 June 2024).
[46] 5G | definition, speed, benefits, health concerns, & conspiracy theories | britannica. https://www.britannica.com/topic/5G. (Accessed 13 June 2024).
[47] W.A. Awan, M. Alibakhshikenari, E. Limiti, Design and analysis of a simple miniaturized fractal antenna for 5G ka-band applications, in: Asia-Pacific Microwave Conference Proceedings, APMC, Institute of Electrical and Electronics Engineers Inc., 2021, pp. 22–24, https://doi.org/10.1109/APMC52720.2021.9661859.
[48] M.V. Yadav, C. Kumar R, S.V. Yadav, T. Ali, J. Anguera, A miniaturized antenna for millimeter-wave 5G-II band communication, Technologies 12 (1) (Jan. 2024), https://doi.org/10.3390/technologies12010010.
[49] M.O.F. Noman, A. Istiaque, M.A. Hossain, Design and analysis of a dual-band miniaturized rectangular patch antenna for millimeter-wave applications, in: 2022 4th International Conference on Sustainable Technologies for Industry 4.0, STI 2022, Institute of Electrical and Electronics Engineers Inc., 2022, https://doi.org/10.1109/STI56238.2022.10103233.
[50] H. Gu, An analysis of miniaturization of 5G massive MIMO base station antenna, in: *Journal Of Physics: Conference Series*, Institute of Physics, 2023, https://doi.org/10.1088/1742-6596/2419/1/012041.
[51] S. Xu, M. Zhang, H. Wen, J. Wang, Deep-subwavelength decoupling for MIMO antennas in mobile handsets with singular medium, Sci. Rep. 7 (1) (Dec. 2017), https://doi.org/10.1038/s41598-017-11281-2.
[52] A. Ghasemi, E.S. Sousa, Collaborative spectrum sensing for opportunistic access in fading environments, in: First IEEE International Symposium on New Frontiers in Dynamic Spectrum Access Networks, 2005. DySPAN 2005, Nov. 2005, pp. 131–136, https://doi.org/10.1109/DYSPAN.2005.1542627.
[53] K. Pandya, et al., Performance analysis of quad-port UWB MIMO antenna system for Sub-6 GHz 5G, WLAN and X band communications, Results in Engineering 22 (Jun) (2024), https://doi.org/10.1016/j.rineng.2024.102318.
[54] A. Morita, J. Hynes, A theoretical analysis of the sum frequency generation spectrum of the water surface, Chemical Physics - CHEM PHYS 258 (Jun. 2000) 371–390, https://doi.org/10.1016/S0301-0104(00)00127-0.
[55] R. Chowdhury, N. Mishra, M.M. Sani, R.K. Chaudhary, Analysis of a wideband circularly polarized cylindrical dielectric resonator antenna with broadside radiation coupled with simple microstrip feeding, IEEE Access 5 (Sep. 2017) 19478–19485, https://doi.org/10.1109/ACCESS.2017.2752210.
[56] Malaysian Communications and Multimedia Commission Suruhanjaya Komunikasi Dan Multimedia Malaysia Public Inquiry Allocation of Spectrum Bands for Mobile Broadband Service in Malaysia." .
[57] Md M. Sani, R. Chowdhury, R.K. Chaudhary, Design and analysis of multiple input multiple output antenna for wideband applications using cylindrical dielectric resonator, AEU - International Journal of Electronics and Communications 131 (2021) 153598, https://doi.org/10.1016/j.aeue.2020.153598.
[58] M.M. Sani, R. Chowdhury, R.K. Chaudhary, An ultra-wideband rectangular dielectric resonator antenna with MIMO configuration, IEEE Access 8 (2020) 139658–139669, https://doi.org/10.1109/ACCESS.2020.3012793.
[59] N. Makul, P. Rattanadecho, D.K. Agrawal, Applications of microwave energy in cement and concrete - a review, Renew. Sustain. Energy Rev. 37 (2014) 715–733, https://doi.org/10.1016/j.rser.2014.05.054.
[60] BfS - specific absorption rates (SAR) for mobile phones. https://www.bfs.de/EN/topics/emf/mobile-communication/protection/sar-mobil/sar-mobile-phone_node.html. (Accessed 13 June 2024).
[61] "Specific Absorption Rate (SAR) For Cell Phones: What It Means For You | Federal Communications Commission." Accessed: June. 13, 2024. [Online]. Available: https://www.fcc.gov/consumers/guides/specific-absorption-rate-sar-cell-phones-what-it-means-you.
[62] G. Ziegelberger, et al., "Guidelines for Limiting Exposure to Electromagnetic Fields (100 kHz to 300 GHz),", Lippincott Williams and Wilkins, May 01, 2020 https://doi.org/10.1097/HP.0000000000001210.
[63] R.H. Elabd, A.J.A. Al-Gburi, Low mutual coupling miniaturized dual-band quad-port MIMO antenna array using decoupling structure for 5G samrtphones, Discov Appl Sci 6 (2024) 189, https://doi.org/10.1007/s42452-024-05765-w.
[64] A. Pant, M. Singh, M. Parihar, A frequency reconfigurable/switchable MIMO antenna for LTE and early 5G applications, AEU - International Journal of Electronics and Communications 131 (Jun. 2021) 153638, https://doi.org/10.1016/j.aeue.2021.153638.
[65] Env 50166-2:1995 - human exposure to electromagnetic fields - high frequency (10 kHz to 300 GHz). https://standards.iteh.ai/catalog/standards/clc/d7d51ee2-b10d-4686-9748-53b2884f8c4d/env-50166-2-1995. (Accessed 14 June 2024).
[66] M. Abdul-Al, et al., Wireless electromagnetic radiation assessment based on the specific absorption rate (SAR): a review case study, Electronics 11 (2022) 511, https://doi.org/10.3390/ELECTRONICS11040511, 11, no. 4, p. 511, Feb. 2022.
[67] T.S. Rappaport, Wireless Communications: Principles and Practice, Prentice Hall, 1996 [Online]. Available: https://nyuscholars.nyu.edu/en/publications/wireless-communications-principles-and-practice-2. (Accessed 14 June 2024).
[68] Great Britain. National Radiological Protection Board, "Board statement on restrictions on human exposure to static and time varying electromagnetic fields and radiation.," (1993) 69. https://books.google.com/books/about/Board_Statement_on_Restrictions_on_Human.html?id=XzqQMQEACAAJ. (Accessed 14 June 2024).
[69] on N.-I. R. Hazards, IEEE Standards Coordinating Committee 28, IEEE-SA Standards Board., and Institute of Electrical and Electronics Engineers., "IEEE standard for safety levels with respect to human exposure to radio frequency electromagnetic fields, 3kHz to 300 GHz (1999) 73.
[70] C95.1-2019 - IEEE Standard for Safety Levels with Respect to Human Exposure to Electric, Magnetic, and Electromagnetic Fields, 0 Hz to 300 GHz.".
[71] R. Matthes, J.H. Bernhardt, A.F. McKinlay, International Commission on Non-Ionizing Radiation Protection, Guidelines on limiting exposure to non-ionizing radiation : a reference book based on the guidelines on limiting exposure to non-ionizing radiation and statements on special applications, 74, International Commission on Non-Ionizing Radiation Protection, 1999, p. 375.
[72] Directive 2002/44/EC of the European Parliament and of the Council of 25 June 2002 on the Minimum Health and Safety Requirements Regarding the Exposure of Workers to the Risks Arising from Physical Agents (Vibration) (Sixteenth Individual Directive within the Meaning of Article 16(1) of Directive 89/391/EEC)." .
[73] C95.1-1991 IEEE Standard for Safety Levels with Respect to Human Exposure to Radio Frequency Electromagnetic Fields, 3 kHz to 300 GHz.". .
[74] N. Azlinda Ahmad, P. Fhazleen Shaharun, SAR measurement from mobile phone and its effect to human body, vol. 22, no. 1, pp. 63–69, www.elektrika.utm.my, 2023.
[75] M.I. Hossain, M.R.I. Faruque, M.T. Islam, Investigation of hand impact on PIFA performances and SAR in human head, J. Appl. Res. Technol. 13 (4) (Aug. 2015) 447–453, https://doi.org/10.1016/J.JART.2015.09.001.
[76] A. Christ, T. Samaras, E. Neufeld, A. Klingenbock, N. Kuster, SAR distribution in human beings when using body-worn RF transmitters, Radiat Prot Dosimetry 124 (1) (Sep. 2007) 6–14, https://doi.org/10.1093/rpd/ncm377.
[77] SAR proximity sensor controls human RF exposure. https://www.engineeringspecifier.com/sensors/sar-proximity-sensor-controls-human-rf-exposure. (Accessed 22 July 2024).
[78] Localized movement sensing for SAR applications • Azoteq. https://www.azoteq.com/localized-movment-sensing-for-sar/. (Accessed 22 July 2024).
[79] M. Sole, C. Musu, F. Boi, D. Giusto, and V. Popescu, "RFID Sensor Network for Workplace Safety Management." .
[80] B. Ivsic, D. Bonefacic, J. Bartolic, Coupling between Antenna and Human Body — Design Issues, Jul. 2018, pp. 1–4, https://doi.org/10.23919/SMAGRIMET.2018.8369840.
[81] W.-T. Chen, H.-R. Chuang, Human body coupling effects on radiation characteristics of superquadric loop antennas for pagers' application, IEEE Antennas and Propagation Society International Symposium 1997. Digest 2 (1997) 1190–1193, https://doi.org/10.1109/APS.1997.631773.
[82] 5G SAR testing: what you need to know - RF exposure lab. https://www.rfexposurelab.com/5g-sar-testing-what-to-know/. (Accessed 23 July 2024).
[83] Cell phone SAR testing regulations - RF exposure lab. https://www.rfexposurelab.com/cell-phone-sar-testing-regulations/. (Accessed 23 July 2024).
[84] T. Ramachandran, M.R.I. Faruque, A.M. Siddiky, M.T. Islam, Reduction of 5G cellular network radiation in wireless mobile phone using an asymmetric square shaped passive metamaterial design, Sci. Rep. 11 (1) (2021), https://doi.org/10.1038/s41598-021-82105-7, 11, no. 1, pp. 1–22, Jan. 2021.
[85] M. Abdul-Al, et al., Wireless electromagnetic radiation assessment based on the specific absorption rate (SAR): a review case study, Electronics (Switzerland) 11 (4) (Feb. 2022), https://doi.org/10.3390/ELECTRONICS11040511.
[86] ANFR-SAR and market surveillance. https://www.anfr.fr/en/maitriser/radio-equipment/specific-absorption-rate-sar/sar-and-market-surveillance. (Accessed 23 July 2024).
[87] T.S. Bird, Mutual coupling between antennas, Mutual Coupling Between Antennas (Jan. 2021) 1–455, https://doi.org/10.1002/9781119565048.
[88] Antenna coupling, mutual coupling. https://www.antenna-theory.com/definitions/mutualcoupling.php. (Accessed 1 June 2024).

[89] B. Virdee, Grand challenges in metamaterial antennas, Frontiers in Antennas and Propagation 1 (2022), https://doi.org/10.3389/fanpr.2022.1032205. Nov.
[90] Z. Wang, L. Zhao, Y. Cai, S. Zheng, Y. Yin, A meta-surface antenna array decoupling (MAAD) method for mutual coupling reduction in a MIMO antenna system, Sci. Rep. 8 (1) (Dec. 2018), https://doi.org/10.1038/s41598-018-21619-z.
[91] S.J.P. Callens, C.H. Arns, A. Kuliesh, A.A. Zadpoor, Decoupling minimal surface metamaterial properties through multi-material hyperbolic tilings, Adv. Funct. Mater. 31 (30) (2021) 2101373, https://doi.org/10.1002/adfm.202101373.
[92] Z. Wang, L. Zhao, Y. Cai, S. Zheng, Y. Yin, A meta-surface antenna array decoupling (MAAD) method for mutual coupling reduction in a MIMO antenna system, Sci. Rep. 8 (1) (Dec. 2018), https://doi.org/10.1038/s41598-018-21619-z.
[93] B. Virdee, Grand challenges in metamaterial antennas, Frontiers in Antennas and Propagation 1 (Nov) (2022), https://doi.org/10.3389/fanpr.2022.1032205.
[94] K. Du, Y. Wang, Y. Hu, Design and Analysis on Decoupling Techniques for MIMO Wireless Systems in 5G Applications, MDPI, Apr. 01, 2022, https://doi.org/10.3390/app12083816.
[95] K. Du, Y. Wang, Y. Hu, Design and Analysis on Decoupling Techniques for MIMO Wireless Systems in 5G Applications, MDPI, Apr. 01, 2022, https://doi.org/10.3390/app12083816.
[96] O. Sokunbi and A. Kishk, "Millimeter-Wave MIMO Antenna with Decoupling Structures for Isolation Enhancement." .
[97] S. Iriqat, S. Yenikaya, M. Secmen, Dual-band 2 × 1 monopole antenna array and its MIMO configuration for WiMAX, sub-6 GHz, and sub-7 GHz applications, Electronics (Switzerland) 13 (8) (Apr. 2024), https://doi.org/10.3390/electronics13081502.
[98] H.M. Marzouk, M.I. Ahmed, A.A. Shaalan, Novel Dual-Band 28/38 GHz MIMO Antennas for 5G Mobile Applications, 2019.
[99] S. Dey, S. Dey, S.K. Koul, Isolation improvement of MIMO antenna using novel EBG and hair-pin shaped DGS at 5G millimeter wave band, IEEE Access 9 (2021) 162820–162834, https://doi.org/10.1109/ACCESS.2021.3133324.
[100] P.B. Nikam, J. Kumar, V. Sivanagaraju, A. Baidya, Dual-band reconfigurable EBG loaded circular patch MIMO antenna using defected ground structure (DGS) and PIN diode integrated branch-lines (BLs), Measurement 195 (May 2022) 111127, https://doi.org/10.1016/j.measurement.2022.111127.
[101] W. Wang, Y. Wu, W. Wang, Y. Yang, Isolation enhancement in dual-band monopole antenna for 5G applications, IEEE Transactions on Circuits and Systems II: Express Briefs 68 (6) (Jun. 2021) 1867–1871, https://doi.org/10.1109/TCSII.2020.3040164.
[102] C. Munusami, R. Venkatesan, A compact boat shaped dual-band MIMO antenna with enhanced isolation for 5G/WLAN application, IEEE Access 12 (2024) 11631–11641, https://doi.org/10.1109/ACCESS.2024.3356078.
[103] M. Munde, A. Nandgaonkar, S. Deosarkar, Performance Optimization of Dual-Feed UWB Annular Ring Antenna with Circular DGS and EBG for SAR Reduction, 2021.
[104] K. Chand Ravi, J. Kumar, T.A. Elwi, M. Mahdi Ali, Compact MIMO antenna for 5G applications, in: 2022 IEEE ANDESCON: Technology and Innovation for Andean Industry, ANDESCON 2022, Institute of Electrical and Electronics Engineers Inc., 2022, https://doi.org/10.1109/ANDESCON56260.2022.9989598.
[105] M. Khalid, et al., 4-port MIMO antenna with defected ground structure for 5G millimeter wave applications, Electronics (Switzerland) 9 (1) (Jan. 2020), https://doi.org/10.3390/electronics9010071.
[106] K. Cuneray, N. Akcam, T. Okan, G.O. Arican, 28/38 GHz dual-band MIMO antenna with wideband and high gain properties for 5G applications, AEU - International Journal of Electronics and Communications 162 (2023), https://doi.org/10.1016/j.aeue.2023.154553. Apr.
[107] B. Aghoutane, S. Das, M. EL Ghzaoui, B.T.P. Madhav, H. El Faylali, A novel dual band high gain 4-port millimeter wave MIMO antenna array for 28/37 GHz 5G applications, AEU - International Journal of Electronics and Communications 145 (2022), https://doi.org/10.1016/j.aeue.2021.154071. Feb.
[108] C. Güler, S.E. Bayer Keskin, A novel high isolation 4-port compact MIMO antenna with DGS for 5G applications, Micromachines 14 (7) (Jul. 2023), https://doi.org/10.3390/mi14071309.
[109] M.A. Abbas, A. Allam, A. Gaafar, H.M. Elhennawy, M.F.A. Sree, Compact UWB MIMO antenna for 5G millimeter-wave applications, Sensors 23 (5) (Mar. 2023), https://doi.org/10.3390/s23052702.
[110] S.Y.A. Fatah, E.K.I. Hamad, W. Swelam, A.M.M.A. Allam, H.A. Mohamed, Design of compact 4-port mimo antenna based on minkowski fractal shape dgs for 5g applications, Prog. Electromagn. Res. C 113 (2021) 123–136, https://doi.org/10.2528/PIERC21042703.
[111] M. Bilal, S.I. Naqvi, N. Hussain, Y. Amin, N. Kim, High-isolation MIMO antenna for 5G millimeter-wave communication systems, Electronics (Switzerland) 11 (6) (Mar. 2022), https://doi.org/10.3390/electronics11060962.
[112] A. Baz, D. Jansari, S.P. Lavadiya, S.K. Patel, Miniaturized and high gain circularly slotted 4×4 MIMO antenna with diversity performance analysis for 5G/Wi-Fi/WLAN wireless communication applications, Results in Engineering 20 (2023), https://doi.org/10.1016/j.rineng.2023.101505. Dec.
[113] A.P. Abhilash, P. Thomas, K.K. Indhu, K. Neema, R. Anil Kumar, C.K. Aanandan, Four-Element Compact and Dual-Band MIMO Antenna with Self-Decoupled Mechanism for 5G Applications, 2022.
[114] M.A. Nassar, H.Y. Soliman, R.M. Abdallah, E.A.F. Abdallah, Improving Mutual Coupling in MIMO Antennas Using Different Techniques, 2023.
[115] S.S. Khade, D.B. Bhoyar, K. Kotpalliwar, C.V. Bawankar, M.S. Kimmatkar, Four element EC slot MIMO antenna for WLAN, wi-fi, and 5G applications, Prog. Electromagn. Res. C 139 (2024) 147–158, https://doi.org/10.2528/PIERC23082201.
[116] A.A. Megahed, M. Abdelazim, E.H. Abdelhay, H.Y.M. Soliman, Sub-6 GHz highly isolated wideband MIMO antenna arrays, IEEE Access 10 (2022) 19875–19889, https://doi.org/10.1109/ACCESS.2022.3150278.
[117] G. Ramyasree, N. Suman, Dual-Band 4-Port Vivaldi MIMO Antenna for 5G mmWave Applications at 28/39 GHz, 2023.
[118] G. Ramyasree, N. Suman, Compact 4-Port Vivaldi MIMO Antenna for 5G Wireless Devices, 2023.
[119] A.M. Hediya, A.M. Attiya, W.S. El-Deeb, Multiple-Input Multiple-Output Antenna for Sub-six GHz 5G Applications Using Coupled Folded Antenna with Defective Ground Surface, 2021.
[120] P. Kumar, et al., Design of a six-port compact UWB MIMO antenna with a distinctive DGS for improved isolation, IEEE Access 10 (2022) 112964–112974, https://doi.org/10.1109/ACCESS.2022.3216889.
[121] Y.Q. Hei, J.G. He, W.T. Li, Wideband decoupled 8-element MIMO antenna for 5G mobile terminal applications, IEEE Antennas Wirel Propag Lett 20 (8) (Aug. 2021) 1448–1452, https://doi.org/10.1109/LAWP.2021.3086261.
[122] S. Dey, S. Dey, Wideband highly efficient eight element MIMO antenna using differential fed open end slot for sub-7 GHz 5G mobile handset applications, IEEE Transactions on Circuits and Systems II: Express Briefs (2024), https://doi.org/10.1109/TCSII.2024.3374729.
[123] T. He, J. Huang, J. Lu, X. Shi, G. Liu, Eight-element dual-band multiple-input multiple-output mobile phone antenna for 5G and wireless local area network applications, Micromachines 14 (12) (Dec. 2023), https://doi.org/10.3390/mi14122200.
[124] H.S. Abubakar, Z. Zhao, S.H. Kiani, U. Rafique, E. Alabdulkreem, H. Elmannai, Eight element dual-band MIMO array antenna for modern fifth generation mobile phones, AEU - International Journal of Electronics and Communications 175 (Feb) (2024), https://doi.org/10.1016/j.aeue.2023.155083.
[125] C. Antennas, Propagation Society. International Symposium 2017 San Diego, IEEE antennas and propagation society, Institute of electrical and electronics engineers, calif, in: IEEE Antennas and Propagation Society International Symposium 2017.07.09-14 San Diego, Calif. IEEE International Symposium on Antennas and Propagation 2017.07.09-14 San Diego, and Calif. AP-S Symposium 2017.07.09-14 San Diego, IEEE Antennas and Propagation Society International Symposium proceedings : July 9-14, 2017, Manchester Grand Hyatt, San Diego, California, USA, 2017.
[126] M. Amiri, A. Ghafoorzadeh-Yazdi, A.A. Heidari, A compact 5G-MIMO antenna with reduced mutual coupling, in: 2023 31st International Conference on Electrical Engineering, ICEE 2023, Institute of Electrical and Electronics Engineers Inc., 2023, pp. 351–355, https://doi.org/10.1109/ICEE59167.2023.10334641.
[127] P. Kumar, et al., High isolated defected ground structure based elliptical shape dual element MIMO antenna for S-band applications, Prog. Electromagn. Res. C 143 (2024) 67–74, https://doi.org/10.2528/PIERC24031304.
[128] S. Ghosh, G.S. Baghel, M.V. Swati, Design of a highly-isolated, high-gain, compact 4-port MIMO antenna loaded with CSRR and DGS for millimeter wave 5G communications, AEU - International Journal of Electronics and Communications 169 (Sep) (2023), https://doi.org/10.1016/j.aeue.2023.154721.
[129] R.H. Elabd, A.J.A. Al-Gburi, Ultra-Compact 4-Port MIMO Antenna with Defected Ground Structure and SAR Analysis for 28/38 GHz 5G Mobile Devices, J Electromagn Waves Appl, May 2024, pp. 1–26, https://doi.org/10.1080/09205071.2024.2354716.
[130] A. Kumar, J. Mohanty, P. Pattanayak, D. Sabat, G. Prasad, Six-port mid-bands Low-SAR MIMO antenna for WLAN, 5G mobile terminals, and C-band applications, AEU - International Journal of Electronics and Communications 166 (Jul) (2023), https://doi.org/10.1016/j.aeue.2023.154665.
[131] A. Khan, A. Wakeel, L. Qu, Z. Zahid, Dual-band 8 × 8 MIMO antenna with enhanced isolation and efficiency for 5G smartphone applications, AEU - International Journal of Electronics and Communications 163 (May 2023), https://doi.org/10.1016/j.aeue.2023.154600.
[132] S.H. Kiani, et al., Dual-polarized wideband 5G N77 band slotted MIMO antenna system for next-generation smartphones, IEEE Access 12 (2024) 34467–34476, https://doi.org/10.1109/ACCESS.2024.3370860.
[133] Y. Fawad, et al., Dual-polarized 8-port sub 6 GHz 5G MIMO diamond-ring slot antenna for smart phone and portable wireless applications, PLoS One 18 (11 November) (Nov. 2023), https://doi.org/10.1371/journal.pone.0288793.
[134] H. Ali, et al., An eight element dual band antenna for future 5g smartphones, Electronics (Switzerland) 10 (23) (Dec. 2021), https://doi.org/10.3390/electronics10233022.
[135] P. Kovács and T. Urbanec, "Electromagnetic Band Gap Structures: Practical Tips and Advice for Antenna Engineers". .
[136] D.M.N. Elsheakh, H.A. Elsadek, E.A. Abdallah, Antenna designs with electromagnetic band gap structures [Online]. Available: www.intechopen.com. (Accessed 3 June 2024).
[137] A.J.A. Al-Gburi, 5G MIMO antenna: compact design at 28/38 GHz with metamaterial and SAR analysis for mobile phones, Przeglad Elektrotechniczny 2024 (4) (2024) 171–174, https://doi.org/10.15199/48.2024.04.32.
[138] G. Expósito-Domínguez, J. Manuel Fernández-González, P. Padilla, and M. Sierra-Castañer, "New EBG Solutions for Mutual Coupling Reduction." .
[139] R.H. Elabd, A.A. Megahed, Isolation enhancement of a two- orthogonal printed elliptical slot MIMO antenna array with EBG structure for millimeter wave 5G applications, Discover Applied Sciences 6 (5) (May 2024), https://doi.org/10.1007/s42452-024-05881-7.

[140] R.H. Elabd, A.A. Megahed, Isolation enhancement of a two- orthogonal printed elliptical slot MIMO antenna array with EBG structure for millimeter wave 5G applications, Discover Applied Sciences 6 (5) (May 2024), https://doi.org/10.1007/s42452-024-05881-7.
[141] R. Aloui, et al., Planar wide-band MIMO antenna using a modified EBG structure, in: 20th SBMO/IEEE MTT-S International Microwave and Optoelectronics Conference, IMOC 2023, Institute of Electrical and Electronics Engineers Inc., 2023, pp. 322–324, https://doi.org/10.1109/IMOC57131.2023.10379714.
[142] A.I. Afifi, A.S. Abd El-Hameed, A. Allam, S.M. Ahmed, A.B. Abdel-Rahman, Dual port MIMO antenna with low mutual coupling based on asymmetric EBG decoupling structure, in: 15th European Conference on Antennas and Propagation, EuCAP 2021, Institute of Electrical and Electronics Engineers Inc., Mar. 2021, https://doi.org/10.23919/EuCAP51087.2021.9411149.
[143] K.S.L. Parvathi, S.R. Gupta, Novel dual-band EBG structure to reduce mutual coupling of air gap based MIMO antenna for 5G application, AEU - International Journal of Electronics and Communications 138 (2021), https://doi.org/10.1016/j.aeue.2021.153902. Aug.
[144] A. Khan, S. Bashir, S. Ghafoor, K.K. Qureshi, Mutual coupling reduction using ground stub and EBG in a compact wideband MIMO-antenna, IEEE Access 9 (2021) 40972–40979, https://doi.org/10.1109/ACCESS.2021.3065441.
[145] E.L.M. Wissem, I. Sfar, L. Osman, J.M. Ribero, A textile EBG-based antenna for future 5G-IoT millimeter-wave applications, Electronics (Switzerland) 10 (2) (Jan. 2021) 1–12, https://doi.org/10.3390/electronics10020154.
[146] K. Sharma, G.P. Pandey, Two Port Compact MIMO Antenna for ISM Band Applications, 2020.
[147] Z. Yang, J. Xiao, Q. Ye, Enhancing MIMO antenna isolation characteristic by manipulating the propagation of surface wave, IEEE Access 8 (2020) 115572–115581, https://doi.org/10.1109/ACCESS.2020.3004467.
[148] P.R.T. Naidu, C. Saha, K. Vamshi Krishna, L.A. Shaik, J.Y. Siddiqui, Y. Antar, Compact multiple EBG cells loaded UWB-narrowband antenna pair with high isolation for cognitive radio (CR) based MIMO applications, AEU - International Journal of Electronics and Communications 127 (Dec. 2020), https://doi.org/10.1016/j.aeue.2020.153420.
[149] H.N. Chen, J.M. Song, J.D. Park, A compact circularly polarized MIMO dielectric resonator antenna over electromagnetic band-gap surface for 5G applications, IEEE Access 7 (2019) 140889–140898, https://doi.org/10.1109/ACCESS.2019.2943880.
[150] T.A. Elwi, et al., On the performance of a photonic reconfigurable electromagnetic band gap antenna array for 5G applications, IEEE Access 12 (2024) 60849–60862, https://doi.org/10.1109/ACCESS.2024.3392368.
[151] M.A.T. Sakib, M.R. Islam, M.S. Islam, G.M. Asadullah, M.S.R. Bashri, Design of quad element MIMO array with EBG structure for mutual coupling reduction, in: Proceedings of the 9th International Conference on Computer and Communication Engineering, ICCCE 2023, Institute of Electrical and Electronics Engineers Inc., 2023, pp. 405–409, https://doi.org/10.1109/ICCCE58854.2023.10246046.
[152] G. Tamminaina, R. Manikonda, Investigation on Performance of Four Port MIMO Antenna Using Electromagnetic Band Gap for 5G Communication, 2023.
[153] A.A. Megahed, M. Abdelazim, E.H. Abdelhay, H.Y.M. Soliman, Sub-6 GHz highly isolated wideband MIMO antenna arrays, IEEE Access 10 (2022) 19875–19889, https://doi.org/10.1109/ACCESS.2022.3150278.
[154] A.K.M.Z. Hossain, N. Bin Hassim, W.H.W. Hassan, W.A. Indra, S.G. Herawan, M.Z. A.B.A. Aziz, A planar 2×2 MIMO antenna array for 5G smartphones, Int. J. Adv. Comput. Sci. Appl. 12 (7) (2021) 710–717, https://doi.org/10.14569/IJACSA.2021.0120781.
[155] A.M. Hediya, A.M. Attiya, W.S. El-Deeb, 5G MIMO Antenna System Based on Patched Folded Antenna with EBG Substrate, 2022.
[156] N. Suresh Babu, A.Q. Ansari, S. Kumar, B.K. Kanaujia, G. Singh, B. Goyal, Octa-Port High Gain MIMO Antenna Backed with EBG for Mm-Wave Applications, 2023.
[157] B. Kumkhet, et al., SAR reduction using dual band EBG method based on MIMO wearable antenna for WBAN applications, AEU - International Journal of Electronics and Communications 160 (2023), https://doi.org/10.1016/j.aeue.2022.154525. Feb.
[158] P.B. Nikam, J. Kumar, V. Sivanagaraju, A. Baidya, Dual-band reconfigurable EBG loaded circular patch MIMO antenna using defected ground structure (DGS) and PIN diode integrated branch-lines (BLs), Measurement 195 (May 2022), https://doi.org/10.1016/j.measurement.2022.111127.
[159] R.H. Elabd, A.J.A. Al-Gburi, Super-compact 28/38 GHz 4-port MIMO antenna using metamaterial-inspired EBG structure with SAR analysis for 5G cellular devices, J. Infrared, Millim. Terahertz Waves 45 (1–2) (Feb. 2024) 35–65, https://doi.org/10.1007/s10762-023-00959-6.
[160] H. Nornikman, B. H. Ahmad, M. Z. A. A. Aziz, A. R. Othman, and F. Malek, "Split Ring Resonator Structure on Microstrip Patch Antenna and Other Microwave Application Design: A Review." .
[161] X. Zhao, Y. Lee, J. Choi, Design of a compact patch antenna using split-ring resonator embedded substrate, Microw. Opt. Technol. Lett. 53 (12) (Dec. 2011) 2786–2790, https://doi.org/10.1002/MOP.26411.
[162] K.B. Alici, E. Ozbay, Electrically small split ring resonator antennas, J. Appl. Phys. 101 (8) (2007), https://doi.org/10.1063/1.2722232.
[163] O.S. Kim, O. Breinbjerg, Miniaturized self-resonant split-ring resonator antenna, Electron. Lett. 12 (4) (2009) 196–197.
[164] A. Christina, J. Malathi, B. Vamsi, K. Reddy, K.R. Phanindra, A Decoupling Method Using Split Ring Resonator (SRR) for Tri-band MIMO Antenna for WLAN LTE Band and 5G Applications, 2024.
[165] H. Nornikman, B. H. Ahmad, M. Z. A. A. Aziz, A. R. Othman, and F. Malek, "Split Ring Resonator Structure on Microstrip Patch Antenna and Other Microwave Application Design: A Review." .
[166] R. Sharma, Geetanjali, R. Khanna, Metamaterial loaded wideband highly isolated compact 2 × 1 MIMO antenna for mmWave applications, in: International Conference on Distributed Computing and Optimization Techniques, ICDCOT 2024, Institute of Electrical and Electronics Engineers Inc., 2024, https://doi.org/10.1109/ICDCOT61034.2024.10515996.
[167] D. Khan, A. Ahmad, D.Y. Choi, Dual-band 5G MIMO antenna with enhanced coupling reduction using metamaterials, Sci. Rep. 14 (1) (Dec. 2024), https://doi.org/10.1038/s41598-023-50446-0.
[168] I.U. Din, S. Ullah, N. Mufti, R. Ullah, B. Kamal, R. Ullah, Metamaterial-based highly isolated MIMO antenna system for 5G smartphone application, Int. J. Commun. Syst. 36 (3) (Feb. 2023), https://doi.org/10.1002/dac.5392.
[169] B. Ali Esmail, S. Koziel, High isolation metamaterial-based dual-band MIMO antenna for 5G millimeter-wave applications, AEU - International Journal of Electronics and Communications 158 (Jan) (2023), https://doi.org/10.1016/j.aeue.2022.154470.
[170] L. Chouikhi, C. Essid, H. Sakli, B. Ben Salah, Metamaterial Decoupling MIMO Antennas for 5G Communication 1 St Linda CHOUIKHI, 2021.
[171] H. Sakli, C. Abdelhamid, C. Essid, N. Sakli, Metamaterial-based antenna performance enhancement for MIMO system applications, IEEE Access 9 (2021) 38546–38556, https://doi.org/10.1109/ACCESS.2021.3063630.
[172] G. Singh, et al., Frequency reconfigurable quad-element MIMO antenna with improved isolation for 5G systems, Electronics (Switzerland) 12 (4) (Feb. 2023), https://doi.org/10.3390/electronics12040796.
[173] J.A. Tirado-Mendez, et al., Metamaterial split-ring resonators applied as reduced-size four-port antenna array for MIMO applications, AEU - International Journal of Electronics and Communications 154 (2022), https://doi.org/10.1016/j.aeue.2022.154338. Sep.
[174] V. Rajeshkumar, R. Rajkumar, SRR Loaded Compact Tri-band MIMO Antenna for WLAN/WiMAX Applications, 2021.
[175] A. Khan, Y. He, Z.N. Chen, An eight-port circularly polarized wideband MIMO antenna based on a metamaterial-inspired element for 5G mmWave applications, IEEE Antennas Wirel Propag Lett 22 (7) (Jul. 2023) 1572–1576, https://doi.org/10.1109/LAWP.2023.3251740.
[176] J. Huang, L. Shen, S. Xiao, X. Shi, G. Liu, A miniature eight-port antenna array based on split-ring resonators for 5G sub-6 GHz handset applications, Sensors 23 (24) (Dec. 2023), https://doi.org/10.3390/s23249734.
[177] A. Christina, J. Malathi, B. Vamsi, K. Reddy, K.R. Phanindra, A Decoupling Method Using Split Ring Resonator (SRR) for Tri-band MIMO Antenna for WLAN LTE Band and 5G Applications, 2024.
[178] J. Zhang, S. Yan, X. Hu, G.A.E. Vandenbosch, Mutual coupling suppression for on-body multiantenna systems, IEEE Trans Electromagn Compat 62 (4) (Aug. 2020) 1045–1054, https://doi.org/10.1109/TEMC.2019.2936679.
[179] T. Saeidi, et al., High gain triple-band metamaterial-based antipodal vivaldi mimo antenna for 5g communications, Micromachines 12 (3) (Mar. 2021) 1–25, https://doi.org/10.3390/mi12030250.
[180] A. Ennajih, A. Sardi, Y. Mouzouna, M. Sadik, A. Errkik, Design of a novel compact low specific absorption rate multiple input multiple output antenna for 5G sub-6 GHz terminals, Bulletin of Electrical Engineering and Informatics 13 (3) (Jun. 2024) 1602–1612, https://doi.org/10.11591/eei.v13i3.6658.
[181] K. Du, Y. Wang, Y. Hu, Design and Analysis on Decoupling Techniques for MIMO Wireless Systems in 5G Applications, MDPI, Apr. 01, 2022, https://doi.org/10.3390/app12083816.
[182] T. Wu, J. Wang, Neutralization-line-based decoupling for miniaturized MIMO antenna array, Microw. Opt. Technol. Lett. 65 (May 2022), https://doi.org/10.1002/mop.33546 n/a-n/a.
[183] R. Liu, X. An, H. Zheng, M. Wang, Z. Gao, E. Li, Neutralization line decoupling tri-band multiple-input multiple-output antenna design, IEEE Access 8 (2020) 27018–27026, https://doi.org/10.1109/ACCESS.2020.2971038.
[184] M. Li, L. Jiang, K.L. Yeung, A general and systematic method to design neutralization lines for isolation enhancement in MIMO antenna arrays, IEEE Trans. Veh. Technol. 69 (6) (Jun. 2020) 6242–6253, https://doi.org/10.1109/TVT.2020.2984044.
[185] A. Dkiouak, M. El Ouahabi, S. Chakkor, M. Baghouri, A. Zakriti, Y. Lagmich, High Performance UWB MIMO Antenna by Using Neutralization Line Technique, 2023.
[186] P. Jha, A. Kumar, D. Sahu, N. Sharma, Isolation enhancement of two element MIMO antenna based on neutralization technique, in: 2023 3rd International Conference on Advancement in Electronics and Communication Engineering, AECE 2023, Institute of Electrical and Electronics Engineers Inc., 2023, pp. 355–359, https://doi.org/10.1109/AECE59614.2023.10428468.
[187] D. Saxena, A. Kumar, R.K. Verma, P. Jha, Metamaterial inspired dual band MIMO antenna with open-ended slot and neutralized line for isolation enhancement, in: Proceedings of the 10th International Conference on Signal Processing and Integrated Networks, SPIN 2023, Institute of Electrical and Electronics Engineers Inc., 2023, pp. 727–732, https://doi.org/10.1109/SPIN57001.2023.10117256.
[188] Z. Wang, W. Mu, M. Yang, C. Li, Design of compact multiband MIMO antenna based on ground neutralization line decoupling, Appl. Comput. Electromagn. Soc. J. 37 (6) (Jun. 2022) 702–715, https://doi.org/10.13052/2022.ACES.J.370606.
[189] P. Sharma, R.N. Tiwari, P. Singh, B.K. Kanaujia, Dual-band trident shaped MIMO antenna with novel ground plane for 5G applications, AEU - International Journal of Electronics and Communications 155 (Oct) (2022), https://doi.org/10.1016/j.aeue.2022.154364.
[190] K.N. Patil, G. Akshay, T. Chaitanya, A.K. Dwivedi, N.K. Narayanaswamy, V. Singh, A two-element MIMO antenna with a small footprint for 5G

connectivity, in: Proceedings of 2022 Workshop on Microwave Theory and Techniques in Wireless Communications, MTTW 2022, Institute of Electrical and Electronics Engineers Inc., 2022, pp. 110–113, https://doi.org/10.1109/MTTW56973.2022.9942621.
[191] I.S. Masoodi, I. Ishteyaq, K. Muzaffar, Extra Compact Two Element Sub 6 GHz MIMO Antenna for Future 5G Wireless Applications, 2022.
[192] A.H. Mousa, M.A. Bin Othman, M.Z. Abidin, A.M. Ibrahim, Fractalh-Vicsek MIMO antenna for 5g communications, Przeglad Elektrotechniczny 1 (6) (2021) 15–20, https://doi.org/10.15199/48.2021.06.03.
[193] C. Du, Z. Zhao, X. Wang, F. Yang, A Compact CPW-Fed Triple-Band MIMO Antenna with Neutralization Line Decoupling for WLAN/WiMAX/5G Applications, 2021.
[194] S. Naga Jyothi Sree Gorre, Nelaturi, Semi-circular MIMO patch antenna using the neutralization line technique for UWB applications, in: V.V. S. S. S, A. J, S. S. C, B. V. Chowdary, P. Satish Rama, Chakravarthy (Eds.), Microelectronics, Electromagnetics and Telecommunications, Springer Singapore, Singapore, 2021, pp. 175–182.
[195] A. Saleh, et al., Mutual coupling reduction of dual-band uni-planar MIMO system using neutralization line technique [Online]. Available: https://www.researchgate.net/publication/344508933, 2020.
[196] P. Mondal, D. Dhara, A.R. Harish, Throughput enhancement of 2\times 2 MIMO system using a novel wideband neutralization line, in: 2020 IEEE International Symposium on Antennas and Propagation and North American Radio Science Meeting, IEEECONF 2020 - Proceedings, Institute of Electrical and Electronics Engineers Inc., Jul. 2020, pp. 1671–1672, https://doi.org/10.1109/IEEECONF35879.2020.9329707.
[197] R. Liu, X. An, H. Zheng, M. Wang, Z. Gao, E. Li, Neutralization line decoupling tri-band multiple-input multiple-output antenna design, IEEE Access 8 (2020) 27018–27026, https://doi.org/10.1109/ACCESS.2020.2971038.
[198] N. Srivastava, P.K. Rao, R. Mishra, Decoupling function for UWB MIMO antenna to enhance bandwidth with neutralization line, in: 2019 IEEE 5th International Conference for Convergence in Technology (I2CT), IEEE, Mar. 2019, pp. 1–3, https://doi.org/10.1109/I2CT45611.2019.9033787.
[199] Y.-T. Chen, Q.-X. Chu, H.-L. Xu, Two-Antenna Array with T-Shaped Neutralization Line for 5G Wideband Application, 2019.
[200] T. Wu, M.J. Wang, J. Chen, Decoupling of MIMO antenna array based on half-mode substrate integrated waveguide with neutralization lines, AEU - International Journal of Electronics and Communications 157 (Dec) (2022), https://doi.org/10.1016/j.aeue.2022.154416.
[201] I. Rosaline, A. Kumar, P. Upadhyay, A.H. Murshed, Four element MIMO antenna systems with decoupling lines for high-speed 5G wireless data communication, Int. J. Antenn. Propag. 2022 (2022), https://doi.org/10.1155/2022/9078929.
[202] Y.Y. Chen, Q.X. Chu, J.F. Bian, A 4-element MIMO antenna with grounded neutralization line for 5G application, in: 13th International Symposium on Antennas, Propagation and EM Theory, ISAPE 2021 - Proceedings, Institute of Electrical and Electronics Engineers Inc., 2021, https://doi.org/10.1109/ISAPE54070.2021.9753425.
[203] E. Fritz-Andrade, R. Gómez-Villanueva, J. Alfredo Tirado-Méndez, L. Alberto Vasquez-Toledo, A. Rangel-Merino, H. Jardón-Aguilar, Broadband Four Elements PIFA Array for Access-Point MIMO Systems, 2020.
[204] J.-F. Bian, Q.-X. Chu, A compact high-isolation MIMO antenna with coupling neutralization line, in: 2020 9th Asia-Pacific Conference on Antennas and Propagation (APCAP), IEEE, Aug. 2020, pp. 1–3, https://doi.org/10.1109/APCAP50217.2020.9245933.
[205] R.N. Tiwari, P. Singh, B.K. Kanaujia, K. Srivastava, Neutralization technique based two and four port high isolation MIMO antennas for UWB communication, AEU - International Journal of Electronics and Communications 110 (Oct. 2019), https://doi.org/10.1016/j.aeue.2019.152828.
[206] M. Singh, M.S. Parihar, A compact 4×4 MIMO antenna with high isolation for 5G application, in: 2019 IEEE Asia-Pacific Microwave Conference (APMC), IEEE, Dec. 2019, pp. 688–690, https://doi.org/10.1109/APMC46564.2019.9038359.
[207] Z. Yu, M. Wang, Y. Xie, An Improved Loop Ultra-wideband MIMO Antenna System for 5G Mobile Terminals, 2020.
[208] D. Serghiou, M. Khalily, V. Singh, A. Araghi, R. Tafazolli, Sub-6 GHz dual-band 8 × 8 MIMO antenna for 5G smartphones, IEEE Antennas Wirel Propag Lett 19 (9) (Sep. 2020) 1546–1550, https://doi.org/10.1109/LAWP.2020.3008962.
[209] X. Cao, Y. Xia, L. Wu, X. Wu, Tri-band MIMO antenna design based on characteristic modes manipulation, AEU - International Journal of Electronics and Communications 155 (Oct. 2022), https://doi.org/10.1016/j.aeue.2022.154318.
[210] W. Jiang, B. Liu, Y. Cui, W. Hu, High-isolation eight-element MIMO array for 5G smartphone applications, IEEE Access 7 (2019) 34104–34112, https://doi.org/10.1109/ACCESS.2019.2904647.
[211] W. Hu, et al., Dual-band ten-element MIMO array based on dual-mode IFAs for 5G terminal applications, IEEE Access 7 (2019) 178476–178485, https://doi.org/10.1109/ACCESS.2019.2958745.
[212] W.-J. Wu, Y.-F. Cheng, G. Wang, Enhancement of antenna decoupling bandwidth by utilizing common and differential modes cancellation, Microw. Opt. Technol. Lett. 65 (6) (2023) 1710–1718, https://doi.org/10.1002/mop.33603.
[213] S. Salama, K. Solbach, Parasitic Elements Based Decoupling Technique for Monopole Four Square Array Antenna, Jul. 2014.
[214] Q.Q. Phung, T.H. Nguyen, N. Michishita, H. Sato, Y. Koyanagi, H. Morishita, A study on decoupling method for two PIFAs using parasitic elements and bridge line, IEICE Trans. Commun. E104B (6) (2021) 630–638, https://doi.org/10.1587/transcom.2020EBP3048.
[215] W. Wu, R. Zhi, Y. Chen, H. Li, Y. Tan, G. Liu, A Compact Multiband MIMO Antenna for IEEE 802.11 A/b/g/n Applications, 2019.
[216] C.Y.D. Sim, V. Dhasarathan, T.K. Tran, J. Kulkarni, B.A. Garner, Y. Li, Mutual coupling reduction in dual-band MIMO antenna using parasitic dollar-shaped structure for modern wireless communication, IEEE Access 11 (2023) 5617–5628, https://doi.org/10.1109/ACCESS.2023.3235761.
[217] V. Sorathiya, A.G. Alharbi, S. Lavadiya, Design and investigation of unique shaped low-Profile material-based superlative two-element printed ultrawideband MIMO antenna for Zigbee/WiFi/5G/WiMAX applications, Alex. Eng. J. 64 (Feb. 2023) 813–831, https://doi.org/10.1016/j.aej.2022.10.051.
[218] V.N.K.R. Devana, N. Radha, P. Sunitha, F.N. Alsunaydih, F. Alsaleem, K. Alhassoon, Compact MIMO UWB antenna integration with Ku band for advanced wireless communication applications, Helliyon 10 (5) (Mar. 2024), https://doi.org/10.1016/j.heliyon.2024.e27393.
[219] H.T. Chou, B.A. Liu, S.C. Chen, Y.J.E. Chen, Dual-band dual-polarized microstrip patch antenna with parasitic elements for 5G antenna-in-package design at millimeter-wave frequencies, IEEE Trans Compon Packaging Manuf Technol 13 (11) (Nov. 2023) 1778–1789, https://doi.org/10.1109/TCPMT.2023.3321610.
[220] H. Yon, et al., Development of c-shaped parasitic mimo antennas for mutual coupling reduction, Electronics (Switzerland) 10 (19) (Oct. 2021), https://doi.org/10.3390/electronics10192431.
[221] U.A. Patil, A.B. Kakade, A.U. Patil, Low cross-polarization high-isolation 2-element MIMO antenna for unmanned aerial vehicle, AEU - International Journal of Electronics and Communications 177 (Apr) (2024), https://doi.org/10.1016/j.aeue.2024.155164.
[222] T. Islam, E.M. Ali, W.A. Awan, M.S. Alzaidi, T.A.H. Alghamdi, M. Alathbah, A parasitic patch loaded staircase shaped UWB MIMO antenna having notch band for WBAN applications, Helliyon 10 (1) (2024), https://doi.org/10.1016/j.heliyon.2023.e23711. Jan.
[223] K. Srividhya, P. Jothilakshmi, Compact coradiator dual polarized MIMO antenna for future 5G, emerging 6G and IoT applications, Engineering Science and Technology, an International Journal 51 (Mar. 2024) 101609, https://doi.org/10.1016/j.jestch.2023.101609.
[224] K.C. Ravi, J. Kumar, Miniaturized parasitic loaded high-isolation MIMO antenna for 5G applications, Sensors 22 (19) (Oct. 2022), https://doi.org/10.3390/s22197283.
[225] S.B. Paiva, A.G. D'Assunção Junior, V.P. Silva Neto, A.G. D'assunção, A new compact dual-polarized MIMO antenna using slot and parasitic element decoupling for 5G and WLAN applications, Electronics (Switzerland) 11 (13) (Jul. 2022), https://doi.org/10.3390/electronics11131943.
[226] Y.F. Lin, W.C. Chen, C.H. Chen, C. Te Liao, N.C. Chuang, H.M. Chen, High-gain MIMO dipole antennas with mechanical steerable main beam for 5G small cell, IEEE Antennas Wirel Propag Lett 18 (7) (Jul. 2019) 1317–1321, https://doi.org/10.1109/LAWP.2019.2914673.
[227] J. Ghimire, K.W. Choi, D.Y. Choi, Bandwidth enhancement and mutual coupling reduction using a notch and a parasitic structure in a UWB-MIMO Antenna, Int. J. Antenn. Propag. 2019 (2019), https://doi.org/10.1155/2019/8945386.
[228] K. Vasu Babu, S. Das, G.N.J. Sree, S.K. Patel, M. Pardha Saradhi, M.R.N. Tagore, Design and development of miniaturized MIMO antenna using parasitic elements and Machine learning (ML) technique for lower sub 6 GHz 5G applications, AEU - International Journal of Electronics and Communications 153 (Aug) (2022), https://doi.org/10.1016/j.aeue.2022.154281.
[229] B.G.P. Shariff, T. Ali, P.R. Mane, P. Kumar, S. Pathan, Compact wideband two-element millimeter wave MIMO antenna with CMT based modified T-shaped decoupling structure for mobile applications with estimated link budget in urban scenario, AEU - International Journal of Electronics and Communications 177 (Apr) (2024), https://doi.org/10.1016/j.aeue.2024.155209.
[230] A.E. Farahat, K.F.A. Hussein, Dual-band (28/38 GHz) wideband MIMO antenna for 5G mobile applications, IEEE Access 10 (2022) 32213–32223, https://doi.org/10.1109/ACCESS.2022.3160724.
[231] W. Wang, Y. Wu, W. Wang, Y. Yang, Isolation enhancement in dual-band monopole antenna for 5G applications, IEEE Transactions on Circuits and Systems II: Express Briefs 68 (6) (Jun. 2021) 1867–1871, https://doi.org/10.1109/TCSII.2020.3040164.
[232] N.O. Parchin, Y.I.A. Al-Yasir, H.J. Basherlou, R.A. Abd-Alhameed, A Closely Spaced Dual-Band MIMO Patch Antenna with Reduced Mutual Coupling for 4G/5G Applications, 2020.
[233] A.M. Ibrahim, I.M. Ibrahim, N.A. Shairi, Compact MIMO antenna with high isolation for 5G smartphone applications, Journal of Engineering Science and Technology Review 12 (6) (2019) 121–125, https://doi.org/10.25103/jestr.126.15.
[234] M. Abu Sufian, N. Hussain, N. Kim, Quasi-binomial series-fed array for performance improvement of millimeter-wave antenna for 5G MIMO applications, Engineering Science and Technology, an International Journal 47 (Nov) (2023), https://doi.org/10.1016/j.jestch.2023.101548.
[235] F. Amin, R. Saleem, T. Shabbir, S. ur Rehman, M. Bilal, M.F. Shafique, A compact quad-element UWB-MIMO antenna system with parasitic decoupling mechanism, Appl. Sci. 9 (11) (Jun. 2019), https://doi.org/10.3390/app9112371.
[236] S. Hassan Ghadeer, et al., An innovative fractal monopole MIMO antenna for modern 5G applications, AEU - International Journal of Electronics and Communications 159 (Feb) (2023), https://doi.org/10.1016/j.aeue.2022.154480.
[237] J. Huang, G. Dong, J. Cai, H. Li, G. Liu, A quad-port dual-band mimo antenna array for 5g smartphone applications, Electronics (Switzerland) 10 (5) (Mar. 2021) 1–9, https://doi.org/10.3390/electronics10050542.
[238] R.N. Tiwari, R. Thirumalaiah, V.R. Naidu, G. Sreenivasulu, P. Singh, S. Rajasekaran, Compact dual band 4-port MIMO antenna for 5G-sub 6 GHz/N38/N41/N90 and WLAN frequency bands, AEU - International Journal of Electronics

and Communications 171 (Nov. 2023), https://doi.org/10.1016/j.aeue.2023.154919.
[239] G. Shankar Das, B. Bikash Chamuah, Y. Beria, P. Protim Kalita, A. Buragohain, Compact four elements SUB-6 GHz MIMO antenna for 5G applications, Mater Today Proc (Jul. 2023), https://doi.org/10.1016/j.matpr.2023.06.344.
[240] Z. Zhou, S. Liu, Compact wideband MIMO antenna with improved isolation for 5G smartphone application, in: International Conference on Communication Technology Proceedings, ICCT, Institute of Electrical and Electronics Engineers Inc., 2021, pp. 440–444, https://doi.org/10.1109/ICCT52962.2021.9658027.
[241] G. Naga Jyothi Sree, K. Vasu Babu, S. Das, T. Islam, Design and optimization of a deep learning algorithm assisted stub-loaded dual band four-port MIMO antenna for Sub-6 GHz 5G and X band satellite communication applications, AEU - International Journal of Electronics and Communications 175 (Feb) (2024), https://doi.org/10.1016/j.aeue.2023.155074.
[242] A. Abbas, et al., Highly selective multiple-notched UWB-MIMO antenna with low correlation using an innovative parasitic decoupling structure, Engineering Science and Technology, an International Journal 43 (Jul. 2023) 101440, https://doi.org/10.1016/j.jestch.2023.101440.
[243] U. Rafique, S. Agarwal, N. Nauman, H. Khalil, K. Ullah, Inset-Fed Planar Antenna Array for Dual-Band 5G MIMO Applications, 2021.
[244] M. Hussain, et al., Isolation improvement of parasitic element-loaded dual-band MIMO antenna for mm-wave applications, Micromachines 13 (11) (Nov. 2022), https://doi.org/10.3390/mi13111918.
[245] M.A. Sufian, N. Hussain, A. Abbas, J. Lee, S.G. Park, N. Kim, Mutual coupling reduction of a circularly polarized MIMO antenna using parasitic elements and DGS for V2X communications, IEEE Access 10 (2022) 56388–56400, https://doi.org/10.1109/ACCESS.2022.3177886.
[246] T. Addepalli, et al., 8-port semi-circular arc mimo antenna with an inverted l-strip loaded connected ground for uwb applications, Electronics (Switzerland) 10 (12) (Jun. 2021), https://doi.org/10.3390/electronics10121476.
[247] J. Guo, S. Zhang, C.Z. Han, L. Zhang, Combined open-slot and monopole 8 × 8 high-isolation broadband MIMO antenna system for sub-6 GHz terminals, Int. J. Antenn. Propag. 2023 (2023), https://doi.org/10.1155/2023/5169206.
[248] N.O. Parchin, et al., Eight-element dual-polarized MIMO slot antenna system for 5G smartphone applications, IEEE Access 7 (2019) 15612–15622, https://doi.org/10.1109/ACCESS.2019.2893112.
[249] M.I. Khan, S. Liu, J. Mao, A. Basit, A. Ahmed, A. Daraz, Electromagnetic coupling suppression of eight-ports MIMO antenna for satellite communication with neutralize block and parasitic elements, AEU - International Journal of Electronics and Communications 170 (Oct. 2023), https://doi.org/10.1016/j.aeue.2023.154821.
[250] M. Abdullah, et al., Future smartphone: MIMO antenna system for 5G mobile terminals, IEEE Access 9 (2021) 91593–91603, https://doi.org/10.1109/ACCESS.2021.3091304.
[251] S. Jayant, G. Srivastava, M. Khari, 8-Port MIMO antenna having two notched bands for chipless UWB-rfid Tags, IEEE Journal of Radio Frequency Identification 6 (2022) 355–360, https://doi.org/10.1109/JRFID.2022.3180196.
[252] L. Cui, J. Guo, Y. Liu, C.Y.D. Sim, An 8-Element dual-band MIMO antenna with decoupling stub for 5G smartphone applications, IEEE Antennas Wirel Propag Lett 18 (10) (Oct. 2019) 2095–2099, https://doi.org/10.1109/LAWP.2019.2937851.
[253] B. Satyanarayana, S.K. Srivastava, M.K. Meshram, Compact 8-port coupled-fed MIMO antenna array for sub-6 GHz 5G smartphone terminals, in: 2021 IEEE MTT-S International Microwave and RF Conference, IMARC 2021, Institute of Electrical and Electronics Engineers Inc., 2021, https://doi.org/10.1109/IMaRC49196.2021.9714563.
[254] Y.Q. Hei, J.G. He, W.T. Li, Wideband decoupled 8-element MIMO antenna for 5G mobile terminal applications, IEEE Antennas Wirel Propag Lett 20 (8) (Aug. 2021) 1448–1452, https://doi.org/10.1109/LAWP.2021.3086261.
[255] I. Khan, et al., A wideband high-isolation microstrip MIMO circularly-polarized antenna based on parasitic elements, Materials 16 (1) (Jan. 2023), https://doi.org/10.3390/ma16010103.
[256] M.Y. Zeain, et al., A new technique of FSS-based novel chair-shaped compact MIMO antenna to enhance the gain for sub-6GHz 5G applications, IEEE Access (2024), https://doi.org/10.1109/ACCESS.2024.3380013.
[257] R.H. Elabd, A.J.A. Al-Gburi, SAR assessment of miniaturized wideband MIMO antenna structure for millimeter wave 5G smartphones, Microelectron. Eng. 282 (Oct. 2023), https://doi.org/10.1016/j.mee.2023.112098.
[258] A.T.Z. Moses, N. Moses, Compact self decoupled MIMO antenna pairs covering 3.4–3.6 GHz band for 5G handheld device applications, AEU - International Journal of Electronics and Communications 141 (Nov) (2021), https://doi.org/10.1016/j.aeue.2021.153971.
[259] S.H. Kiani, et al., High performance eight-port dual-band MIMO antenna system for 5G devices, Micromachines 13 (6) (Jun. 2022), https://doi.org/10.3390/mi13060959.